PREPARATION, CHARACTERIZATION, AND INTRAMOLECULAR ELECTRON TRANSFER IN PENTAAMMINERUTHENIUM-MODIFIED DERIVATIVES OF CYTOCHROME b_5 AND AZURIN

Thesis by

Bradley Anson Jacobs

In Partial Fulfillment of the Requirements

for the Degree of

Doctor of Philosophy

California Institute of Technology

Pasadena, California

1991

(Submitted September 10, 1990)

ACKNOWLEDGMENTS

First, I would like to thank my parents, whom I love and respect, for instilling in me, by encouragement and example, the value of hard work and doing one's best. Professor Cirila Djordjevic nurtured my interest in chemistry by introducing me to the research laboratory. Professor Harry Gray, through his limitless energy and enthusiasm for teaching and research, helped me to develop independence and an appreciation for how seemingly unrelated fields of chemistry often share fundamental principles.

Members of the Gray group, past and present, have made significant contributions to the progress of my research project through practical help and advice. As Tad once told me, the Gray group always has an opinion for the best way to do something, and often has many. Specifically, Mike A. gave me invaluable help with the computers and flash-photolysis instrumentation. Grant and Marcia saved me the joys of isolating cytochrome b_5 from beef liver, and Cindy did likewise with azurin. But more importantly, aside from just passing the time, discussions of the "nerve center" (Adrienne, Mike T., Tom M., Jeff, Debbie, and Ramy) during the interminable hours waiting for Amicons or the FPLC helped me to refine my professional goals. I had the opportunity to live vicariously through several career choices, with all of the pros and cons considered. I am particularly grateful to Adrienne for giving my propositions and thesis a careful, critical reading. And, of course, a special thanks goes to Andrew B. Canard, just for not being there.

The guys at 114 S. Meridith helped fill my premarital leisure hours with companionship and humor. There, I learned how the other half lives, while getting unforgettable firsthand experience with the extremes of temperature in Pasadena.

And finally, I would like to thank my wife, Lila, for her love, patience, and friendship. Lila, you make it all worthwhile.

ABSTRACT

Wild-type, mutant, and deuteroporphyrin-substituted bovine cytochrome b_5 have been modified with pentaammineruthenium (a_5Ru) for intramolecular electron-transfer (ET) studies. The reactivity of the three surface histidines of the wild-type trypsin-solubilized protein (WT-b_5) with $[a_5Ru(OH_2)]^{2+}$ increases in the order His-15 < His-80 < His-26. Intramolecular ET rates from Fe(II) to Ru(III) have been measured by flash photolysis for a_5Ru(His-26)-modified WT-b_5, Ru(H26)WT-b_5; mutant (Asn-57 to Asp, Gln-13 to Glu, Glu-11 to Gln, His-15 to Asn, His-80 to Asn) lipase-solubilized cyt b_5, Ru(H26)LM-b_5; and deuteroporphyrin-substituted WT-b_5, Ru(H26)DP-b_5. The observed rates display a weak concentration dependence (0.5 - 3 μM protein, μ = 0.5 M sodium phosphate, pH 7.0, 25 °C): k_{ET} = 1.4(1) s^{-1}, Ru(H26)WT-b_5; 5.9(5) s^{-1}, Ru(H26)LM-b_5; and 0.2(1) s^{-1}, Ru(H26)DP-b_5. The rates do not directly correspond to differences in driving force (-0.08, -0.10, -0.13 eV) or edge-to-edge, donor-acceptor separation (12.1, 12, 12.9 Å). Evaluation of the donor-acceptor electronic coupling (H_{AB}) in terms of specific through-bond and through-space interactions in the intervening medium for Ru(H26)WT-b_5 and Ru(H26)LM-b_5 revealed a probable ET pathway consisting of eight covalent bonds from Cγ of His-26 to the end of the Leu-25 side chain, then a through-space jump (R = 3.8, 3.7 Å) to the heme 2-vinyl. Ru(H26)DP-b_5 lacks the 2-vinyl, requiring a longer jump (R = 4.5 Å) to the heme 3-methyl. Because H_{AB} is predicted to decay rapidly with R, the calculated rate constants (assuming λ = 1.2 eV) reflect the differences in R for the three derivatives: Ru(H26)WT-b_5, 1.9 s^{-1}; Ru(H26)LM-b_5, 4.4 s^{-1}; Ru(H26)DP-b_5, 0.16 s^{-1}. The close agreement of calculated and observed rate constants indicates that the electronic coupling in this system is reasonably described by the (His-26)(Leu-25)(through-space jump to heme) pathway. The ET rate in a mutant (His-26 to Arg), trypsin-solubilized cyt b_5 modified with a_5Ru^{3+} at His-80 was also measured. As expected from the long donor-acceptor separation

(21Å) and poor electronic coupling predicted by pathway analysis, k_{ET} was within experimental error of 0 s^{-1}.

Azurin from *Alcaligenes denitrificans* was singly modified at His-83 with a_5Ru^{3+}; the other surface histidine (32) was not successfully modified. The intramolecular ET rate from Ru(II) to Cu(II) for Ru(H83)Az was measured (1.0(3) s^{-1}) and was found to be comparable to that reported for the analogous ruthenium-modified *P. a.* azurin. These rates are slower than would be expected for a similar distance in cytochrome *c*. The application of a pathway theoretical model to both the *P. a.* and *A. d.* azurin systems showed no evidence that the β-sheet secondary structure of azurin precludes effective electronic coupling. This suggests that weak electronic coupling to the copper site itself is responsible for the low k_{ET}'s in azurin.

TABLE OF CONTENTS

LIST OF FIGURES

CHAPTER I

CHAPTER II

CHAPTER IV

LIST OF TABLES

CHAPTER I

INTRODUCTION

Electron transfer (ET) reactions play a key role in biological processes such as respiration and photosynthesis.[1-3] The redox-active prosthetic groups of metalloproteins that mediate these reactions are often buried in the protein interior, making ET across distances of 10 to 25 Å likely.[4,5] Yet redox reactions of metalloproteins are highly specific, implicating chemical and/or physical mechanisms that control the rate of long-range ET. As a result, there is intense interest in elucidating the factors contributing to the observed rates.[4,6]

Semiclassical ET theory gives the rate constant for intramolecular ET (k_{ET}) as [7]

$$k_{ET} = \upsilon_N \kappa_E \exp [-(\Delta G^\circ + \lambda)^2 /4\lambda RT]$$

where ΔG° is the free energy change for the reaction, λ is the inner-shell and solvent nuclear reorganization energy, υ_N is a frequency factor describing the dynamics of nuclear motion, and κ_E is the electronic coupling between the donor and the acceptor. Figure 1 schematically represents the energetics described by the exponential term; the vibrational energies of the reactant (R) and the product (P) nuclear configurations are approximated as those of harmonic oscillators. At the crossing point (C), the activation energy, $\Delta G^\ddagger = [-(\Delta G^\circ + \lambda)^2 /4\lambda]$, has been attained; if $\kappa_E = 1$ (an adiabatic process), there is unit probability that the reaction will proceed from the reactant to the product surface. In protein ET reactions, however, the electronic coupling is often poor; i. e., $\kappa_E < 1$ (a nonadiabatic process). Once the nuclei reach a configuration allowing charge transfer, the electron still must tunnel through the barrier presented by the peptide matrix between the donor and the acceptor.

Determining how proteins mediate ET has attracted considerable attention. Recent investigations involving derivatives of myoglobin,[8] horse-heart cytochrome *c*,[9,10] and hemoglobin [11] have indicated that the ET rates in these proteins fall off exponentially with increasing donor-acceptor distance:[7]

$$\kappa_E = \kappa_E^\circ \exp [-\beta (D - D_o)]$$

Figure 1. A schematic diagram of the reactant (R) and product (P) potential energy surfaces for an ET reaction. See the text for discussion.

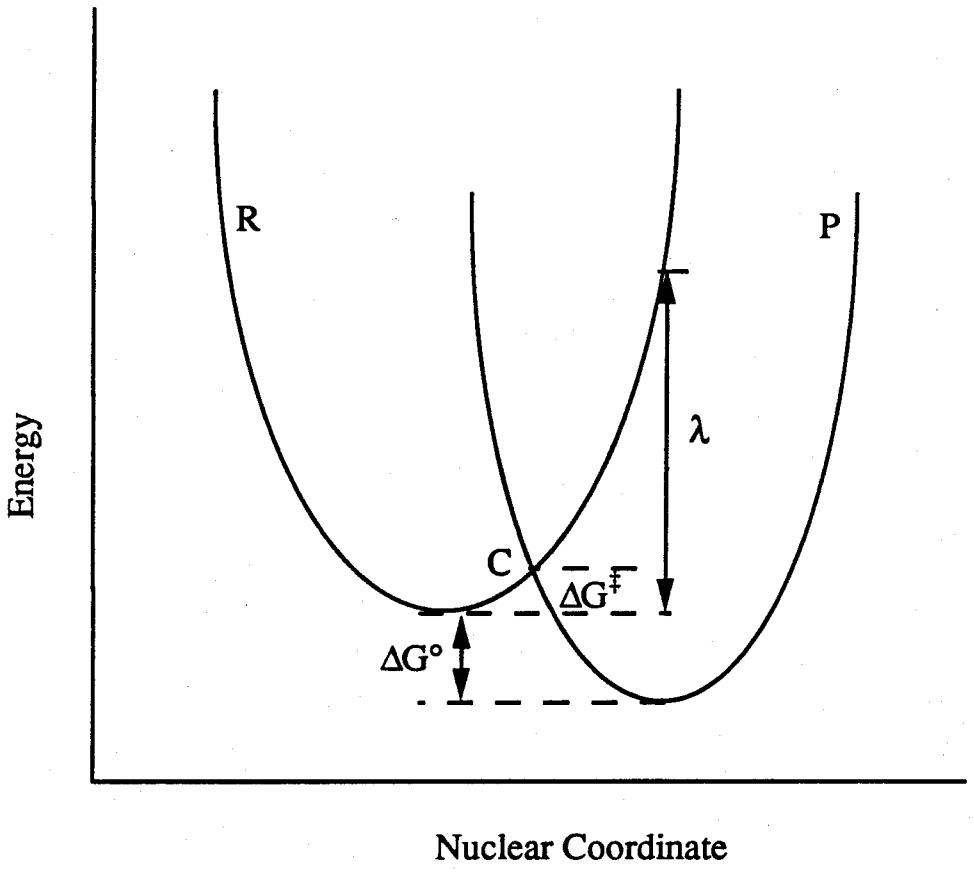
R
P
λ
C
ΔG‡
ΔG°
Energy
Nuclear Coordinate

with values of β in the range of 0.8 to 0.9 $Å^{-1}$. ($\kappa_E°$ is the electronic coupling at donor-acceptor contact (D_0), normally taken to be 3 Å.) However, rates higher than predicted by simple exponential decay relationships have been found in ruthenium-modified *Candida krusei* cytochrome *c*,[12] and unusually low rates have been observed in ruthenated derivatives of cytochrome c_{551},[13] plastocyanin,[14] azurin,[15] and the high-potential, iron-sulfur protein (HIPIP) from *Chromatium vinosum*.[16] What is responsible for the differences in these rates? Does each protein have an inherently different value of β? Perhaps the electronic coupling is not homogeneous within a protein but instead depends on the structural details of the peptide folds in the ET pathway. Several theoretical treatments have been developed to consider these possibilities.[17]

This thesis presents experimental research directed towards defining the role of the peptide medium in controlling ET rates. Two natural electron-transport metalloproteins were chosen for study: an iron-heme protein, cytochrome b_5, and a blue-copper protein, azurin. The general experimental approach used is one that has met success in the past for investigating ET in a number of other proteins.[8-10,12-16] By chemically modifying a redox metalloprotein with a metal complex, a two-site, donor-acceptor system can be constructed; the electron donor and acceptor are in one molecule but are separated by peptide folds rather than by a short covalent link. For example, solvent-accessible histidines will substitute for the aquo ligand in complexes of the form $[(NH_3)_5Ru(OH_2)]^{2+}$.[4-6] The resulting $(NH_3)_5$Ru-His complex is substitutionally inert, particularly in the Ru(III) oxidation state.[18] Since only surface residues are modified, the ruthenation method is not expected to perturb the protein structure significantly.[19] Thus, if the protein has been crystallographically characterized, the site-to-site distance and the nature of the intervening medium can be estimated by computer modeling. By changing the site of surface modification, the ET distance, intervening medium, and/or relative orientation of the redox centers can be varied. ET rates can then be measured by flash photolysis or by pulse radiolysis.

Chapter II discusses the physical properties of cyt b_5 and the preparation, purification, and characterization of several ruthenium-modified derivatives. Chapter III describes the methodology developed to study ET in ruthenated cyt b_5 by flash photolysis. This chapter also reports intramolecular ET rate constants for the modified proteins prepared in Chapter II and evaluates the results with respect to current theory. Finally, Chapter IV provides a comparative investigation of ET in ruthenium-modified azurin from *Alcaligenes denitrificans*.

REFERENCES

(1) Hatefi, Y. *Ann. Rev. Biochem.* **1985**, *54*,1015.

(2) Devault, D., *Quantum Mechanical Tunnelling in Biological Systems*; Cambridge University Press: Cambridge, 2nd Ed., 1985.

(3) Gray, H. B.; Malmstrom, B. G. *Biochemistry* **1989**, *28*, 7499-7505.

(4) McLendon, G. *Acc. Chem. Res.* **1988**, *21*, 160-167.

(5) Mayo, S. L.; Ellis, W. R., Jr.; Crutchley, R. J.; Gray, H. B. *Science* **1986**, *233*, 948-952.

(6) a) Therien, M. J.; Chang, J.; Raphael, A. R.; Bowler, B. E.; Gray, H. B. *Structure and Bonding*; Palmer, G., Ed.; in press. b) Bowler, B. E.; Raphael, A. L.; Gray, H. B. *Prog. Inorg. Chem.*, in press.

(7) Marcus, R. A.; Sutin, N. S. *Biochim. Biophys. Acta* **1985**, *811*, 265-322.

(8) Axup, A. W.; Albin, M.; Mayo, S. L.; Crutchley, R. J.; Gray, H. B. *J. Am. Chem. Soc.* **1988**, *110*, 435-439.

(9) Nocera, D. G.; Winkler, J. R.; Yocom, K. M.; Bordignon, E.; Gray, H. B. *J. Am. Chem. Soc.* **1984**, *106*, 5145-5150.

(10) a) Elias, H.; Chou, M. H.; Winkler, J. R. *J. Am. Chem. Soc.* **1988**, *110*, 429-434. b) Durham, B.; Pan, L. P.; Long, J. P.; Millett, F. *Biochemistry* **1989**, *28*, 8659-8665.

(11) Peterson-Kennedy, S. E.; McGourty, J. L.; Kalweit, J. A.; Hoffman, B. M. *J. Am. Chem. Soc.* **1986**, *108*, 1739-1746.

(12) Therien, M. J.; Selman, M.; Gray, H. B.; Chang, I. -J.; Winkler, J. R. *J. Am. Chem. Soc.* **1990**, *112*, 2420-2422.

(13) Osvath, P.; Salmon, G. A.; Sykes, A. G. *J. Am. Chem. Soc.* **1988**, *110*, 7114-7118.

(14) Jackman, M. P.; McGinnis, J.; Powls, R.; Salmon, G. A.; Sykes, A. G. *J. Am. Chem. Soc.* **1988**, *110*, 5880-5887.

(15) Margalit, R.; Kostic, N. M.; Che, C. -M.; Blair, D. F.; Chiang, H. -J.; Pecht, I.; Shelton, J. B.; Shelton, J. R.; Schroeder, W. A.; Gray, H. B. *Proc. Natl. Acad. Sci., USA* **1984**, *81*, 6554-6558.

(16) Jackman, M. P.; Lim, M. -C.; Salmon, G. A.; Sykes, A. G. *J. Chem. Soc., Dalton Trans.* **1988**, 2843-2850.

(17) a) Beratan, D. N.; Onuchic, J. N. *Photosynthesis Research* **1989**, *22*, 173-186. b) Beratan, D. N.; Onuchic, J. N.; Hopfield, J. J. *J. Phys. Chem.* **1987**, *86*, 4488-4498. c) Beratan, D. N.; Onuchic, J. N.; Betts, J. N.; Bowler, B. E.; Gray, H. B. *J. Am. Chem. Soc.*, in press. d) Siddarth, P; Marcus, R. A. *J. Chem. Phys.*, in press.

(18) a) Yocom, K. M.; Shelton, J. B.; Shelton, J. R.; Schroeder, W. A.; Worosila, G.; Isied, S. S.; Bordignon, E.; Gray, H. B. *Proc. Natl. Acad. Sci., USA* **1982**, *79*, 7052-7055. b) Yocom, K. M.; Winkler, J. R.; Nocera, D. G.; Bordignon, E.; Gray, H. B. *Chemica Scripta*, **1983**, *21*, 29-33.

(19) a) Go, M.; Miyazawa, S. *Int. J. Pept. Protein Res.* **1980**, *15*, 211-224. b) Alber, T.; Dao-pin, S.; Nye, J. A.; Muchmore, D. C.; Matthews, B. W. *Biochemistry* **1987**, *26*, 3754-3758. c) Baldwin, R. L.; Eisenberg, D. In *Protein Engineering*; Oxender, D. L. and Fox, C. F., Eds.; Alan R. Liss: New York, 1987, pp. 127-148.

CHAPTER II

PREPARATION AND CHARACTERIZATION OF RUTHENIUM-MODIFIED CYTOCHROME b_5 DERIVATIVES

INTRODUCTION

Cytochrome b_5 (cyt b_5) is a natural ET protein with an iron-heme prosthetic group. The microsomal form consists of a water-soluble, heme-binding domain (MW ≈ 10 kdal) and a short, hydrophobic tail that serves to anchor it to the endoplasmic reticulum membrane. This form participates in fatty-acid elongation [1] and desaturation,[2] cholesterol biosynthesis,[3] and the cytochrome P-450 catalytic cycle.[4] Figure 2 shows the amino-acid sequence of bovine cyt b_5. Treatment with lipase or with trypsin solubilizes the protein by cleaving the hydrophobic tail but leaves the functional globular region intact. This head region closely resembles a soluble form of the cyt b_5 responsible for methemoglobin reduction in erythrocytes.[5] (Refer to Figure 2 for comparative cleavage sites.)

Cyt b_5 is attractive for intramolecular ET studies for several reasons. The crystal structure of the lipase-solubilized bovine form [6,7] indicates that there are three surface histidines potentially accessible to ruthenium modification.[8,9] His-26, His-15, and His-80 (Figure 3) span a wide range of distances from the heme (12, 15, and 21 Å), making cyt b_5 a good candidate for an ET distance-dependence investigation. The direct path from His-26 to the heme passes through Phe-58, which is parallel to the Fe-binding His-63 (Figure 4). Thus, a ruthenated derivative at this position will provide insight into the importance of intervening aromatic residues in affecting ET. In addition, the expression of rat [10] and bovine [11] cyt b_5 in *E. coli* allows the construction of site-specific mutants that could be valuable in studies of long-range, donor-acceptor interactions.

Bimolecular ET kinetics of cyt b_5 both with small molecules[12-16] and with other metalloproteins [17,18] have been investigated. These studies suggest that a ring of eleven negative side chains around the heme serve to facilitate redox partner recognition and binding (Figure 5). The net charge of cyt b_5 has been estimated from the amino-acid sequence to be -6.5; however, the clustering of acidic residues near the heme makes the

Figure 2. The amino-acid sequence of bovine, microsomal cytochrome b_5. Numbering is based on the crystallographic convention. Cleavage sites (*) used for solubilization are distinguished by "L" (lipase) or by "T" (trypsin). "R" denotes the cleavage sites for the soluble cyt b_5 found in red blood cells. Heme ligands are indicated by "Fe," and native surface histidines, of interest in the present work, are emphasized with their sequence numbers.

L T
(X - Ala , Glx , Glx - Ser * Lys * Ala - Val - Lys - Tyr - (6)

11 13 15
Tyr - Thr - Leu - Glu - Glu - Ile - Gln - Lys - His - Asn - (16)

26
Asn - Ser - Lys - Ser - Thr - Trp - Leu - Ile - Leu - His - (26)

Tyr - Lys - Val - Tyr - Asp - Leu - Thr - Lys - Phe - Leu - (36)

Fe
Glu - Glu - His - Pro - Gly - Gly - Glu - Glu - Val - Leu - (46)

Arg - Glu - Gln - Ala - Gly - Gly - Asp - Ala - Thr - Glu - (56)

Fe
Asn - Phe - Glu - Asp - Val - Gly - His - Ser - Thr - Asp - (66)

Ala - Arg - Glu - Leu - Ser - Lys - Thr - Phe - Ile - Ile - (76)

80 T
Gly - Glu - Leu - His - Pro - Asp - Asp - Arg * Ser - Lys - (86)

R L/R
Ile - Thr - Lys - Pro - Ser * Glu - Ser * Ile - Ile - Thr - (96)

Thr - Ile - Asp - Ser - Asn - Pro - Ser - Trp - Trp - Thr - (106)

Asn - Trp - Leu - Ile - Pro - Ala - Ile - Ser - Ala - Leu - (116)

Phe - Val - Ala - Leu - Ile - Tyr - His - Leu - Tyr - Thr - (126)

Ser - Glu - Asn - COOH

Figure 3. The crystal structure of lipase-solubilized bovine cytochrome b_5.[14,15] The peptide backbone (plus the amide-nitrogen hydrogens) is shown in blue, the iron protoporphyrin IX (heme) in red, the iron axial ligands in green, and the surface histidines in orange. The globular cyt b_5 structure consists of two hydrophobic cavities (one of which contains the heme) surrounded by strands of α-helix and separated by a central β-sheet.

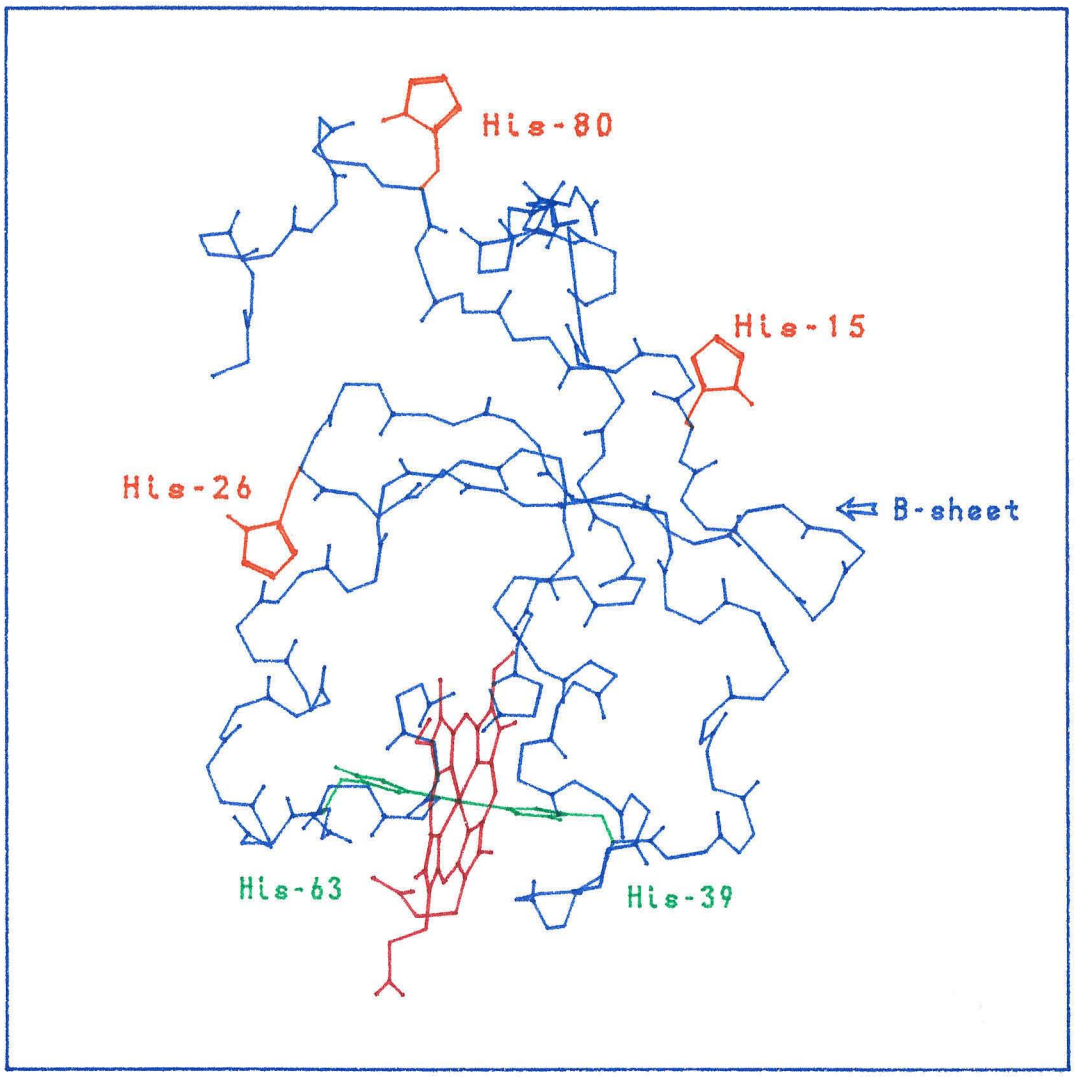
His-80
His-15
His-26
B-sheet
His-63
His-39

Figure 4. The direct path between His-26 and the heme. The aromatic side chain of Phe-58 lies in the path and is parallel to a heme ligand, His-63.

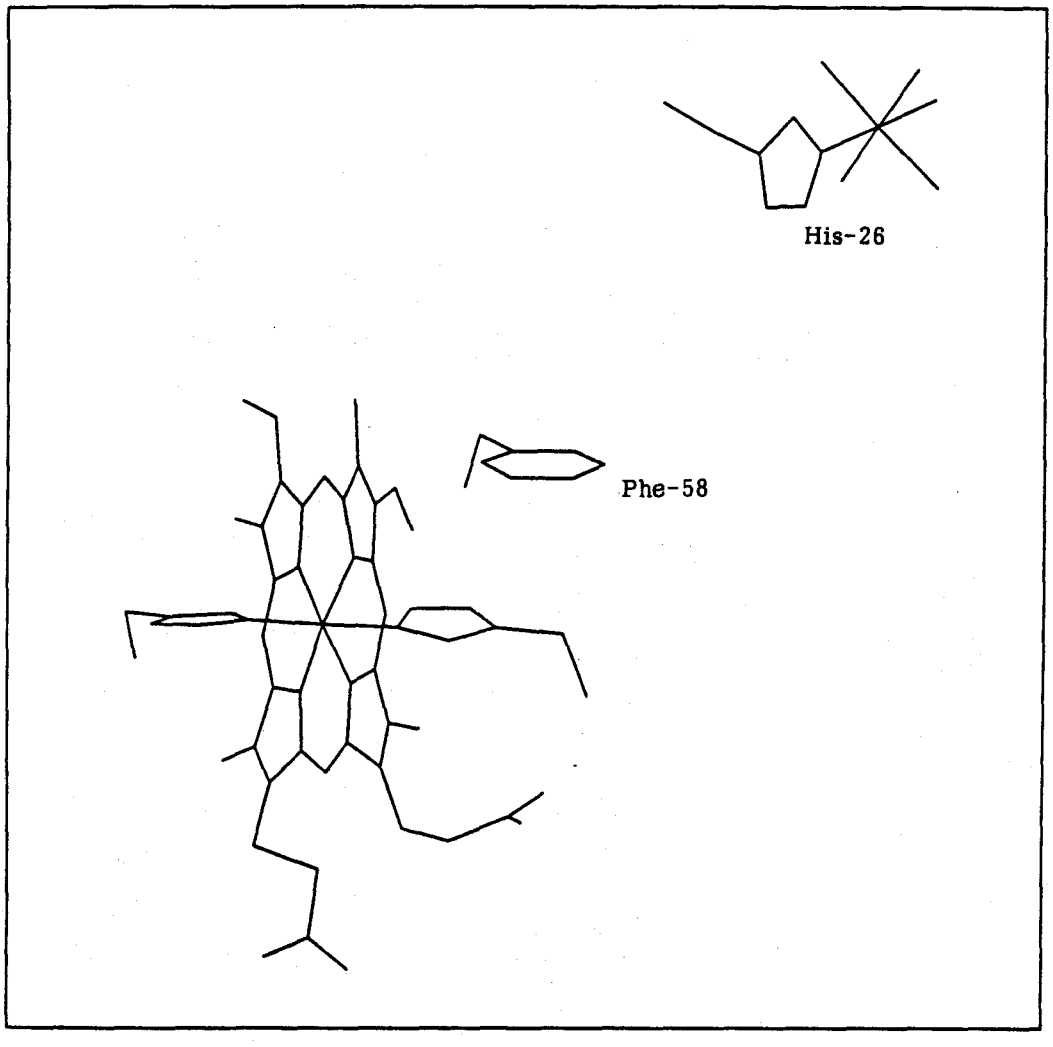
His-26
Phe-58

Figure 5. The negative heme area in cyt b_5. The side chains of the acidic amino-acid residues surrounding the heme are shown in red. The two porphyrin propionates are also negatively charged, but only propionate-6 extends into the solvent.

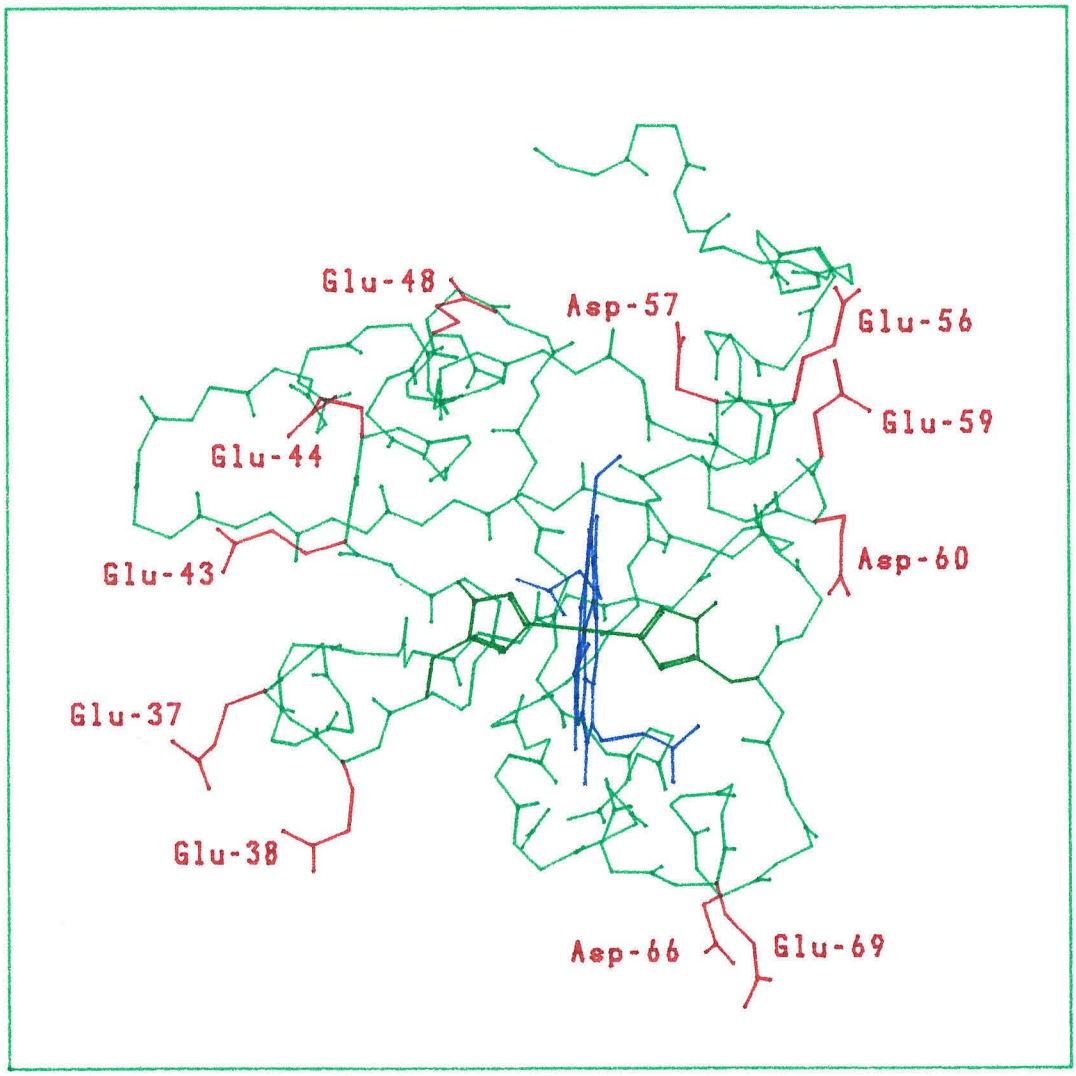
Glu-48
Asp-57
Glu-56
Glu-59
Glu-44
Asp-60
Glu-43
Glu-37
Glu-38
Asp-66
Glu-69

effective charge towards small metal complexes equal to -14.2.[16] The heme itself has two anionic propionates; one (propionate-7) projects out into solvent, and the other (propionate-6) is folded back into the protein interior.[6] The negative charge of propionate-6 is thought to stabilize Fe^{3+},[6c] a possible explanation for cyt b_5's low reduction potential ($E°(Fe^{3+/2+})$ = 5.1 mV vs. NHE)[19] compared to other cytochromes.†

Because cyt b_5 has a low reduction potential, ET from the heme to a_5Ru^{3+} ($E°(Ru^{3+/2+})$ = 80 mV vs. NHE)[8,22] should occur, and changes in the protein's UV-vis spectrum with oxidation state (Figure 6) should make ET readily observable. As characteristic of cytochrome *c*, the iron is low-spin in both oxidation states; thus its contribution to ET reorganization energy is small. Unlike the *c*-type cytochromes, however, because the heme is covalently bound to the apoprotein only by the axial histidines, it can be replaced by other porphyrins [23] with different electronic properties for ET experiments.

The work on cyt b_5 described in this thesis made use of several forms of the protein (kindly provided by the Mauk group at the University of British Columbia). Wild-type bovine-sequence cyt b_5, WT-b_5, was isolated from bovine liver and solubilized by tryptic digestion, or later, was produced in *E. coli* by recombinant DNA techniques.[11] With the purpose of probing the importance of pathways in ET (Chapter III), the native iron protoporphyrin IX was replaced with iron deuteroporphyrin IX to make DP-b_5. The two porphyrins differ only at positions 2 and 4, as shown in Figure 7.

Initial attempts to express bovine cyt b_5 in bacteria used a gene synthesized from a published amino-acid sequence,[24] which incorrectly assigned the amidation status of three

---

† Recent studies of cytochrome *c* have suggested that axial ligation may play a key role in determining heme reduction potential. Replacing the native Met-80 of cyt *c* with histidine by semisynthesis yields a cyt b_5-like *bis*-histidine protein with $E°(Fe^{3+/2+})$ = 41(10) mV vs. NHE,[20] compared to wild-type cyt *c*, which has $E°(Fe^{3+/2+})$ = 260 mV.[21]

Figure 6. The UV-visible spectra of oxidized (—) and reduced (- - -) WT-b_5. The concentration of protein is identical in each spectrum (μ = 100 mM NaPi, pH 7.0). The absorbance below 370 nm in the reduced spectrum is due to added $Na_2S_2O_4$ reductant.

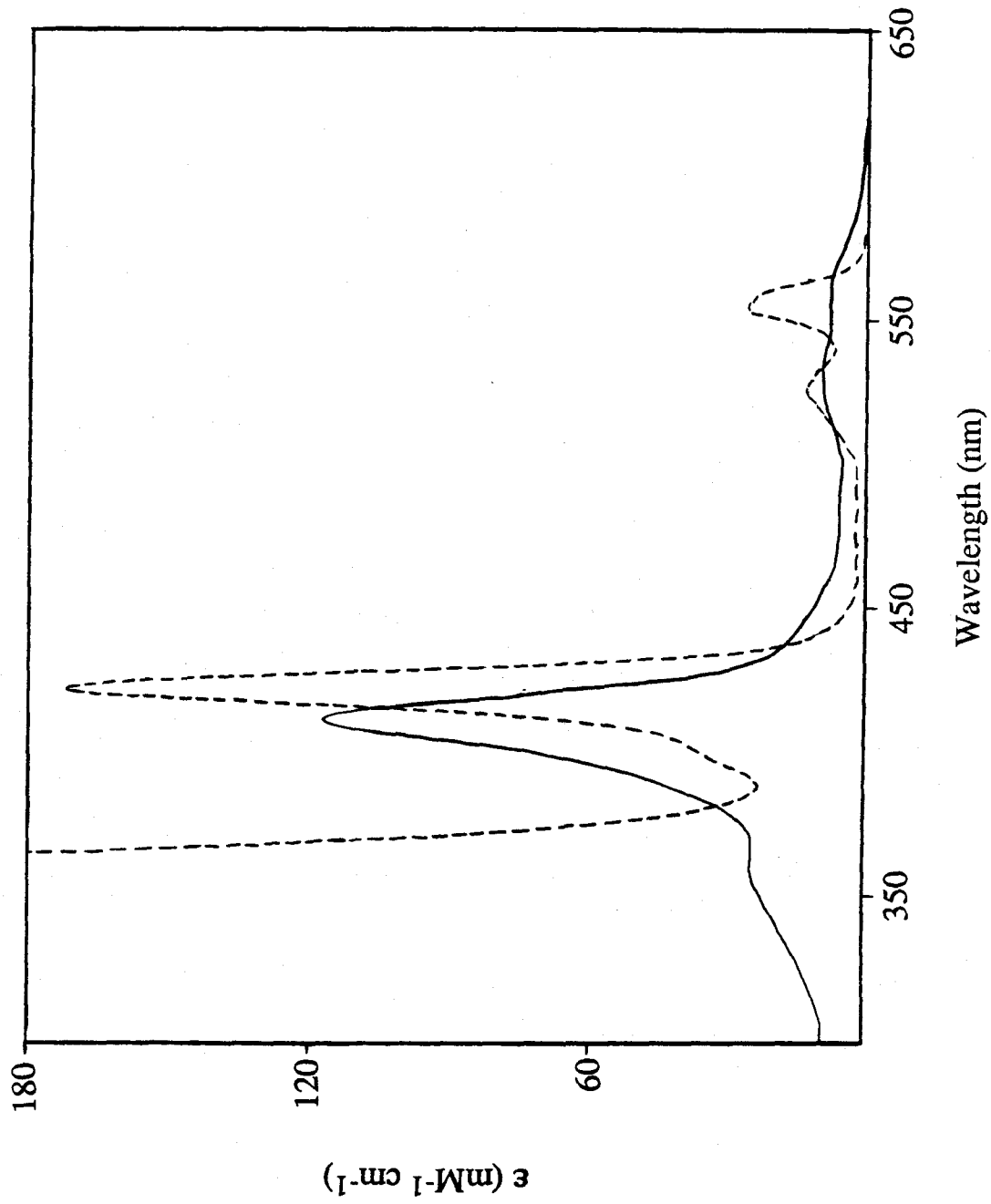
180
120
60
ε (mM-1 cm-1)
350
450
550
650
Wavelength (nm)

Figure 7. The structure of a general iron porphyrin. For protoporphyrin IX, R = $-CH=CH_2$; for deuteroporphyrin IX, R = H.

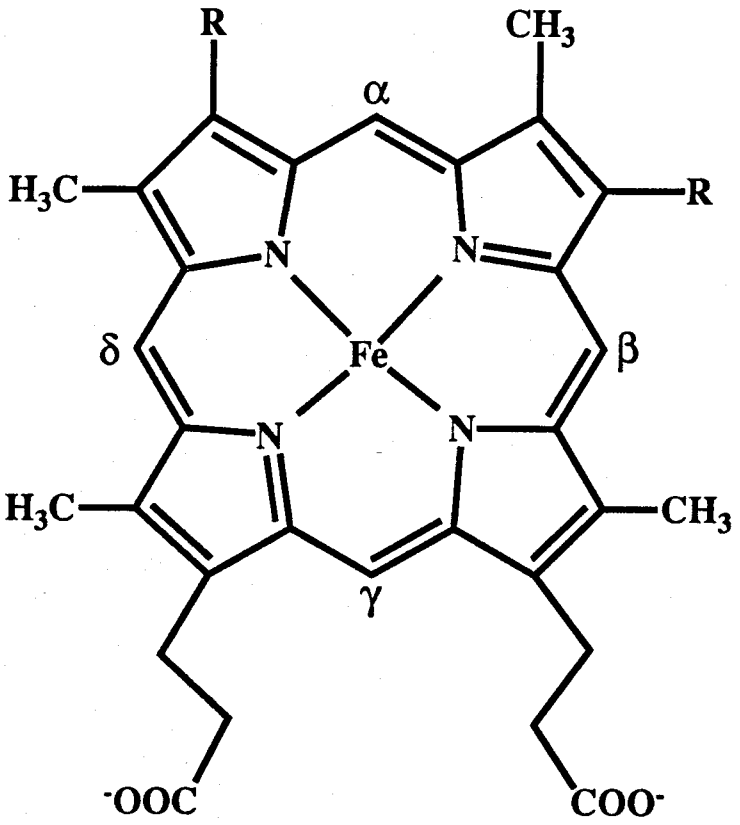
R
CH3
α
H3C
R
N
N
δ
Fe
β
N
N
H3C
CH3
γ
-OOC
COO-

residues. The lipase-sequence triple mutant, LTM-b_5 (Asn-57 to Asp, Gln-13 to Glu, Glu-11 to Gln), showed different electrochemical ($E°(Fe^{3+/2+})$ = -14 mV vs. NHE), chromatographic, cytochrome *c* binding, and methemoglobin binding behavior from the authentic protein.[11] A crystal structure of LTM-b_5 was determined, and it revealed a close correspondence but slight changes from the wild-type structure.[11] An overlay of the alpha-carbon backbones is shown in Figure 8, and a plot of the average deviations of backbone and side chain atoms is given in Figure 9.

The inadvertent expression of LTM-b_5 provided a fortuitous opportunity for ET studies. Being so closely related to WT-b_5, LTM-b_5 allowed a parallel ET investigation using a well-characterized protein having small structural variations. Any difference in ET behavior between ruthenium-modified WT-b_5 and LTM-b_5 can be attributed to subtle differences in the proteins' structures; thus the role of the peptide medium in controlling ET can be examined. To increase the yield of His-26-modified protein, a mutant with His-15 and His-80 replaced with asparagine, LM-*b5*, was made with the expectation that these conservative surface mutations would be nonperturbative.[25]

Two additional mutants studied had native histidines replaced with residues unreactive towards ruthenium modification in order to increase the yields of singly modified products. For example, in a protein denoted "TNN-b_5," the amino-acid sequence was the same as WT-b_5, except that His-15 and His-80 were substituted with asparagine. Similarly, TR26-b_5 retained His-15 and His-80, but the most reactive residue, His-26, was replaced with arginine.

The abbreviations given above will be used throughout this thesis to identify specific proteins studied. Prefixes such as Ru(H26)- or Ru(H80)- denote derivatives singly modified with a_5Ru^{3+} at the indicated histidine.

Figure 8. Stereoview overlaying the structures of WT-b_5 (thin lines) and LTM-b_5 (thick lines). The residues differing by the inadvertent mutations are indicated. (Figure provided by A. G. Mauk.)

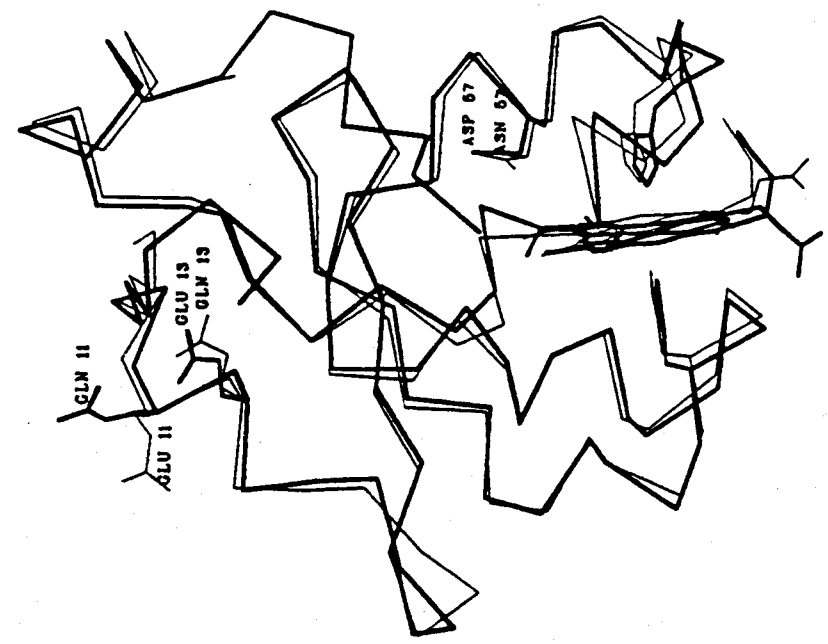
ASP 67
GLU 13
GLN 13
GLN 11
GLU 11

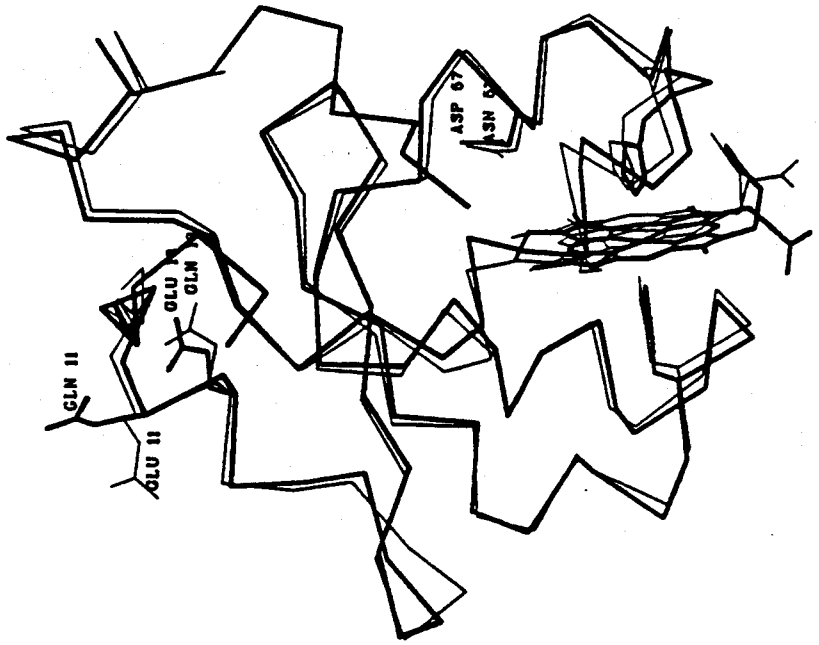
ASP 67
GLN 11
GLU 11

Figure 9. Plot of the structural deviations between WT-b_5 and LTM-b_5. The thick line represents main chain atoms, and the thin line represents side chain atoms. (Figure provided by A. G. Mauk.)

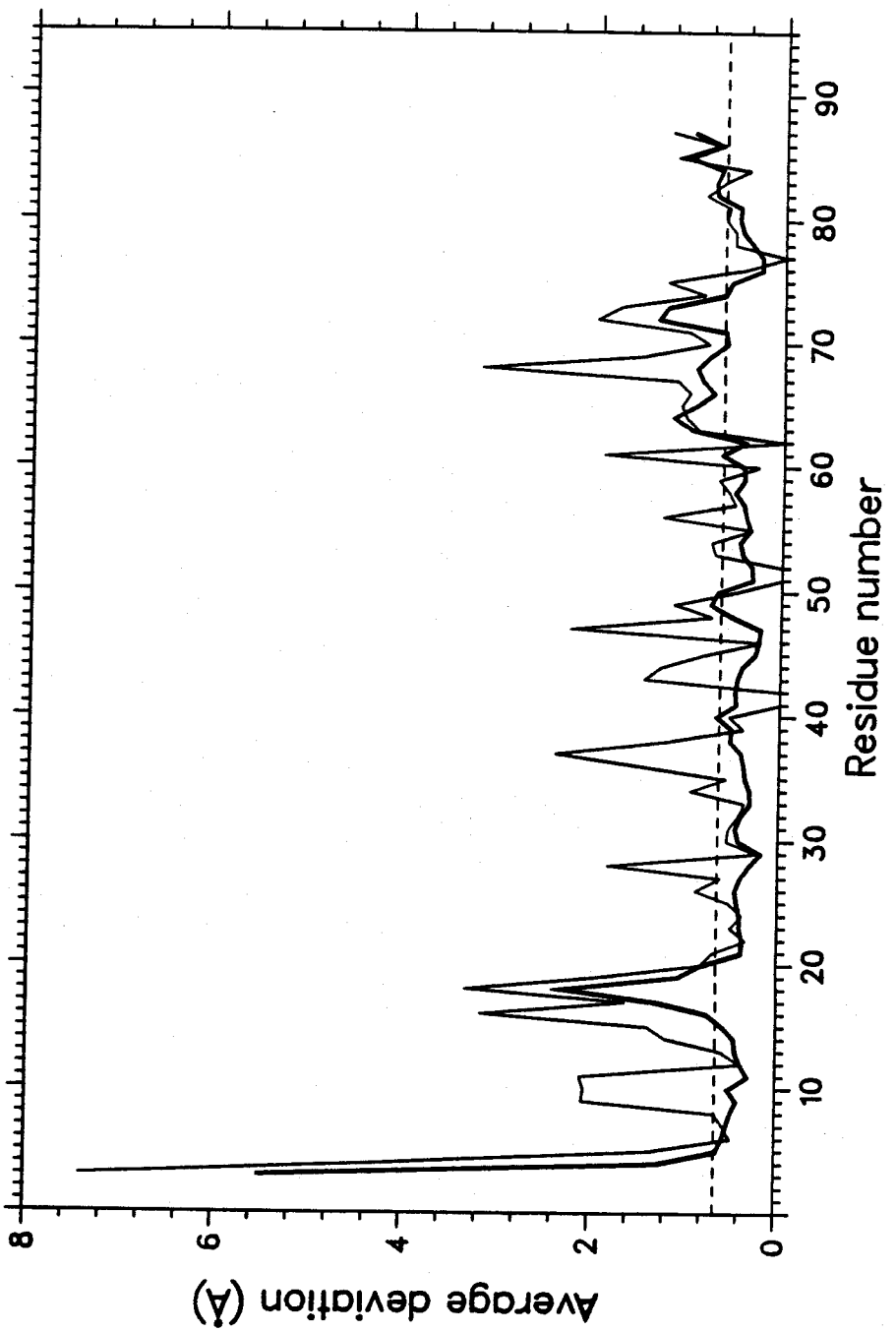
Average deviation (Å)
0
2
4
6
8
10
20
30
40
50
60
70
80
90
Residue number

EXPERIMENTAL

Materials and General Methods

Distilled water, passed through a Barnstead Nanopure purification system (No. 2794, specific resistance > 18 MΩ-cm), was used to prepare all aqueous solutions. Sodium phosphate (NaPi); 2,2',2"-nitrilotriethanol (TEA); and [4-(2-hydroxyethyl)-1-piperazineethanesulfonic acid] (HEPES) buffers were prepared with analytical grade reagents.

Protein samples were deoxygenated by at least five vacuum/purge cycles on a dual-manifold vacuum argon (manganese oxide scrubbed) line. Nonprotein reagents were degassed with at least five freeze, pump, thaw cycles and were handled by standard Schlenk techniques. Other air-sensitive manipulations were performed under Ar in a Vacuum Atmospheres Co. HE-493 Dri-Train glove box.

Proteins were concentrated and buffers were changed using either Amicon (YM-5 membrane, 5 kdal cutoff) or Centricon (YM-10, 10 kdal cutoff) ultrafiltration. Unless otherwise noted, all proteins were handled and stored at 4 °C (when in routine use) or were frozen in liquid N_2 and stored at -50 °C. At all times care was taken to rinse tubes and pipets when transferring protein solutions in order to conserve the limited quantities available.

Preparation of Modified Proteins

Ruthenium-Modified WT-b_5

A concentrated solution of 20 - 50 mg (MW 10,060) wild-type or recombinant trypsin-solubilized bovine sequence cyt b_5 in 325 mM HEPES, pH 7.5, and extra HEPES in a separate flask were degassed by the Ar-purge method. A 25-fold molar excess of $[a_5Ru(OH_2)](PF_6)_2$ (a = NH_3)[26] was taken into the glove box as a solid (prepared < 2 weeks before use and stored in a vacuum dessicator), dissolved in the extra HEPES, and filtered (Millipore 0.2 μm syringe-tip filter) into the protein solution (2

mg/mL final protein concentration; $\varepsilon_{413}(Fe^{3+}) = 117\ mM^{-1}\ cm^{-1}$).[23] The resulting salmon-pink, reduced protein solution was stirred briefly, then allowed to react at room temperature. The optimum reaction time of 2 h was determined by FPLC chromatography (see below) of aliquots quenched at various times using a gel filtration column (G-25; 1.5 x 47 cm) equilibrated and eluted with 20 mM TEA, pH 7.3, to remove unbound ruthenium complexes. Air oxidation was sufficient to produce the substitutionally inert a_5Ru^{III}(His).[9] The product mixture was washed with several Centricon ultrafiltration cycles into TEA in preparation for separation by FPLC chromatography.

Ruthenium-Modified LM-b_5

LM-b_5 (lipase fragment; Asn-57 to Asp, Gln-13 to Glu, Glu-11 to Gln, His-15 to Asn, His-80 to Asn) was modified by a procedure similar to the above, except that the protein concentration was 1.4 mg/mL (MW 11,250), a 30-fold excess of $[a_5Ru(OH_2)](PF_6)_2$ was used, and the reaction was allowed to run for 12 h.

Ruthenium-Modified DP-b_5

The native protoporphyrin IX was extracted from WT-b_5 to produce the apoprotein by the method of Teale,[27] as modified by Reid *et al.*[13] Ferric deuteroporphyrin IX (Porphyrin Products) was reconstituted with the apoprotein according to published procedures.[12] The resulting deuteroporphyrin-cyt b_5, DP-b_5 (ε_{403} = 122 $mM^{-1}\ cm^{-1}$),[23] was modified with ruthenium, employing the same conditions as for WT-b_5.

Ruthenium-Modified TR26-b_5

A 2 mg/mL solution of TR26-b_5 (tryptic fragment; His-26 to Arg) in 325 mM HEPES, pH 7.5, was reacted for 2 h with a 75-fold molar excess of $[a_5Ru(OH_2)](PF_6)_2$. The reaction was quenched on a G-25 gel filtration column as above.

Ruthenium-Modified LTM-b_5

The ruthenation of LTM-b_5 (lipase fragment; Asn-57 to Asp, Gln-13 to Glu, Glu-11 to Gln) was handled differently than above. A 1.25 mg/mL solution of LTM-b_5 in 50 mM HEPES, pH 7.5, was reacted with a 28-fold excess of $[a_5Ru(OH_2)](PF_6)_2$ for 20 minutes. To quench the reaction quickly, a procedure developed by M. Mauk was employed.[28] Bio-Gel P2 (200-400 mesh; Bio-Rad) swollen and equilibrated to 20 mM TEA, pH 7.3, was packed by centrifugation in 3 mL syringes fitted with 0.45 μm Millipore filters. The syringes were suspended in heavy-walled centrifuge tubes to allow eluate collection. Protein mixtures loaded onto such columns were effectively quenched by centrifugation in 5 minutes .

Ruthenium-Modified TNN-b_5

A 1 mg/mL solution of TNN-b_5 (tryptic fragment; His-15 and His-80 to Asn) in 325 mM HEPES was reacted with a 30-fold excess of $[a_5Ru(OH_2)](PF_6)_2$ for 12 h. The reaction was quenched using Bio-Gel, as above, or simply by washing the reaction mixture by Amicon ultrafiltration.

Recycling of Multiply Modified Products

Since the protein samples were in short supply, all FPLC fractions representing undesired elution bands were pooled (with like protein) for reductive recycling. The samples were washed into fresh 20 mM TEA, pH 7.3, and degassed. In the glove box or under a flow of Ar, an excess (spatula tip) of $Na_2S_2O_4$ was added to reduce pendant

ruthenium complexes. The salmon-pink protein solution was stirred for 2 h at 4 °C, then run down a G-25 gel filtration column equilibrated to TEA. The early eluting, column-oxidized protein was then repurified by FPLC chromatography.

FPLC Chromatography Conditions

Ruthenium-modified product mixtures were separated using a Pharmacia FPLC chromatography system equipped with a Mono Q (HR 5/5 or 10/10) anion-exchange column, which was eluted with a gradual salt gradient at room temperature. Generally, 1-2 mg (5/5 column) or up to 20 mg (10/10 column) of the protein in buffer A (20 mM TEA, pH 7.3) were eluted with buffer B (buffer A + 1 M NaCl) according to the gradient programs in Figure 10. The eluate was monitored by absorbance at 280 nm, and fractions were collected at regular volume intervals (1 - 4 mL). Since cyt b_5 has a high negative charge, increasing amounts of bound Ru^{3+} are expected to decrease elution volumes for an anion-exchange column. Thus, runs were often stopped after elution of the native protein band, and later bands eluting in the high-salt wash were discarded as decomposition products.

Determining Ru/Fe Ratios

Samples of bands from FPLC separation of ruthenium-modification reactions were frozen in liquid N_2 and shipped on dry ice to Brookhaven National Laboratory for atomic-absorption analysis (performed by E. L. Norton, Analytical Services). Samples were approximately 20 μM protein in 20 mM TEA, pH 7.3.

Before shipping, the same samples were examined by UV-vis spectroscopy. Using $\varepsilon_{412} = 117\ mM^{-1}\ cm^{-1}$ for pure oxidized WT-b_5 and TR26-b_5 samples, extinction values of $\varepsilon_{304} = 9200$ and $8800\ M^{-1}\ cm^{-1}$ were empirically determined. Since $[a_5Ru\text{-}Im]^{3+}$ (Im = imidazole) absorbs at 304 nm ($\varepsilon_{304} = 1880\ M^{-1}\ cm^{-1}$),[26]

$$C_{Ru} = (A_{304} - \varepsilon_{Fe}C_{Fe}) / \varepsilon_{Ru},$$

Figure 10. FPLC gradient programs for the separation of ruthenium-modification product mixtures of cyt b_5. The program for the Mono Q 10/10 column was patterned after that for the Mono Q 5/5 column (4-fold increase in volumes) to facilitate direct scale-up of separations and to allow easy comparison of chromatograms from each. Buffer A: 20 mM TEA, pH 7.3. Buffer B: A + 1 M NaCl. In each program, the numbers in the left-hand column are in mL eluate.

Mono Q 5/5

0.00	CONC %B	0.0
0.00	ML/MIN	0.50
0.00	CM/ML	0.30
2.00	VALVE.POS	1.2
4.00	VALVE.POS	1.1
4.00	CONC %B	0.0
8.00	CONC %B	15.0
8.00	PORT.SET	6.1
60.00	CONC %B	24.0
70.00	CONC %B	40.0
70.00	CONC %B	100
70.00	ML/MIN	2.00
74.00	CONC %B	100
74.00	PORT.SET	6.0
74.00	CONC %B	0.0
76.00	CONC %B	0.0

Mono Q 10/10

0.00	CONC %B	0.0
0.00	ML/MIN	2.00
0.00	CM/ML	0.07
8.00	VALVE.POS	1.2
16.00	VALVE.POS	1.1
16.00	CONC %B	0.0
32.00	CONC %B	15.0
32.00	PORT.SET	6.1
320.00	CONC %B	27.5
360.00	CONC %B	40.0
360.00	CONC %B	100
376.00	CONC %B	100
376.00	PORT.SET	6.0
376.00	CONC %B	0.0
380.00	CONC %B	0.0

where A is absorbance, and C is concentration. To check for heme loss (which increases the apparent Ru/Fe), the ratio $R_{412/280}$ was calculated for each of the samples. Pure cyt b_5 has $R_{412/280}$ = 5.7 - 6.0.[16]

Proton NMR Spectra

^1H NMR spectra were recorded on a Bruker AM500 spectrometer at 298 K, and referenced to DSS (sodium 2,2-dimethyl-2-silapentane-5-sulfonate). Samples were prepared by washing the fully oxidized protein into D_2O (≥ 4 times) and then into μ = 100 mM NaPi in D_2O (uncorrected pH 7.0; ≥ 4 times) by Centricon ultrafiltration. Resonance from residual water was not suppressed. The sharp histidine C_2H resonances were enhanced by Gaussian multiplication, and their assignments [14] were verified by pH titration with DCl and NaOD.

Differential Pulse Voltammetry

Generally, protein samples used were 0.5 to 2 mM in an electrolyte of μ = 100 mM NaPi, pH 7.0, with 10 mM 4, 4'-bipyridine added to facilitate electron transfer. Solutions were degassed *in situ* by maintaining an Ar blanket and occasional stirring for >30 minutes before a run. The 2 mm-diameter, Au button (Bioanalytical Systems, Inc.) working electrode was polished with an alumina slurry prior to each run. A Pt wire was used for a counter electrode, and the reference was SCE (KCl) (E° = +0.246 V vs. NHE). Potentials were controlled by a Princeton Applied Research polarographic analyzer (model 174A) and were monitored using a Keithley 177 microvolt digital multimeter. Scans were initiated by manually adjusting the potential from the rest value to > 200 - 300 mV positive of the expected reduction wave, then by scanning cathodically with a rate of 2-5 mV s^{-1}, a drop time of 0.5 s, and a 25 mV modulation amplitude. Scan direction was reversed approximately 200 mV negative of the reduction wave, with the

run finishing at the starting potential. Reported DPV E° values are averages of forward and reverse peak potentials and are referenced to the normal hydrogen electrode (NHE).

RESULTS AND DISCUSSION

Ruthenium-modified WT-b_5

WT-b_5 has three surface histidines (His-26, His-15, and His-80) potentially accessible to ruthenium modification. By introducing a second metal center into the protein at any one of these residues, a two-site donor-acceptor system can be produced for intramolecular ET investigations; ideally, three singly modified isomers would be prepared and isolated. Preliminary studies indicated that trypsin-isolated cyt b_5 could be effectively modified with a 20-fold molar excess of $[a_5Ru(OH_2)](PF_6)_2$ in 10 minutes, producing the a_5Ru-WT-b_5 derivatives.[28] An FPLC elution profile of the product mixture is shown in Figure 11. Development of a method using a more gradual salt gradient and a slower flow rate (Figures 10 and 12) gave superior product purity.

As was found with binding studies using diethyl pyrocarbonate (DEP),[29] the most solvent-accessible of cyt b_5's three surface histidines, His-26, is the most reactive toward ruthenium modification (percent solvent accessibility for His-26, His-80, and His-15 are 37.0, 33.4, and 19.1 %).[29,†] Unlike DEP binding, reactivity of the other two

---

† In calculating the percent accessibility, the authors used 159 Å^2 for the maximum surface area, which was determined from the accessible surface area of a histidine side chain in a random coil peptide. BIOGRAF was used to calculate the surface area accessible to a 1.4 Å diameter spherical probe (a model for water) of a histidine side chain on a tripeptide lacking the two adjacent side chains. The maximum area found was a much lower 82 Å^2. The reason for the discrepancy is not clear; one would actually expect less surface area to be accessible in a random coil. Using 86 Å^2 as the maximum area increases the percent accessibility by a factor of 1.9 to 71.7, 64.8, and 37.0 %. Unfortunately, increasing the estimation of the surface area does not affect the residues' reactivity!

Figure 11. FPLC trace from a preliminary WT-b_5 modification. A 5/5 Mono Q column was used to separate 2.5 mg protein. Separation was carried out at 25 °C in 20 mM TEA, pH 7.3, with a NaCl gradient; flow rate 2.0 mL/min. Peak A is unmodified WT-b_5; peaks B, C, and D may be singly modified derivatives. (Figure prepared by M. R. Mauk.)[28]

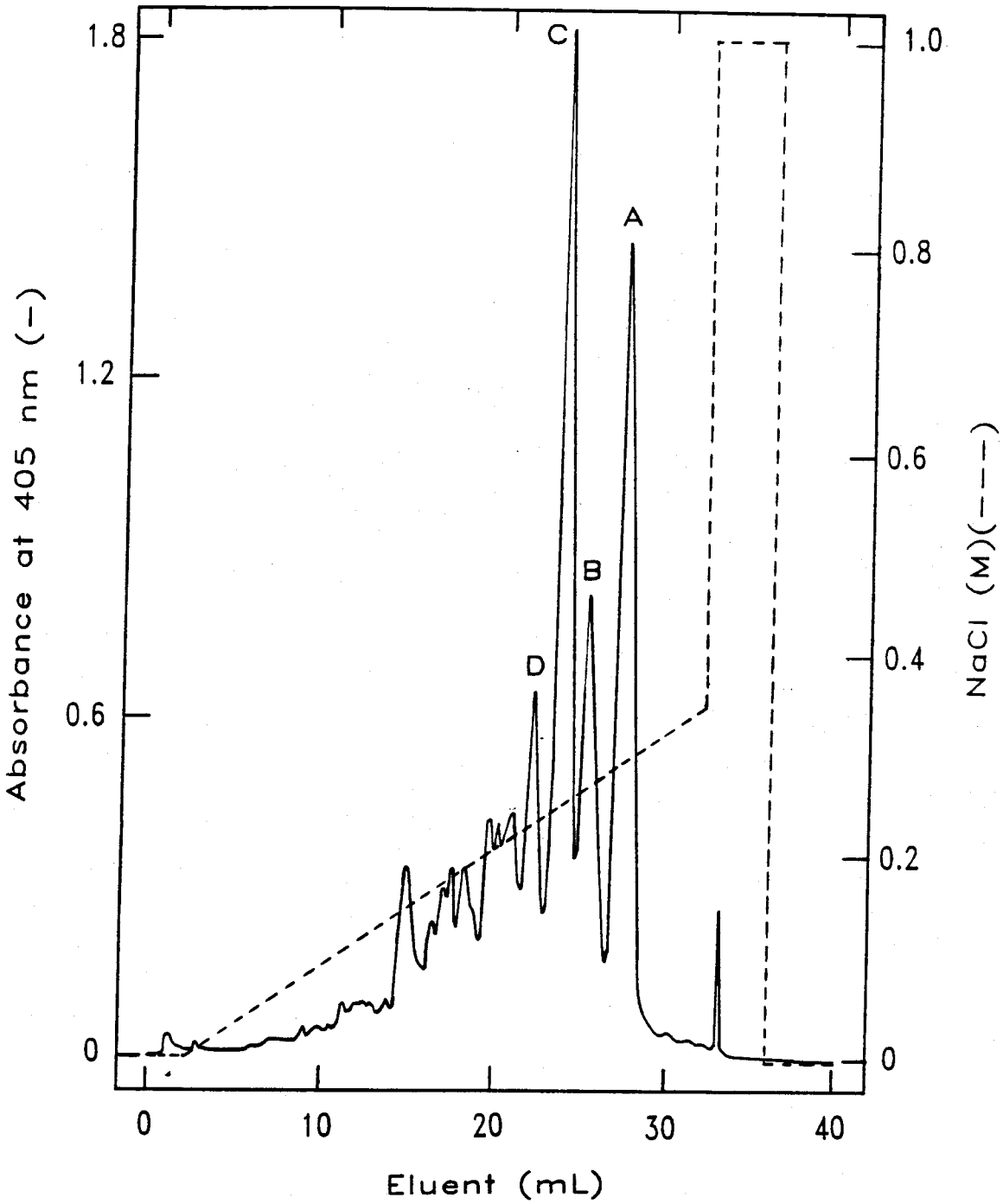
1.8
1.2
0.6
0
Absorbance at 405 nm (—)
1.0
0.8
0.6
0.4
0.2
0
NaCl (M)(— — —)
C
A
B
D
0
10
20
30
40
Eluent (mL)

Figure 12. Elution profile by FPLC (Mono Q 5/5; 20 mM TEA, pH 7.3; NaCl gradient generated using the gradient program in Figure 10) of the reaction mixture from a_5Ru-modification of WT-b_5 quenched after 2 h. The salt gradient (- - -) has been corrected for the horizontal pen displacement on the chart recorder used (subsequent FPLC figures have been corrected similarly). Peak A is unreacted native WT-b_5, peaks B and C are singly modified derivatives, and peak D is Ru(H26)WT-b_5. Early eluting peaks were assumed to be multiply modified derivatives and decomposition products; the corresponding fractions were recycled by reduction.

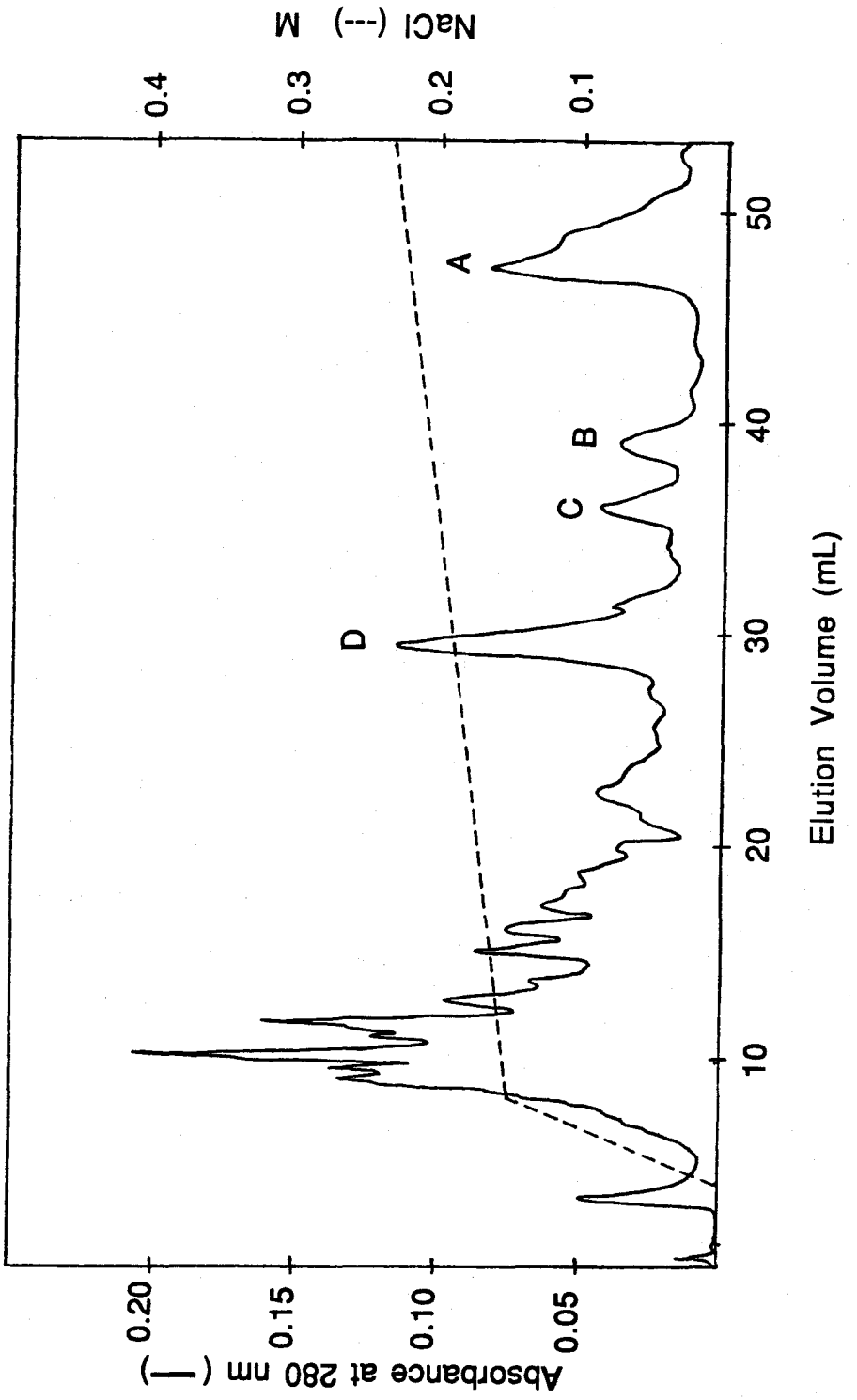
Absorbance at 280 nm (—)
0.20
0.15
0.10
0.05
NaCl (---) M
0.4
0.3
0.2
0.1
A
B
C
D
10
20
30
40
50
Elution Volume (mL)

histidines also reflects solvent exposure, with His-80 > His-15. With three surface histidines, there are four possible combinations of multiply histidine-modified products. However, many early eluting products are made (Figure 12), indicating nonspecific binding to the negatively charged protein surface. These competing multiply modified side products were minimized at high ionic strength (325 mM HEPES) and could be recycled to native protein by reduction. However, because of this competition, reaction times were necessarily limited to prevent singly modified products from reacting further. At the optimum reaction time of 2 h, the size of band A (Figure 12) indicates a considerable amount of unreacted native protein, but longer reactions did not increase the yields of singly modified products. Typical isolated yields of FPLC bands B, C, and D were 1.5%, 3%, and 12%. Confirmation that band A was unmodified native protein and that bands B, C, and D were singly modified a_5Ru-cyt b_5 was provided by the results of atomic absorption and UV-vis measurements (Table 1).

Tryptic mapping was used to make preliminary assignments of FPLC bands to ruthenium-modified isomers.[28] Native WT-b_5 was cleaved by trypsin into nine peptides (T1-T9; Figure 13) and separated by HPLC to make a tryptic map (Figure 14). When FPLC bands A-D were treated similarly, the ruthenium-modified peptides precipitated. As a result, the HPLC elution profiles (monitored at the peptide bond absorbance maximum, 210 nm) showed comparatively smaller peak integrations for ruthenated peptides. This method was the basis for the modification site assignments: A, unreacted native; B, His-80-modified; D, His-26-modified. Unfortunately, the precipitation of ruthenated peptides introduced uncertainty in quantifying the results and precluded the use of parallel HPLC runs monitored for ruthenium absorbance at 300 nm. In addition, the small size (and thus low ε_{210}) of the His-15-containing peptide T3 and its co-elution with peptide T1 prevented assignment of His-15-modified samples (thought to be peak C).

Proton NMR gave more conclusive results; hence, it was the preferred method for identifying ruthenated isomers. Figure 15 shows the aromatic regions of ^{1}H NMR

Table 1. Ru/Fe ratios determined by atomic absorption and by UV-vis spectroscopy for peaks from FPLC separation of ruthenium-modification reaction mixtures a) of WT-b_5, peaks A - D, Figure 12; and b) of TR26-b_5, peaks A and B, Figure 25. Samples were 20 μM protein in 20 mM TEA, pH 7.3.

Sample	Ru/Fe Expected	Ru/Fe Found (A. A.)[a]	Ru/Fe Found (UV-vis)[b]
a) Pure WT-b5	0.0	< 0.1	0
A	0.0	< 0.1	n.a.
B	1.0	1.2	0
C	1.0	1.3	1.3[c]
D	1.0	1.2	1.1[c]
b) Pure TR26-b5	0.0	< 0.1	0
A	0.0	< 0.1	0.8[d]
B	1.0	1.1	1.0[c]

[a] Performed by Analytical Services (E. L. Norton) at Brookhaven National Laboratory. Estimated uncertainties: $[Fe^{3+}] = \pm 10\%$, $[Ru^{3+}] = \pm 20\%$ (giving Ru/Fe = ± 0.2).
[b] See Experimental Section for method of calculation.
[c] $R_{412/280}$ = 5.2 - 5.4, which indicates some heme (Fe^{3+}) loss during preparation.
[d] $R_{412/280}$ = 4.3, which indicates substantial heme (Fe^{3+}) loss during preparation.

Figure 13. The peptides resulting from digesting denatured apo-WT-b_5 with trypsin. Residues are numbered according to the nonproteolytically cleaved protein; subtract four to obtain numbers by the crystallographic convention.

T1(7-9)	Ala - Val - Lys
T2(10-18)	Tyr - Tyr - Thr - Leu - Glu - Gln - Ile - Glu - Lys
T3(19-23)	His - Asn - Asn - Ser - Lys
T4(24-32)	Ser - Thr - Trp - Leu - Ile - Leu - His - Tyr - Lys
T5(33-38)	Val - Tyr - Asp - Leu - Thr - Lys
T6(39-51)	Phe - Leu - Glu - Glu - His - Pro - Gly - Gly - Glu
	Glu - Val - Leu - Arg
T7(52-72)	Glu - Gln - Ala - Gly - Gly - Asp - Ala - Thr - Glu
	Asp - Phe - Glu - Asp - Val - Gly - His - Ser - Thr
	Asp - Ala - Arg
T8(73-76)	Glu - Leu - Ser - Lys
T9(77-88)	Thr - Phe - Ile - Ile - Gly - Glu - Leu - His - Pro
	Asp - Asp - Arg

4 ALA	2 GLN	8 LEU	4 SER
3 ARG	11 GLU	6 LYS	6 THR
2 ASN	6 GLY	0 MET	1 TRP
7 ASP	5 HIS	3 PHE	4 TYR
0 CYS	4 ILE	2 PRO	4 VAL

Figure 14. Tryptic map for a) native, and b) modified WT-b_5. Conditions: 0.05% trifluoroacetic acid, 0 - 60% acetonitrile in 135 min, 60 - 75% acetonitrile from 135 - 150 min, 30 °C. The eluate was monitored at 210 nm, and peaks were quantified by integration.[28]

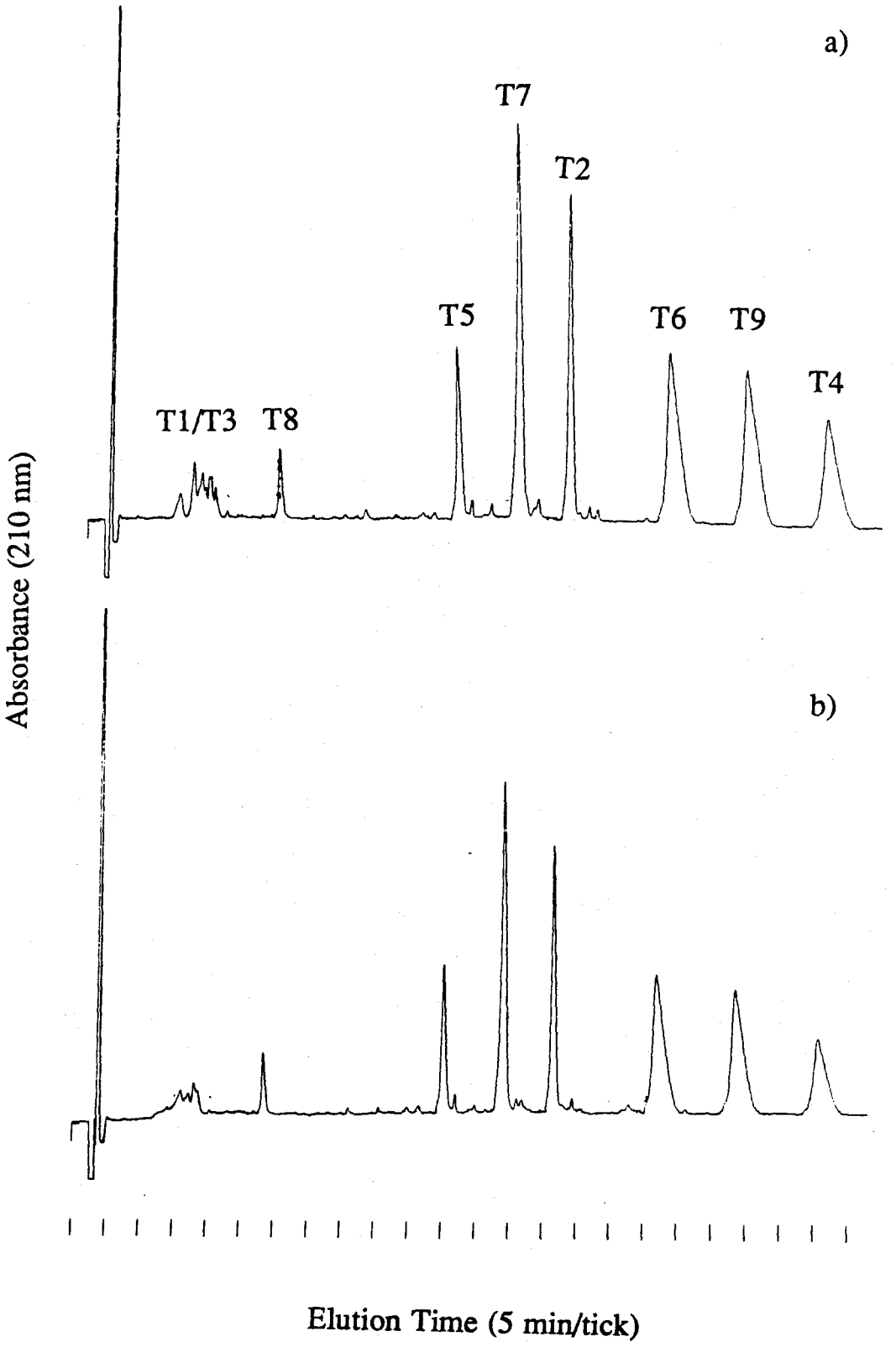
a)
T7
T2
T5
T6
T9
T4
T1/T3
T8
b)
Absorbance (210 nm)
Elution Time (5 min/tick)

Figure 15. The aromatic region of the ^1H NMR spectra (Bruker AM500, 50 mM D_2O NaPi, pH 7.1) of a) FPLC peak D (Figure 12), assigned as Ru(H26)WT-b_5, and b) unmodified WT-b_5. The His-26 C_2H resonance is absent (*) in the modified sample.

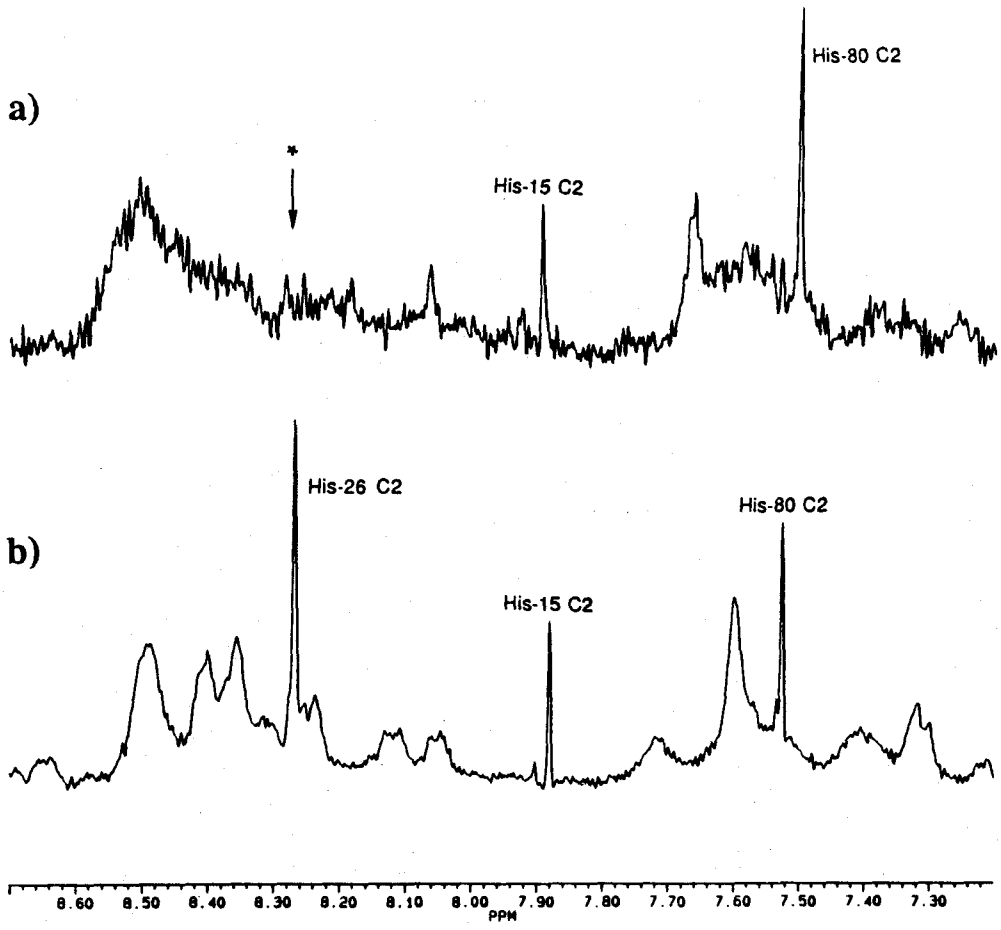
a)
His-80 C2
His-15 C2
b)
His-26 C2
His-80 C2
His-15 C2
8.60
8.50
8.40
8.30
8.20
8.10
8.00
7.90
7.80
7.70
7.60
7.50
7.40
7.30
PPM

spectra for WT-b_5 and for FPLC band D from Figure 12. The three sharp histidine imidazole C_2H (Figure 16) resonances (8.23, 7.84, 7.46 ppm; pH 7.1, 24 °C) in the spectrum of WT-b_5 correlate well with literature assignments for surface histidines 26, 15, and 80 (8.32, 7.89, 7.52 ppm; pH 6.9, 24 °C)[14] Notably, the His-26 resonance is absent for the modified sample because of paramagnetic shifting and broadening by the bound Ru^{3+}. Thus, the spectra clearly identify band D as the isomer singly modified at His-26, Ru(H26)WT-b_5.

Another observation to be made from the ^1H NMR spectra is that aside from changing the modified histidine resonance, spectra for native and modified samples are quite similar. This supports the assumption that the pendant ruthenium is structurally nonperturbative, which is important for the interpretation of electron-transfer rates as described in following chapters. Additional support can be obtained by examining the UV-visible spectra of the two samples (Figure 17), which are nearly identical; the spectrum of the modified sample has a slight increase in absorbance at 300 nm because of a_5Ru-His.

In order to estimate ET driving forces accurately, the donor and acceptor reduction potentials must be known. A thorough spectroelectrochemical study of WT-b_5 reported $E°(Fe^{3+/2+}) = 5.1$ mV vs. NHE (μ = 100 mM NaPi, pH 7.0).[19] In the present work, differential-pulse voltammetry (DPV) gave a value of $E°(Fe^{3+/2+}) = 25(5)$ mV vs. NHE for WT-b_5 in μ = 100 mM NaPi, pH 7.0 with 10 mM 4,4'-bipyridine added to enhance heterogeneous electron transfer to the heme (Figure 18a). A DPV measurement of WT-b_5 in μ = 500 mM NaPi, pH 7.0 was also attempted to check the potential under flash-photolysis conditions (Chapter III), but the poor solubility of 4,4'-bipyridine at this high ionic strength limited response currents. However, Reid et al. reported a shift of only 10 mV with an increase in ionic strength to μ = 500 mM NaPi.[19]

The primary goal of the DPV experiments was to characterize the modified protein, Ru(H26)WT-b_5. As expected, the heme potential was not significantly different

Figure 16. A representation of the histidine side chain modified with a_5Ru. The imidazole 2- and 4- carbons, important for NMR assignments in the present work, are indicated.

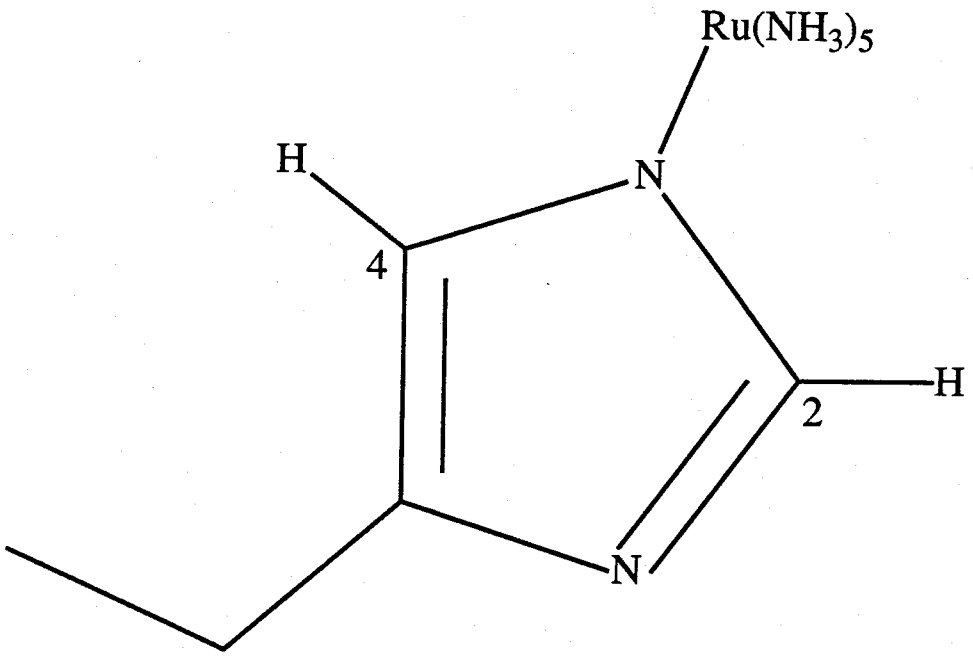
Ru(NH3)5
H
N
4
H
2
N

Figure 17. UV-visible spectra of oxidized WT-b_5 (A) and Ru(H26)WT-b_5 (B). Protein concentrations are 20 μM in 20 mM TEA, pH 7.3. Spectrum A: $R_{412/280}$ = 5.81, $R_{412/305}$ = 12.75. Spectrum B: $R_{412/280}$ = 5.30, $R_{412/305}$ = 10.38.

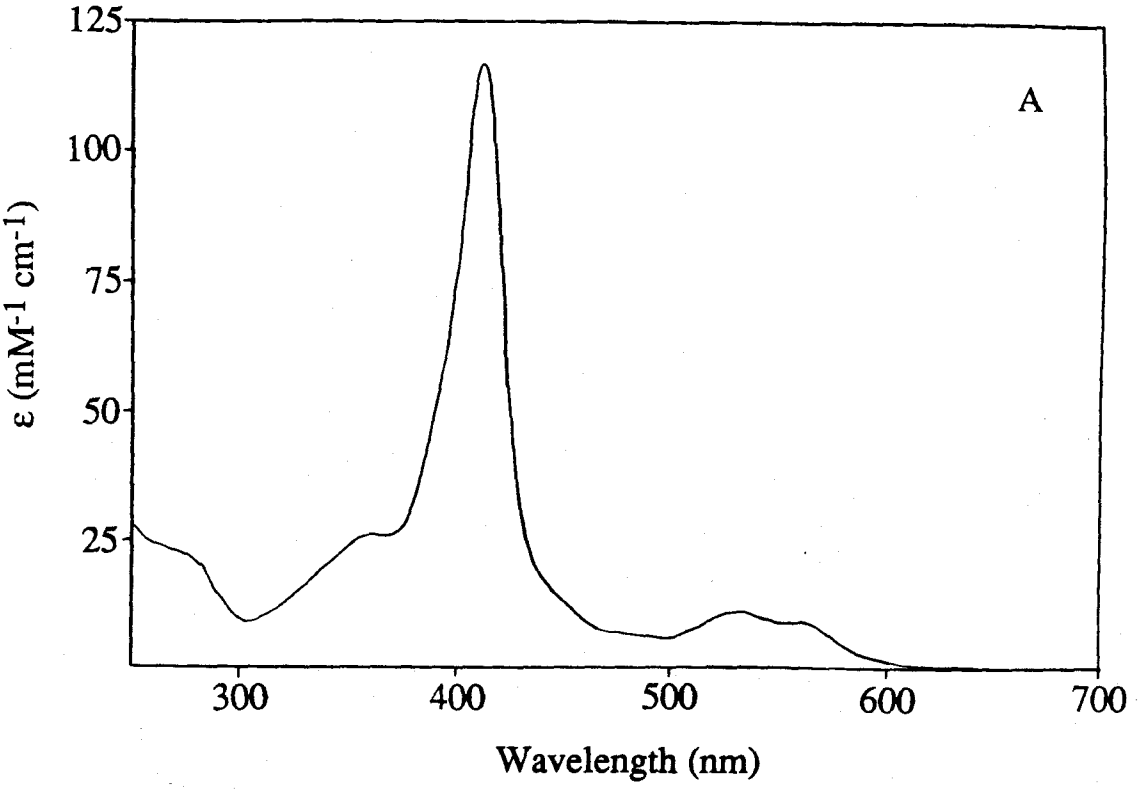
125
100
75
50
25
ε (mM-1 cm-1)
A
300
400
500
600
700
Wavelength (nm)

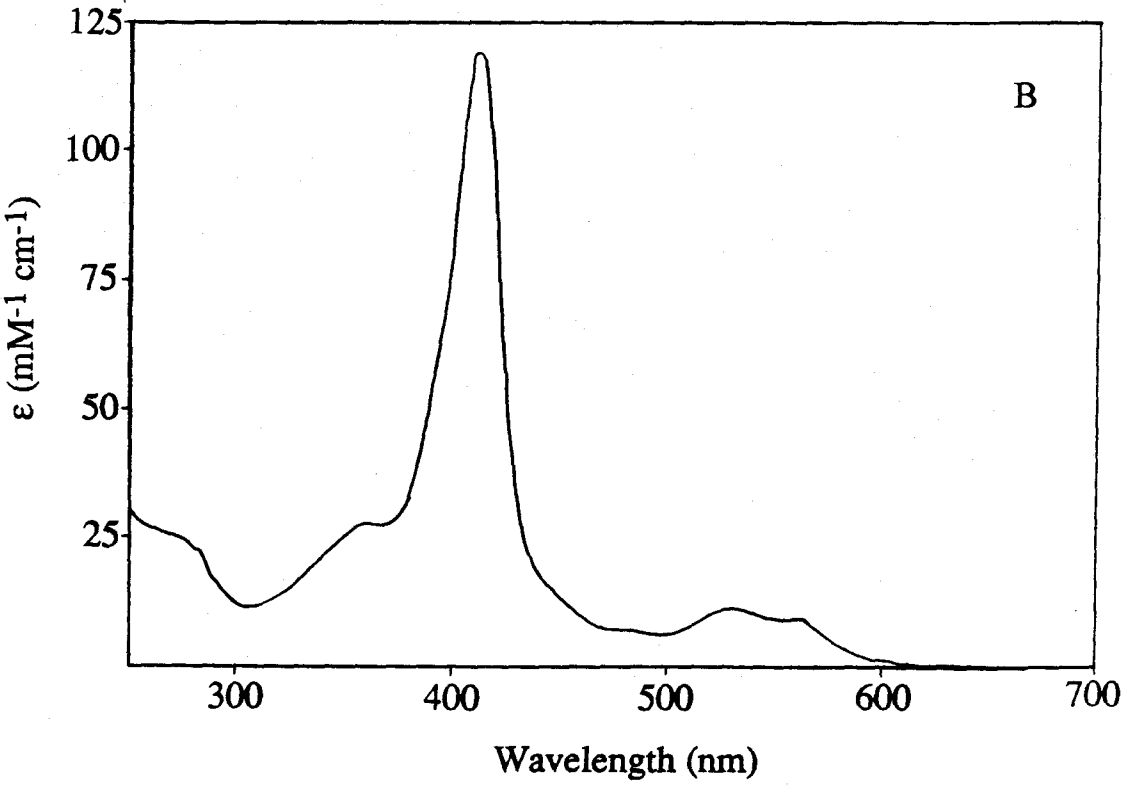
125
100
75
50
25
ε (mM-1 cm-1)
B
300
400
500
600
700
Wavelength (nm)

Figure 18. Differential pulse voltammograms of a) WT-b_5 (E° = 25(5) mV vs. NHE), and b) Ru(H26)WT-b_5 (E° = 40(10) mV vs. NHE) in μ = 100 mM NaPi, pH 7.0, plus 10 mM 4,4'-bipyridine (25 °C). Refer to the Experimental Section for more details.

a)

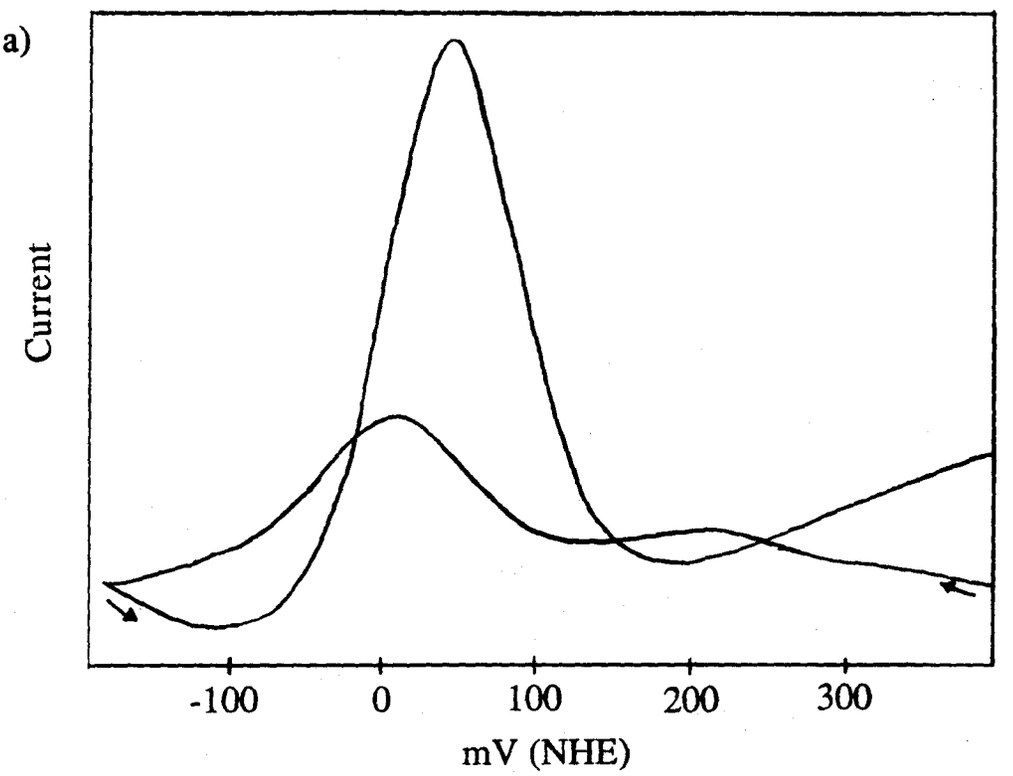
Current
-100
0
100
200
300
mV (NHE)

b)

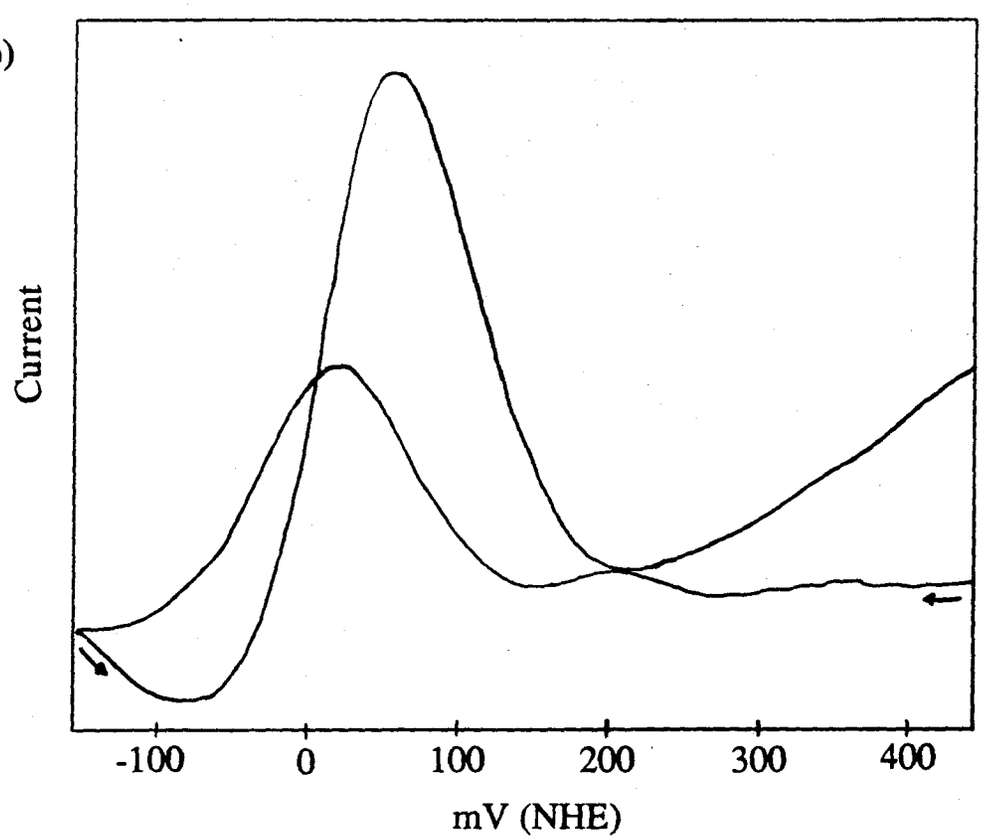
Current
-100
0
100
200
300
400
mV (NHE)

in Ru(H26)WT-b_5 ($E°(Fe^{3+/2+})$ = 40(10) mV vs. NHE; Figure 18b). Unfortunately, the $Ru^{3+/2+}$ couple for this protein was not observed by DPV. To see if the $Ru^{3+/2+}$ peak was unresolved (buried under the heme reduction), the peak width was examined. In the DPV experiment, an ideal peak width at half-maximum ($W_{1/2}$) for a one-electron process is 90 mV, while that for two electrons is 45 mV (real peaks are wider).[30] In measurements performed using both WT-b_5 and Ru(H26)WT-b_5, however, $W_{1/2}$ was equal to 110 mV, which suggests that the $Ru^{3+/2+}$ couple was not buried under the $Fe^{3+/2+}$ peak. This argument is supported by DPV experiments using freshly ruthenated samples without the 4,4'-bipyridine mediator. Even with low levels of heme reduction no ruthenium reduction was evident. Presumably, the modified protein sticks to the electrode in a fashion facilitating ET to the heme but not to the attached a_5Ru. For the purposes of interpreting electron-transfer experiments, it will be assumed that $E°(Ru^{3+/2+})$ = 80 mV, as in ruthenated cytochrome *c* and myoglobin.[8,22,31]

Other Ruthenium-Modified WT-b_5 Peaks

Because of the limited yields of peaks B and C (Figure 12), they were not extensively characterized. Studies of site-directed mutants aimed at increasing yields of His-15- and His-80-modified products will be discussed below.

Ruthenium-Modified LTM-b_5 and LM-b_5

The histidines of the lipase fragment mutant LTM-b_5 were much less reactive than were those of WT-b_5, possibly because of subtle changes in the structure (Figures 8, 9) or interference from the extra nine C-terminal residues (which are in close spatial proximity to His-26). Ruthenation reaction times were limited to only 20 minutes because of the rapid appearance of large amounts of multiply modified products with a considerable amount of unreacted native protein remaining (Figure 19). Typical yields for bands 1-4 were less than one percent.

Figure 19. Elution profile by FPLC (Mono Q 10/10; 20 mM TEA, pH 7.3; NaCl gradient generated using the gradient program in Figure 10) of the reaction mixture from a_5Ru-modification of LTM-b_5 quenched after 20 min. Peak A is unreacted native LTM-b_5, and peak B is expected to be Ru(H26)LTM-b_5.

Absorbance at 280 nm (——)
0.12
0.08
0.04
NaCl (- - -) M
0.6
0.4
0.2
A
B
50
100
150
200
250
Elution Volume (mL)

In order to circumvent this problem, a mutant with Asn in place of His-15 and His-80 was made by site-directed mutagenesis (LM-b_5).[11] With only one surface histidine, a longer reaction time (12 h) to increase the yield of band B (up to 8 %) was possible with less multiple modification (Figure 20). The early eluting multiply modified peaks present even in the chromatogram of this one-surface-histidine mutant confirms the hypothesis that nonspecific binding of positively charged ruthenium complexes to the highly negative cyt b_5 occurs.

Ambiguity in finding the one remaining C_2H resonance in the ^1H NMR spectrum for LM-b_5 (Figure 21) was resolved by titration of the protein solution with NaOD. The histidine peak displayed the characteristic upfield shift with increased pH (8.15 ppm, pH 7.2; 7.9 ppm, pH 7.7). Its absence in the spectrum of band B (Ru(H26)LM-b_5) confirmed that His-26 was the site of modification.

Ruthenium-Modified DP-b_5

Deuteroporphyrin-substituted cyt b_5 was prepared in good yield (65% from the apoprotein, 52% from WT-b_5) by literature methods.[13,27] The reported 403 nm maximum (ε_{403} = 122 mM^{-1} cm^{-1})[23] in the UV-vis spectrum was successfully reproduced (Figure 22) and was used to determine concentrations. A ^1H NMR spectrum of DP-b_5 is shown in Figure 23. The C_2H resonances for His-26, 15, and 80 at 8.27, 7.90, and 7.52 ppm (pH 7.1, uncorrected) closely agree with those for WT-b_5 (Figure 15), indicating that in DP-b_5 there are no significant changes from the parent protein.

Reactivity of DP-b_5 towards ruthenium modification and separation of the products by FPLC chromatography (Figure 24) were similar to the behavior of WT-b_5, as expected. The isolated yield of band B was 3.3%, and its assignment as Ru(H26)DP-b_5 was made by comparison to the FPLC elution profile of ruthenated WT-b_5 (Figure 12).

Figure 20. Elution profile by FPLC (Mono Q 10/10; 20 mM TEA, pH 7.3; NaCl gradient generated using the gradient program in Figure 10) of the reaction mixture from a_5Ru-modification of LM-b_5 quenched after 12 h. Peak A is unreacted native LM-b_5, and peak B is Ru(H26)LM-b_5.

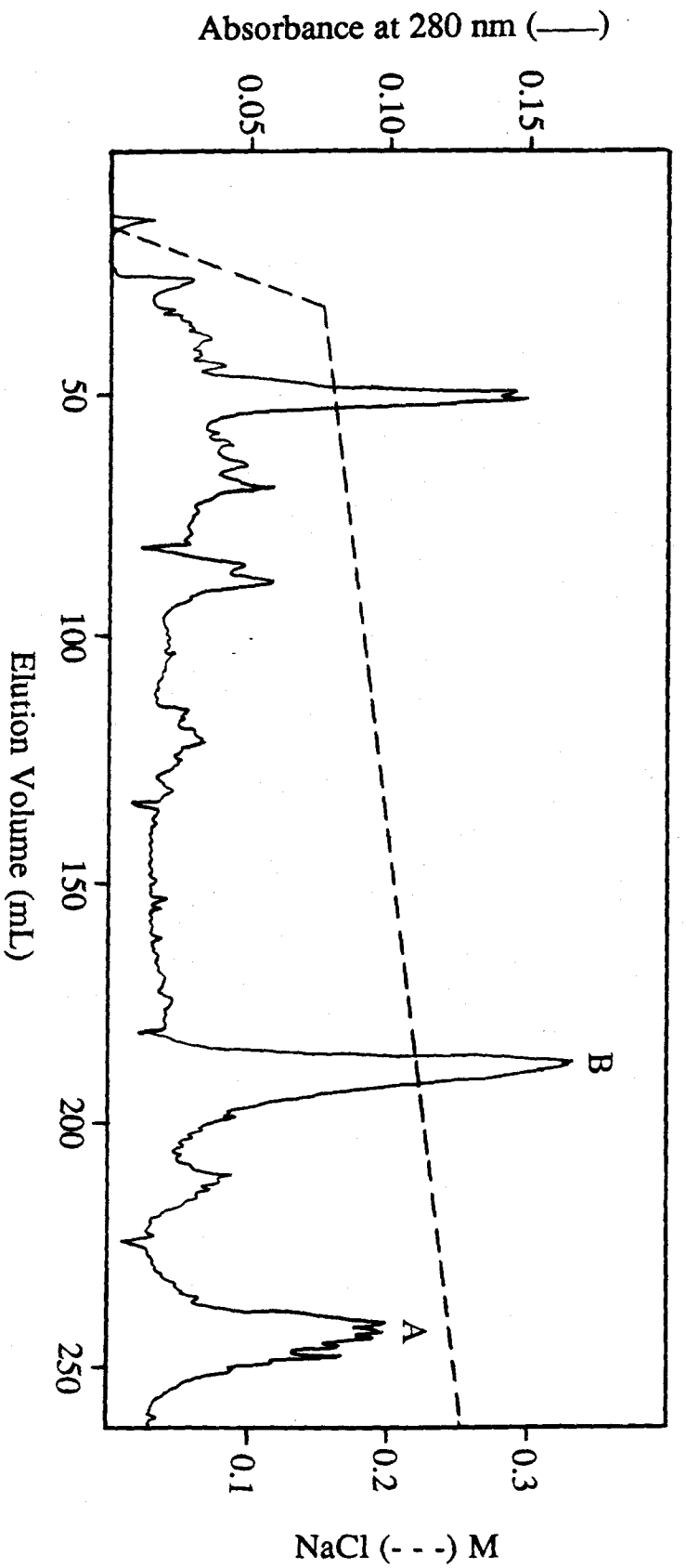
Absorbance at 280 nm (——)
0.05
0.10
0.15
50
100
150
200
250
Elution Volume (mL)
B
A
0.1
0.2
0.3
NaCl (- - -) M

Figure 21. The aromatic region of the ^1H NMR spectra (50 mM D_2O NaPi) of a) LM-b_5, pH 7.2, b) LM-b_5, pH 7.7, and c) FPLC peak B (Figure 20), pH 7.2, assigned as Ru(H26)LM-b_5. The His-26 C_2H resonance is absent (*) in the modified sample.

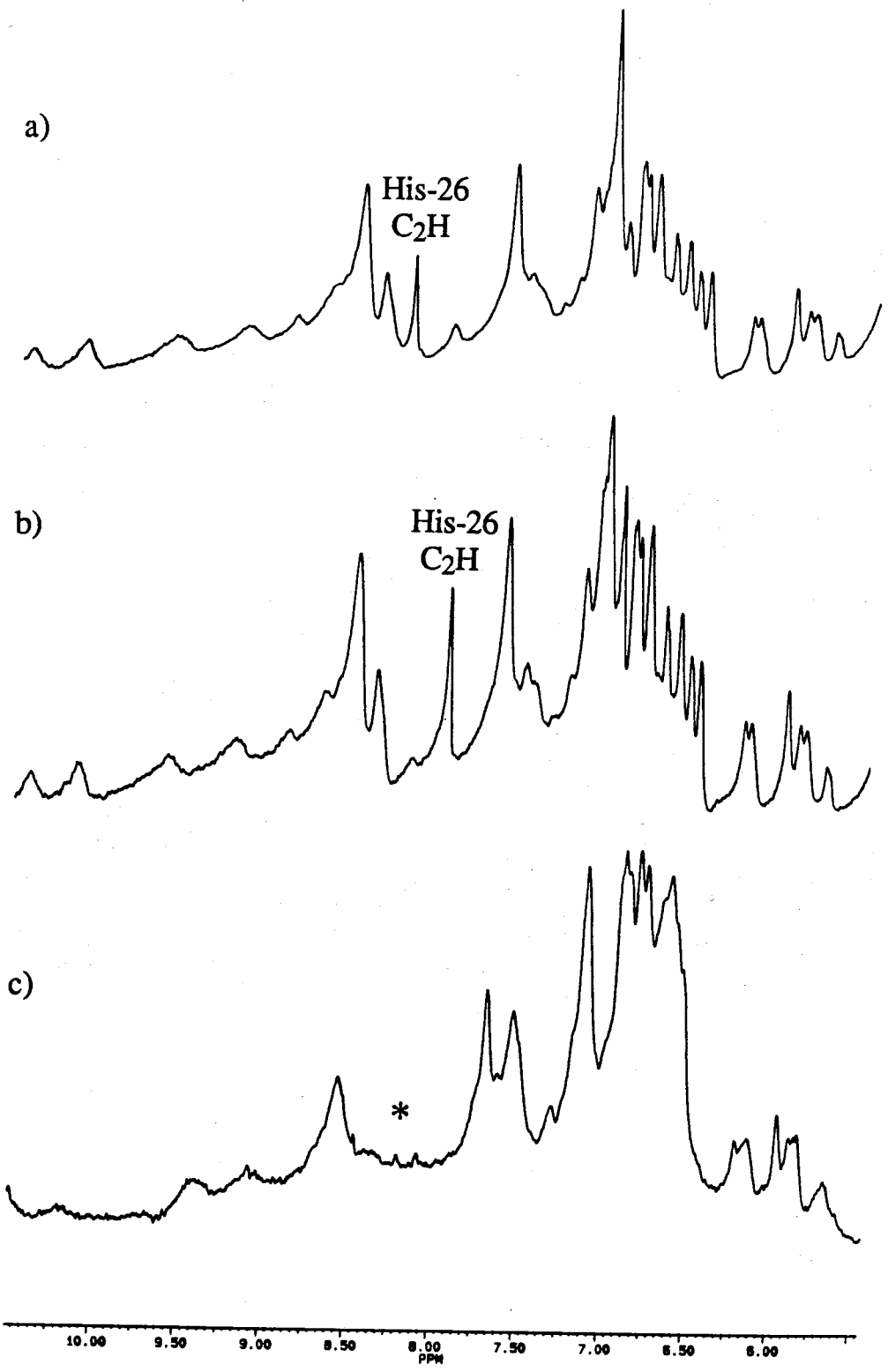
a)
His-26
C_2H
b)
His-26
C_2H
c)
*
10.00
9.50
9.00
8.50
8.00
PPM
7.50
7.00
6.50
6.00

Figure 22. UV-vis spectrum of DP-b_5 in 20 mM TEA, pH 7.3. The Soret band maximum is at 403 nm.

140
70
250
350
450
550
650
Wavelength (nm)
ε (mM-1 cm-1)

Figure 23. The aromatic region of the ^1H NMR spectrum of DP-b_5, pH 7.2 (50 mM D_2O NaPi). The C_2H peaks for His-26, His-15, and His-80 are at 8.27, 7.90, and 7.50 ppm.

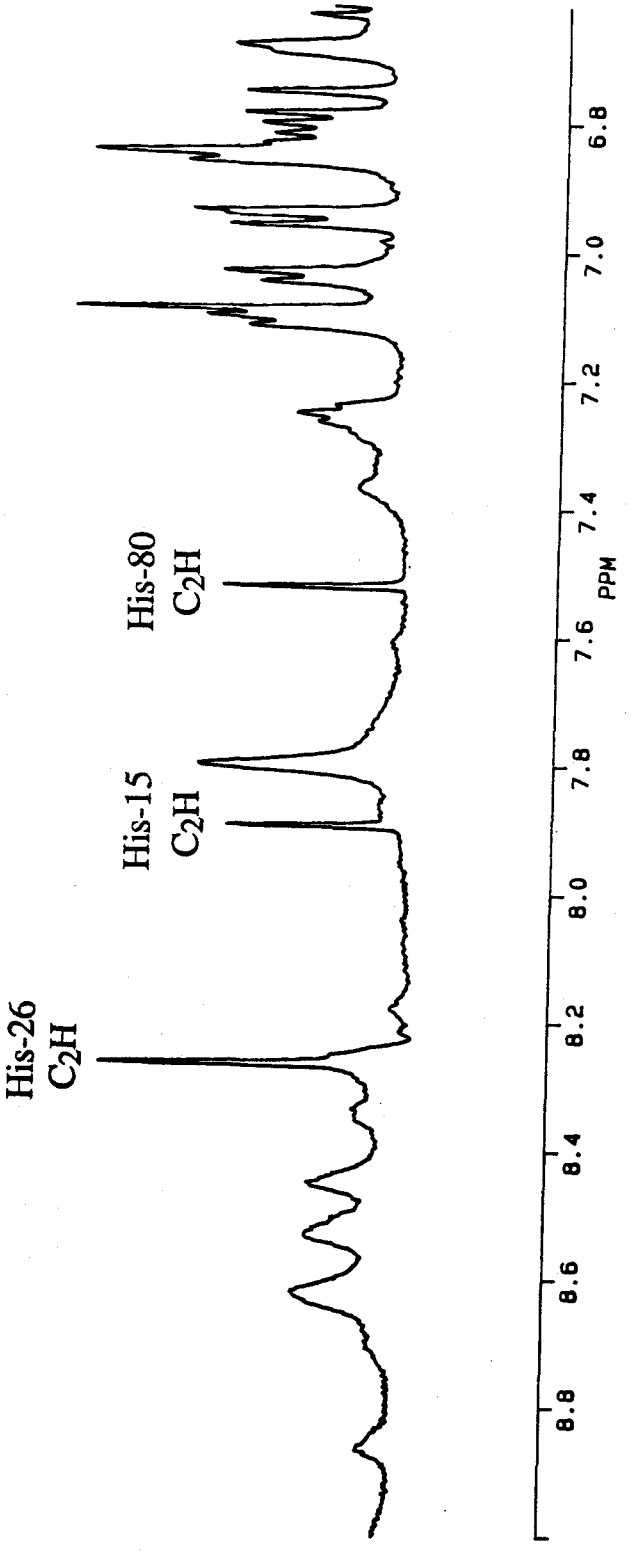
His-26
C_2H
His-15
C_2H
His-80
C_2H
8.8
8.6
8.4
8.2
8.0
7.8
7.6
PPM
7.4
7.2
7.0
6.8

Figure 24. Elution profile by FPLC (Mono Q 10/10; 20 mM TEA, pH 7.3; NaCl gradient generated using the gradient program in Figure 10) of the reaction mixture from a_5Ru-modification of DP-b_5 quenched after 2 h. Peak A is unreacted native DP-b_5, and peak B is Ru(H26)DP-b_5.

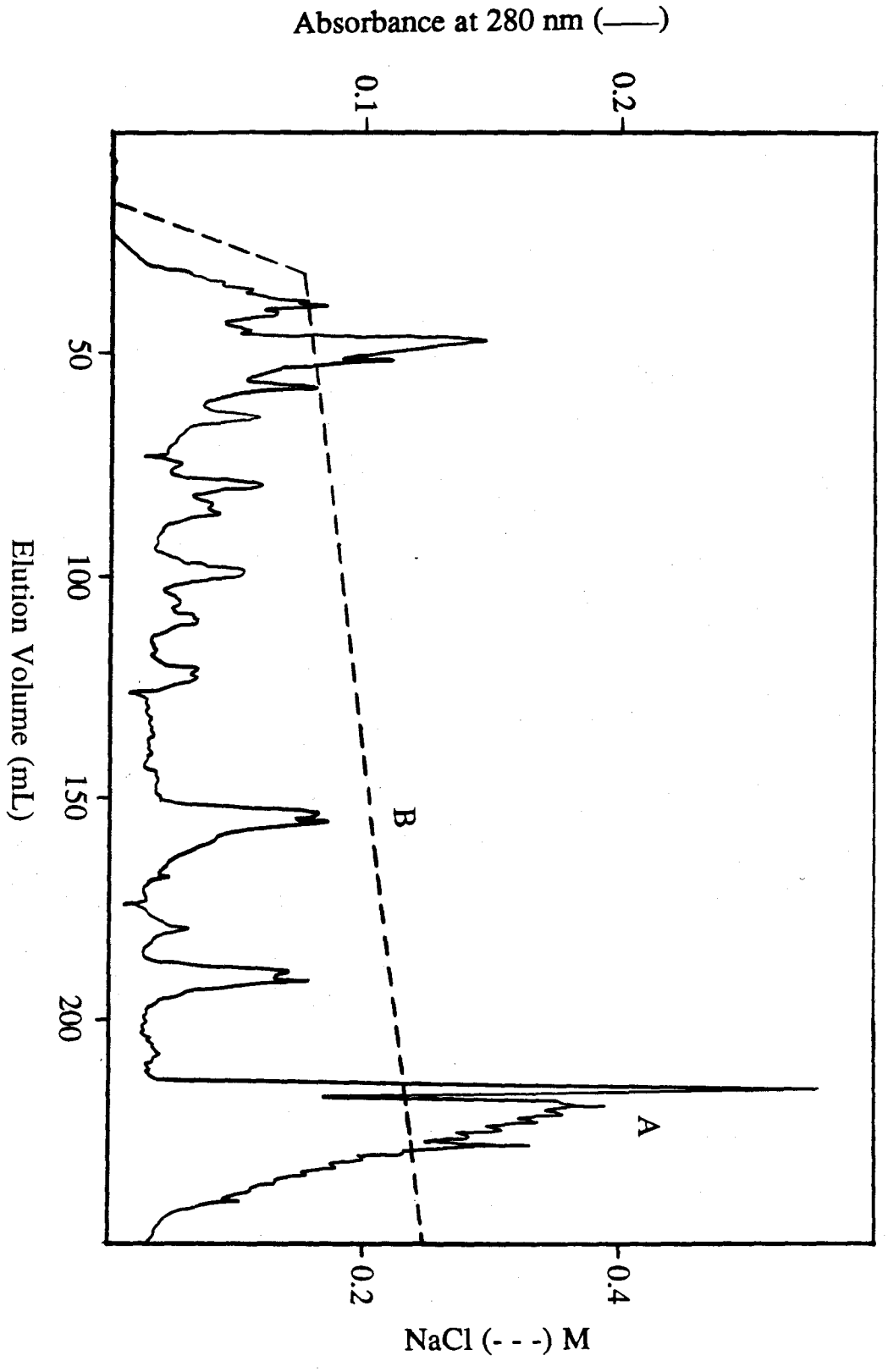
Absorbance at 280 nm (——)
0.1
0.2
50
100
150
200
Elution Volume (mL)
B
A
0.2
0.4
NaCl (- - -) M

Ruthenium-Modified TR26-*b*$_5$

With the most reactive His-26 replaced with Arg, this mutant was designed to increase the yields of His-15- and His-80-modified derivatives. As a result, using a higher molar excess (75-fold) of $[a_5Ru(OH_2)](PF_6)_2$ in the ruthenation reaction was possible without prohibitive multiple modification. As with WT-*b*$_5$, the optimum reaction time was 2 h; FPLC elution profiles of aliquots from longer times showed a decrease in the amount of unreacted native protein, but the same or decreased amounts of singly modified products. Figure 25 shows that there were only two major late-eluting bands, A and B. Table 1 gives the results of atomic absorption and UV-vis peak ratio analysis, which indicate that peak A is unreacted native TR26-*b*$_5$ and that peak B is singly modified.

A ^{1}H NMR spectrum of TR26-*b*$_5$ (Figure 26a) confirmed the literature assignment of the His-26 C_2H resonance in WT-*b*$_5$ spectra,[14] since it was indeed absent for this Arg-26 mutant. On the other hand, the resonances for His-15 and His-80 were unperturbed by the mutation. Disappearance of the latter peak in a spectrum of band B (Figure 26b) suggested that His-80 was modified, but an additional peak at 8.45 ppm is unidentified. The 8.45 ppm peak's sharpness suggests a histidine resonance, but the only other histidines in cyt *b*$_5$ are His-63 and His-39, the heme axial ligands. To determine if one of these residues had dissociated from iron and the subsequent protonation gave rise to the new peak, the heme was extracted from TR26-*b*$_5$ to make the apoprotein (as in the preparation of DP-*b*$_5$, Experimental Section). Initially, the ^{1}H NMR spectrum of apo-TR26-*b*$_5$ at pH 7.1 lacked an 8.45 ppm peak, but upon titration with NaOD it appeared (Figure 26c). The peak's onset at higher pH (and because it remained when the sample was titrated back to pH 7.1 with DCl) suggests that protonation was not limited by pK_a but by a pH-dependent conformational change opening the heme pocket. Recently, an extensive NMR study of apo-cytochrome *b*$_5$ by Moore and Lecomte [32] assigned the resonances for the two axial histidines, lending support to this hypothesis: His-63, δ =

Figure 25. Elution profile by FPLC (Mono Q 10/10; 20 mM TEA, pH 7.3; NaCl gradient generated using the gradient program in Figure 10) of the reaction mixture from a_5Ru-modification of TR26-b_5 quenched after 2 h. Peak A is unreacted native TR26-b_5, and peak B is Ru(H80)TR26-b_5.

Absorbance at 280 nm (——)
0.06
0.04
NaCl (- - -) M
0.4
0.2
A
B
50
100
150
200
Elution Volume (mL)

Figure 26. The aromatic region of the ^1H NMR spectra (50 mM D_2O NaPi) of a) TR26-b_5, pH 7.1 (note the absence (*) of the His-26 C_2H resonance in this Arg-26 mutant), and b) FPLC peak B (Figure 25), pH 7.1, assigned as Ru(H80)TR26-b_5 (the His-80 C_2H resonance is absent (*)). Spectrum c) is of apo-TR26-b_5 titrated to pH 7.4 with NaOD. The peak at 8.45 ppm is assigned as a C_2H resonance by either His-63 or His-39.

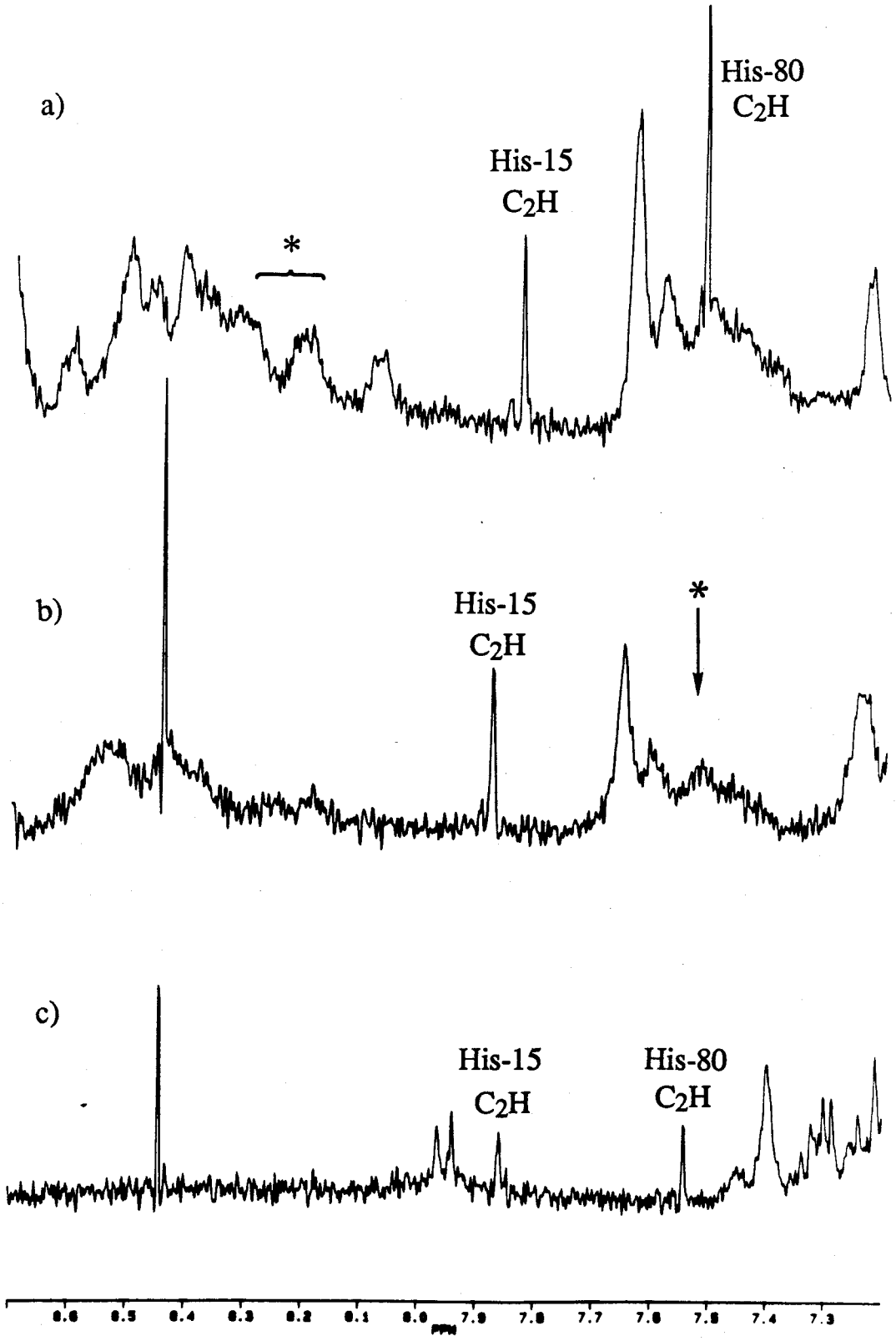
a)
His-80
C_2H
His-15
C_2H
*
b)
His-15
C_2H
*
c)
His-15
C_2H
His-80
C_2H
8.6
8.5
8.4
8.3
8.2
8.1
8.0
7.9
7.8
7.7
7.6
7.5
7.4
7.3
ppm

8.5 ppm (pH 6.2, $pK_a \approx 7.5$), and His-39, $\delta = 8.59$ and 8.37 ppm (pH 6.2 and 7.0; $pK_a \approx 7+$).

From the NMR results one can conclude that the TR26-b_5 mutant is less stable than WT-b_5 and that ruthenation results in some heme loss. Alternatively, an equilibrium of heme ligand dissociation may be operative; variable-temperature studies of WT-b_5 have indicated that in the range 55 - 65 °C an axial ligand reversibly dissociates from the iron to produce a five-coordinate, high-spin species.[33] Dissociation may occur at lower temperatures in TR26-b_5, but reasons for this relative instability are not obvious. The replaced histidine side chain lacks hydrogen bonds, is very solvent-accessible, and is the most reactive towards modification of the three native surface histidines, all observations that suggest a minimal structural role. Perhaps the new Arg side chain forms some destabilizing hydrogen bonds.

The TR26-b5 mutant was designed to increase the yields of a_5Ru modification at residues His-80 and His-15 by removing competition from the more reactive His-26, yet His-15 still did not appear to react. In DEP binding studies, on the other hand, His-15 was more reactive than His-80.[29] One explanation for this reversal in reactivity may be that the ruthenium complex is more sterically demanding than is DEP; of the three surface histidines, His-15 has the lowest solvent accessibility (about half that of His-26).[29] In addition, its imidazole ring is hydrogen-bonded to the backbone carbonyl of residue 11,[6d] making it less likely to react.

Ruthenium-Modified TNN-b_5

The purpose of this Asn-15, Asn-80, tryptic-sequence mutant was to increase the yield of His-26-modified protein. The long reaction times made possible by having only one surface histidine did result in high yields of Ru(H26)TNN-b_5 (Figure 27). However, this mutant had low yields of expression by *E. coli*; thus not enough native protein was available for detailed study.

Figure 27. Elution profile by FPLC (Mono Q 5/5; 20 mM TEA, pH 7.3; NaCl gradient generated using the gradient program in Figure 10) of the reaction mixture from a_5Ru-modification of TNN-b_5 quenched after 12 h. Peak A is unreacted native TNN-b_5, and peak B is expected to be Ru(H26)TNN-b_5.

Absorbance at 280 nm (——)
0.04
0.02
NaCl (- - -) M
0.4
0.2
A
B
15
30
45
60
Elution Volume (mL)

SUMMARY

WT-b_5 was successfully modified with a_5Ru^{3+}, and the products were separated by FPLC anion exchange chromatography. Performing the reaction at high buffer concentration was found to minimize multiply modified side products. The order of reactivity of the three surface histidines was His-15 < His-80 < His-26. The derivative singly modified at His-26, Ru(H26)WT-b_5 , was characterized by UV-vis spectroscopy, atomic absorption analysis, tryptic mapping, ^{1}H NMR spectroscopy, and differential pulse voltammetry.

The native iron protoporphyrin was extracted and replaced with iron deutero-porphyrin to make DP-b_5 . This protein was characterized by UV-vis and ^{1}H NMR spectroscopies, and appeared to have no significant structural changes (aside from the intended missing 2- and 4- vinyls) from WT-b_5 . The reaction of DP-b_5 towards a_5Ru^{2+} and the chromatographic behavior of the products were similar to WT-b_5 .

Several cyt b_5 mutants were also studied. The histidines of LTM-b_5 proved to be unreactive towards ruthenium modification, but modification of the related mutant LM-b_5 at His-26 and isolation of the singly modified product by FPLC chromatography were successful. Ru(H26)LM-b5 was characterized by UV-vis and ^{1}H NMR spectroscopies.

Ruthenation of a cyt b_5 mutant with the most reactive histidine (26) replaced with arginine produced a good yield of the His-80-modified product; His-15 was unreactive. The singly modified derivative, Ru(H80)TR26-b_5 , was characterized by atomic absorption and UV-vis and 1H NMR spectroscopies. This mutant was found to be less thermally stable than the wild-type protein, as indicated by the appearance of a new ^{1}H NMR resonance at 8.45 ppm, attributed to an axial histidine dissociated from the iron.

The one remaining surface histidine (His-26, Asn-15, Asn-80) in TNN-b_5 was found to be quite reactive towards ruthenation, but not enough native protein was available for extensive study.

REFERENCES

(1) Keyes, S. R.; Alfano, J. A.; Jansson, I.; Cinti, D. *J. Biol. Chem.* **1979**, *254*, 7778.

(2) Strittmatter, P.; Spatz, L.; Corcoran, D.; Rogers, M. J.; Setlow, B.; Redline, R. *Proc. Natl. Acad. Sci., USA* **1974**, *71*, 4565.

(3) Fukushima, H.; Grinstead, G. F.; Gaylor, J. L. *J. Biol. Chem.* **1981**, *256*, 4822.

(4) a) Jansson, I.; Schenkman, J. B. *Arch. Biochem. Biophys.* **1977**, *178*, 89. b) Peterson, J. A.; Prough, R. A. In *Cytochrome P-450. Structure, Mechanism, and Biochemistry*; Ortiz de Montellano, P. R., Ed.; Plenum Press: New York, 1986, p. 89.

(5) a) Sannes, L. G.; Hultquist, D. E. *Biochim. Biophys. Acta* **1978**, *544*, 547. b) Kuma, F. *J. Biol. Chem.* **1981**, *256*, 5518.

(6) a) Mathews, F.S.; Levine, M.; Argos, P. *J. Mol. Biol.* **1972**, *64*, 449-464. b) Mathews, F.S.; Argos, P.; Levine, M. *Cold Spring Harbor Symposium* **1972**, *36*, 387-395. c) Argos, P.; Mathews, F. S. *J. Biol. Chem.* **1975**, *250*, 747-751. d) Mathews, F. S.; Czerwinski, E. W.; Argos, P. In *The Porphyrins*; Dolphin, D., Ed.; Academic Press: New York, 1979; Vol. VII, pp. 107-147.

(7) Mathews, F. S. *Biochim. Biophys. Acta* **1980**, *622*, 375-379.

(8) Nocera, D. G.; Winkler, J. R.; Yocom, K. M.; Bordignon, E.; Gray, H. B. *J. Am. Chem. Soc.* **1984**, *106*, 5145-5150.

(9) a) Yocom, K. M.; Shelton, J. B.; Shelton, J. R.; Schroeder, W. A.; Worosila, G.; Isied, S. S.; Bordignon, E.; Gray, H. B. *Proc. Natl. Acad. Sci., USA* **1982**, *79*, 7052-7055. b) Yocom, K. M.; Winkler, J. R.; Nocera, D. G.; Bordignon, E.; Gray, H. B. *Chemica Scripta*, **1983**, *21*, 29-33.

(10) von Bodman, S. B.; Schuler, M. A.; Jollie, D. R.; Sligar, S. G. *Proc. Natl. Acad. Sci., USA* **1986**, *83*, 9443-9447.

(11) Funk, W. D.; Lo, T. P.; Mauk, M. R.; Brayer, G. D.; MacGillivray, R. T. A.; Mauk, A. G., *Biochemistry* **1990**, *29*, 5500-5508.

(12) Reid, L. S.; Lim, A. R.; Mauk, A. G. *J. Am. Chem. Soc.* **1986**, *108*, 8197-8201.

(13) Reid, L. S.; Mauk, M. R.; Mauk, A. G. *J. Am. Chem. Soc.* **1984**, *106*, 2182-2185.

(14) Reid, L. S.; Gray, H. B.; Dalvit, C.; Wright, P. E.; Saltman, P. *Biochemistry* **1987**, *26*, 7102-7107.

(15) a) Chapman, S. K.; Davies, D. M.; Vuik, C. P. J.; Sykes, A. G. *J. Am. Chem. Soc.* **1984**, *106*, 2692-2696.

(16) Reid, L. S.; Mauk, A. G. *J. Am. Chem. Soc.* **1982**, *104*, 841-845.

(17) Dixon, D. W.; Hong, X.; Woehler, S. E.; Mauk, A. G.; Shishta, B. P. *J. Am. Chem. Soc.* **1990**, *112*, 1082-1088.

(18) a) Mauk, M. R.; Mauk, A. G.; Weber, P. C.; Matthew, J. B. *Biochemistry* **1986**, *25*, 7085-7091. b) Rodgers, K. K.; Pochapsky, T. C.; Sligar, S. G. *Science* **1988**, *240*, 1657-1659. c) Hartshorn, R. T.; Mauk, A. G.; Mauk, M. R.; Moore, G. R. *FEBS Lett.* **1987**, *213*, 391-395. d) Wendoloski, J. J.; Mattew, J. B.; Weber, P. C.; Salemme, F. R. *Science* **1987**, *238*, 794-797. e) Tamburini, P. P.; Schenkman, J. B.; *Arch. Biochem. Biophys.* **1986**, *245*, 512-522.

(19) Reid, L. S.; Taniguchi, V. T.; Gray, H. B.; Mauk, A. G. *J. Am. Chem. Soc.* **1982**, *104*, 7516-7519.

(20) Raphael, A. L.; Gray, H. B. *Proteins* **1989**, *6*, 338-340.

(21) Taniguchi, V. T.; Sailasuta-Scott, N.; Anson, F. C.; Gray, H. B. *Pure Appl. Chem.* **1980**, *52*, 2275-2281.

(22) Axup, A. W.; Albin, M.; Mayo, S. L.; Crutchley, R. J.; Gray, H. B. *J. Am. Chem. Soc.* **1988**, *110*, 435-439.

(23) Ozols, J.; Strittmatter, P. *J. Biol. Chem.* **1964**, *239*, 1018-1023.

(24) Ozols, J.; Strittmatter, P. *J. Biol. Chem.* **1969**, *244*, 6617-6618.

(25) a) Go, M.; Miyazawa, S. *Int. J. Pept. Protein Res.* **1980**, *15*, 211-224. b) Alber, T.; Dao-pin, S.; Nye, J. A.; Muchmore, D. C.; Matthews, B. W. *Biochemistry* **1987**, *26*, 3754-3758. c) Baldwin, R. L.; Eisenberg, D. In *Protein Engineering*; Oxender, D. L. and Fox, C. F., Eds.; Alan R. Liss: New York, 1987, pp 127-148.

(26) Ford, P.; Rudd, De F. P.; Gaunder, R.; Taube, H. *J. Am. Chem. Soc.* **1968**, *90*, 1187-1194.

(27) Teale, F. W. J. *Biochim. Biophys. Acta* **1959**, *35*, 543.

(28) Mauk, M. R., unpublished results.

(29) Altman, J.; Lipka, J. J.; Kuntz, I.; Waskell, L. *Biochemistry* **1989**, *28*, 7516-7523.

(30) Bard, A. J.; Faulkner, L. R. *Electrochemical Methods: Fundamentals and Applications*; John Wiley & Sons: New York; 1980.

(31) Mayo, S. L.; Ellis, W. R.,Jr.; Crutchley, R. J.; Gray, H. B. *Science* **1986**, *233*, 948-952.

(32) a) Moore, C. D.; Lecomte, J. J. *Biophys. J.* **1990**, *57(2)*, 228. b) Private communication, C. D. Moore.

(33) a) Sugiyama, T.; Miura, R.; Yamano, T.; Shiga, K.; Watari, H. *Biochem. Biophys. Res. Comm.* **1980**, *97*, 22-27. b) Kitigawa, T.; Sugiyama, T.; Yamano, T. *Biochemistry* **1982**, *21*, 1680-1686.

CHAPTER III

INTRAMOLECULAR ELECTRON TRANSFER IN RUTHENIUM-MODIFIED CYTOCHROME b_5 DERIVATIVES

INTRODUCTION

The strategy for studying ET in cyt b_5 was patterned after those used for other metalloproteins. By modifying a histidine on the protein surface with a ruthenium complex, a second redox site is introduced. Intramolecular ET is then initiated by using a flash of light to produce the highly reactive triplet state of $[Ru(bpy)_3]^{2+}$.[1-3] In a fast bimolecular step, an excess of $[Ru(bpy)_3]^{2+*}$ either oxidizes or reduces a portion of the metal centers in the protein sample, depending on their initial oxidation states (Scheme I). A sacrificial oxidant or reductant is used as a scavenger to prevent regenerating $[Ru(bpy)_3]^{2+}$ by back ET. As long as the protein products are not made in equilibrium concentrations, ET can then be followed spectroscopically. The selection of a scavenging system depends on the expected (or preferred) dominant direction of ET. A reductive scavenging system (Scheme Ia) was developed to study ET from surface-bound Ru^{2+} to the heme Fe^{3+} in cytochrome *c* [1,2,4] and myoglobin,[5] whereas an oxidative system (Scheme Ib) has been used to study ET in the opposite direction.[3]

As discussed in Chapter II, cyt b_5 provides an interesting system for ET studies because of its unique physical characteristics. But its differences from previously studied proteins were also manifest in new practical challenges for kinetics investigations. Important properties that affect the kinetics properties of ruthenium-modified cyt b_5 include the large negative charge near the heme (effective charge = -14.2)[6] and the high solvent accessibility of the heme edge. The low heme reduction potential of cyt b_5 [$E°(Fe^{3+/2+})$= 5 mV] [7] results in a driving force favoring ET from the heme to the pendant a_5Ru^{3+} ($E°(Ru^{3+/2+})$ = 80 mV)[1,4], which has implications for the choice of quenching system. In addition, because cyt b_5 is not commercially available, limited quantities required careful selection of experiments.

Scheme I. Flash Photolysis Chemistry.

a) Protein Initially Oxidized

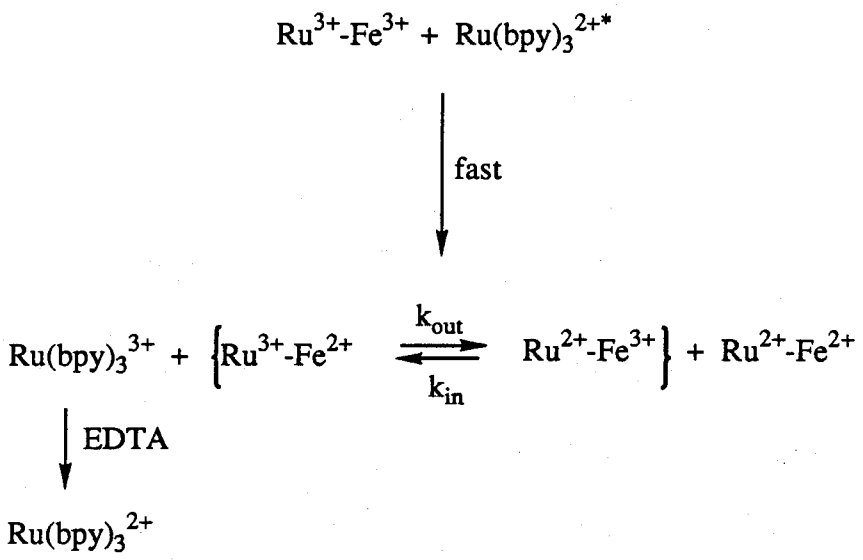

b) Protein Initially Reduced

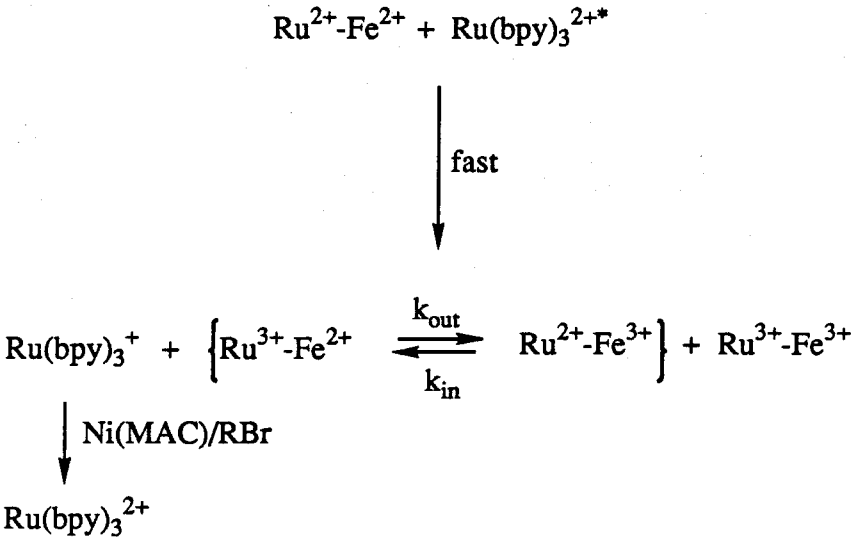

EXPERIMENTAL

Flash-Photolysis Sample Preparation

Initially Oxidized Protein

Flash photolysis was carried out using a 15-cm pathlength, water-jacketed (25 °C) cell containing approximately 11 mL of the following solution: 7.25 mM Na_2EDTA, 65 μM $[Ru(bpy)_3]Cl_2$ (bpy = 2,2'-bipyridine),[2] and 0.5 to 3 μM protein, in μ = 500 mM NaPi, pH 7.0. The component solutions were degassed separately and mixed in a glove box. To prevent premature $[Ru(bpy)_3]^{2+}$ excitation, the loaded cell was kept dark prior to flashing, and the probe light was filtered (cutoff < 523 nm). Electron-transfer reactions were followed by monitoring the protein oxidation state by visible absorption at 555 nm (WT-b_5, LM-b_5, TR26-b_5) or at 545 nm (DP-b_5), and only data from the first flash were used.

Initially Reduced Protein

Flash solutions contained 5 mM Ni (II) [Hexamethyl-tetraazacyclodecane] $2ClO_4$, Ni(MAC);[3,8] 10 mM 3-bromopropionic acid, RBr (purified by vacuum sublimation); and 65 μM $[Ru(bpy)_3]Cl_2$ in μ = 100 mM NaPi, pH 7.0, deoxygenated by Ar purging. Cyt b_5 was reduced by stirring solutions with suspended Pt black under a blanket of H_2 for >30 minutes and was filtered (Millipore 0.2 μm) before use. Protein concentrations flashed were 2.6 μM (to give A_{555} = 1 for ε_{555} = 25,600; 15-cm path).

Flash-Photolysis Instrumentation

Kinetics measurements were made using a microsecond flash-photolysis system described previously [9] with some modifications; a schematic diagram is provided in Figure 28. The Biomation was replaced with an AT-compatible computer equipped with a 12-bit A/D card (Microway A2D-160). A variable amplifier was added, and the probe

Figure 28. A schematic diagram of the updated flash-photolysis instrumentation. (Adapted from a figure prepared by Michael Albin.)

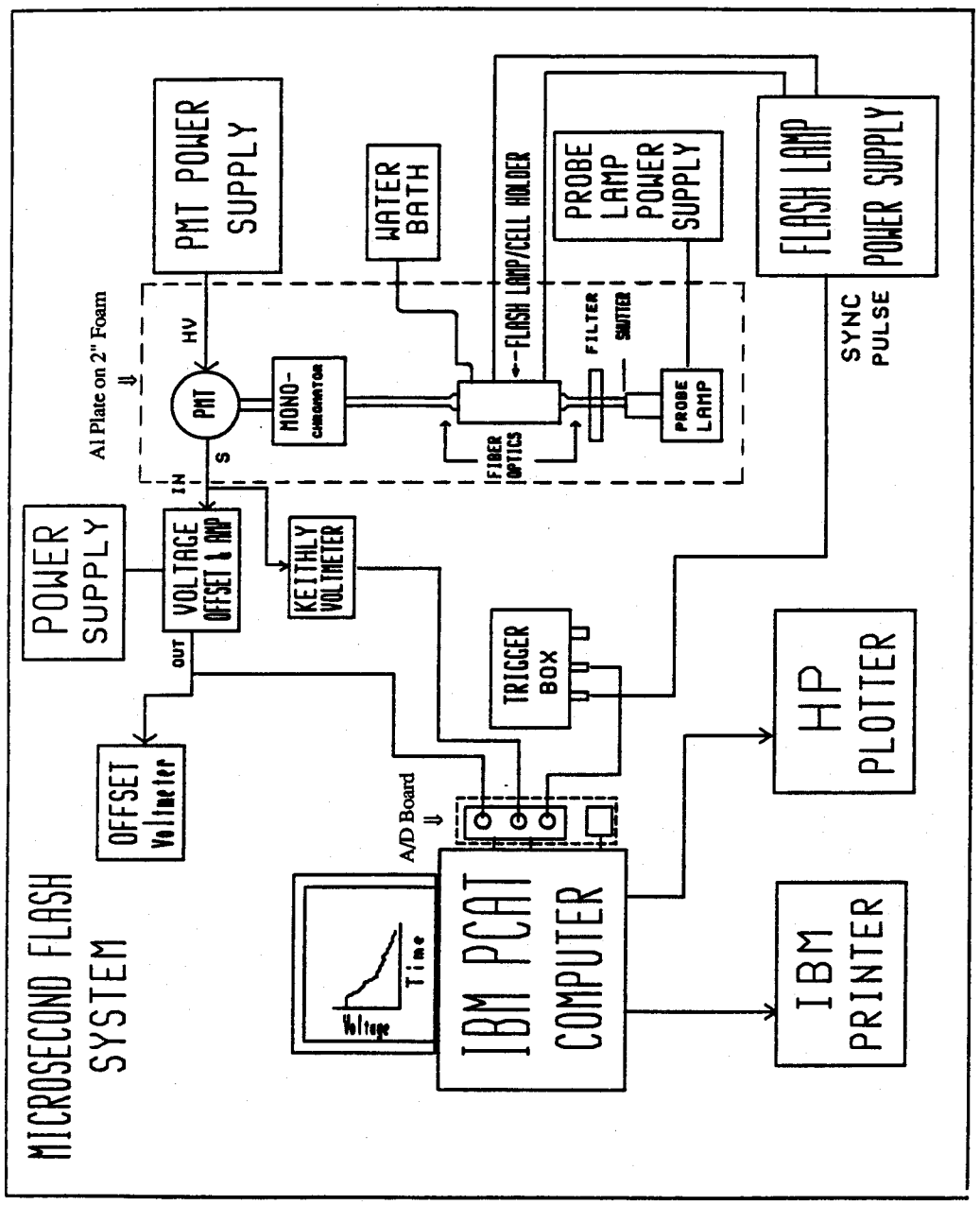
MICROSECOND FLASH SYSTEM
POWER SUPPLY
VOLTAGE OFFSET & AMP
KEITHLY VOLTMETER
OFFSET Voltmeter
OUT
IN
S
Al Plate on 2" Foam
HV
PMT
MONO-CHROMATOR
PMT POWER SUPPLY
WATER BATH
FLASH LAMP/CELL HOLDER
FIBER OPTICS
FILTER
SHUTTER
PROBE LAMP
PROBE LAMP POWER SUPPLY
FLASH LAMP POWER SUPPLY
SYNC PULSE
TRIGGER BOX
A/D Board
Time
Voltage
IBM PCAT COMPUTER
HP PLOTTER
IBM PRINTER

light was directed by fiber optics. In addition, all optical components were mounted on an Al plate supported by 2" foam rubber to dampen vibrational noise. Data collection was controlled from the computer using software commands (UnkelScope, version 2.25, Unkel Software, Inc.). A typical USCOPE parameter file is given in Figure 29.

Treatment and Analysis of Flash-Photolysis Data

Scaling and Fitting of Raw Data

The flash-photolysis instrumentation used to measure ET rates employed a single-beam probe light passed along a 15-cm pathlength cell and detected by a Hamamatsu R928 photomultiplier tube (PMT). The PMT output in volts varied with the intensity of light (I) of a given wavelength transmitted through the sample. Since rates are proportional to concentrations (and hence to absorbances), a conversion from recorded voltage (V) to absorbance (A) was necessary. A is related to I (and V) by the simple relation $A = \log (I_0/I) = \log (V_0/V)$, but measuring I_0 (V_0) with a single-beam instrument would be cumbersome, requiring a reading with an empty (or water-filled) cell. Thus the following method for converting V to A was employed.

Before the flash-photolysis apparatus was upgraded to permit computer-automated data collection and analysis, V vs. time (t) curves plotted on a strip chart recorder were hand-digitized (usually about 8 points) and converted to absorbance for fitting by a logarithm plot. The computer algorithm used to convert V_i to A_i was patterned after the method used in this manual approach. The Guggenheim relation for analysis of first-order reactions [10] was used,

$$\ln (A_{i+\tau} - A_i) = -kt_i + \text{constant}, \qquad (1)$$

where A_i and $A_{i+\tau}$ are absorbances at times t_i and $t_{i+\tau}$. By substituting $\log (V_0/V)$ for A, the following expression can be derived:

$$A_i = \log (V_i/V_{i+\tau}). \qquad (2)$$

Figure 29. A typical USCOPE parameter file. Vertical trace 1 was scaled to accept positive offset voltages (V_i) collected by channel 1 (relevant for initially oxidized cyt b_5), and vertical trace 2 (channel 2) collected raw PMT voltages (V_K). Runs were initiated from the keyboard with the flash triggered after 64 points of baseline had been recorded.

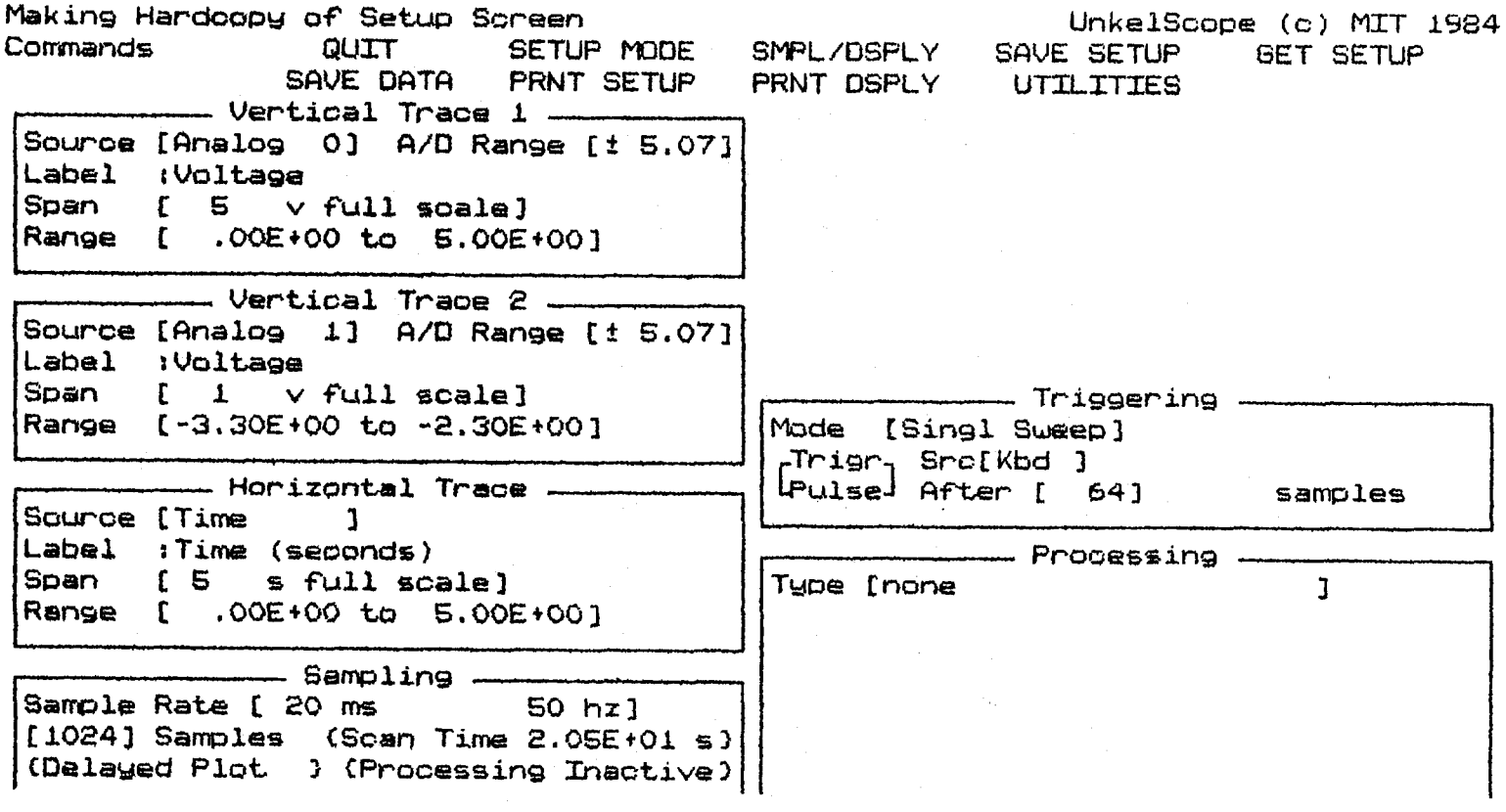
Making Hardcopy of Setup Screen
UnkelScope (c) MIT 1984
Commands
QUIT
SETUP MODE
SMPL/DSPLY
SAVE SETUP
GET SETUP
SAVE DATA
PRNT SETUP
PRNT DSPLY
UTILITIES
Vertical Trace 1
Source [Analog 0] A/D Range [± 5.07]
Label :Voltage
Span [5 v full scale]
Range [.00E+00 to 5.00E+00]
Vertical Trace 2
Source [Analog 1] A/D Range [± 5.07]
Label :Voltage
Span [1 v full scale]
Range [-3.30E+00 to -2.30E+00]
Horizontal Trace
Source [Time]
Label :Time (seconds)
Span [5 s full scale]
Range [.00E+00 to 5.00E+00]
Sampling
Sample Rate [20 ms 50 hz]
[1024] Samples (Scan Time 2.05E+01 s)
(Delayed Plot) (Processing Inactive)
Triggering
Mode [Singl Sweep]
Trigr
Pulse
Src[Kbd]
After [64] samples
Processing
Type [none]

No zero-absorbance value (V_0) is required to compute A_i. As the time increment , τ, increases, the method becomes more accurate, providing $\tau > 3$ times the decay half-life.[10] In the computer analysis, Equation 2 was used with $V_{i+\tau} = V_\infty$ (an average of the last 25 voltage points collected) rather than with increments of τ; thus data with flat end points were required for accurate V_∞'s.

The large raw voltages (V_k) from the PMT were offset using a null balance; i.e., a counter-voltage equal to $-(V_k - V_b)$ was added electronically. The residual voltages (V_b, the baseline reading prior to the flash, and V_i, data points after the flash) were amplified (V_i') to enhance the resolution of small signals (typically 10 - 50 mV for protein flashes) during analog-to-digital conversion. In analysis, voltages were scaled by dividing V_i' by the gain to give V_i again; then

$$A_i = \log \{(V_i + V_k - V_b) / (V_\infty + V_k - V_b)\}. \qquad (3)$$

A separate channel was used to record V_{ki} values automatically, and the first 62 V_{ki}'s collected before the flash were averaged to give V_k in Equation 3.

Fitting routines (FLASHIT.BAS and BIEXP.BAS) written by Albin and Gray,[11] and my program T2A.BAS (a code printout is given in Figure 30), used to format data for analysis with the purchased program SI-FIT, incorporate Equation 3 to convert raw V_i's to A_i's before fitting data traces to calculate rate constants.

To check the validity of this approach, several data sets (Ru(H33)Cyt *c* and Ru(H26)WT-b_5 ET, and the decay of excited Zn-substituted cyt *c*) were analyzed both by hand and by computer, giving similar results. Likewise, an approach to calculating A from V used by Osvath *et al.*,[12] $\Delta A = \log (V_i/V_b)$, was checked also (program T2ASYK.BAS), and it gave comparable rate constants for experimental data.

Figure 30. Basic code for T2A.BAS. This program converts ASCII voltage vs. time files created from USCOPE data by BINASC (Unkel Software, Inc.) into absorbance vs. time files suitable for analysis using SI-FIT (On-line Instrument Systems, Inc.).

```
10 OPTION BASE 1 : CHO1=0
20 DIM MSA$(100), MSA2$(35), MSA3$(50), MSA4$(100), MSA5$(100), COMM$(80)
30 CLS
40 DIM OFFVLT(4100), VLT2ABS(4100)
50 PRINT "THIS PROGRAM CONVERTS USCOPE ASCII VOLTAGES TO SINGLE COLUMN"
60 PRINT "ASCII ABSORBANCES.  (BAJ 9/12/89)"
70 PRINT
80 PRINT "NOTE:  THE LAST 25 POINTS ARE AVERAGED FOR V INFINITY"
81 PRINT "AND A'S ARE DIVIDED BY A 15 CM PATHLENGTH"
90 PRINT
100 INPUT "ENTER DRIVE:FILE.EXT OF DATA SET"; INDATA$
110 INPUT "ENTER NAME FOR OUTPUT FILE"; OUTDATA$
120 LINE INPUT "COMMENTS:"; COMM$
130 OPEN INDATA$ FOR INPUT AS #2
140 MSA2$=INPUT$(35,#2)
150 INPUT #2, GAIN
160 PRINT
170 PRINT "GAIN= ",GAIN
180 INPUT #2, MSA3$
190 LINE INPUT #2, MSA$
200 REM
210 INPUT #2, NOPTS
220 PRINT "# OF POINTS= ",NOPTS
230 FOR I=1 TO NOPTS
240 INPUT #2, OFFVLT (I)
250 OFFVLT(I)=OFFVLT(I)/GAIN
260 IF I=1032 THEN LINE INPUT #2, MSA5$
270 NEXT I
280 INPUT #2, MSA4$
290 INPUT #2, TIME
300 PRINT "TIME PER POINT= ",TIME," SEC"
310 FOR I=1 TO (NOPTS-1)
320 INPUT #2, DISCARD
330 NEXT I
340 INPUT #2, MSA5$
350 FOR I=1 TO NOPTS
360 NEXT I
370 MIN=TIME/60
380 LINE INPUT #2, MSA4$
390 LINE INPUT #2, MSA4$
400 LINE INPUT #2, MSA4$
410 KV=0
420 FOR I=1 TO 62
430 INPUT #2, BKGD
440 KV=KV+BKGD
450 NEXT I
460 CLOSE #2
470 KV=KV/62
480 VO=0
490 FOR I=1 TO 60
500 VO=VO+OFFVLT(I)
510 NEXT I
520 VO=VO/60
530 REM
540 VF=0
550 FOR I=(NOPTS-25) TO (NOPTS-1)
560 VF=VF+OFFVLT(I)
570 NEXT I
580 VF=VF/25
590 OPEN OUTDATA$ FOR OUTPUT AS #1
600 PRINT #1, COMM$
610 PRINT #1, "ABSORBANCE"
620 PRINT #1, NOPTS
630 PRINT #1, TIME
640 FOR I=1 TO NOPTS
650 NUM=OFFVLT(I)+KV-VO
660 DEN=VF+KV-VO
670 QT=ABS(NUM/DEN)
680 VLT2ABS(I)=((LOG(QT))/(2.303*15))
690 PRINT #1, VLT2ABS(I)
700 NEXT I
710 CLOSE #1
720 PRINT
730 PRINT "OUTPUT FILE", OUTDATA$,"HAS BEEN CREATED."
740 END
```

Determining k_{ET} from k_{obs}

To extract the intramolecular rate constant, k_{ET}, from a k_{obs} including bimolecular (pseudo-first-order) components, the following approach was used. Abbreviations below represent modified protein in different oxidation states.

$$R = Fe^{2+}, Ru^{3+}$$

$$O = Fe^{3+}, Ru^{2+}$$

$$RR = Fe^{2+}, Ru^{2+}$$

$$OO = Fe^{3+}, Ru^{3+}$$

Since only the heme oxidation state is observed (by monitoring at 555 or 545 nm),

$$\text{Rate} = - d[R]/dt = k_{ET}[R] + k_2[R]^2 + k_2'[R][OO]$$

$$= k_{obs}[R].$$

Assuming that $k_2 \approx k_2'$,

$$k_{obs} = k_{ET} + k_2([R] + [OO]), \qquad (4)$$

Immediately after the flash (with quantum yields of Fe^{3+} and Ru^{3+} reduction represented by Φ_{Fe} and Φ_{Ru}), the spike concentrations are

$$[R]_s = \Phi_{Fe}C \qquad (5)$$

$$[OO]_s = C\,(1 - \Phi_{Fe} - \Phi_{Ru}), \qquad (6)$$

where C is the concentration of all protein in solution (and is constant). Substituting Equations 5 and 6 into Equation 4,

$$k_{obs} = k_{ET} + k_2\,[\,\Phi_{Fe}C + C - \Phi_{Fe}C - \Phi_{Ru}C]$$

$$= k_{ET} + k_2\,(1 - \Phi_{Ru})C.$$

Plots of k_{obs} vs. C will give an intercept = k_{ET}, but unlike typical expressions found in textbooks, the slope $\neq k_2$. Without knowing Φ_{Ru} one cannot determine k_2 by this approach.

Why is there a nonzero return?

A return of the signal to the preflash baseline is often a good indication in unimolecular photochemical studies that the reaction is reversible and that no side products are formed. In the protein flash experiments discussed in this thesis, however, the reactions of interest are unimolecular, but they are initiated by irreversibly injecting an electron (from $[Ru(bpy)_3]^{2+*}$) into a doubly oxidized system. Thus the products are not expected to have the same equilibrium as the ground-state reactants. The final difference ($V_\infty - V_b$) arises from the final concentration of R, which is in equilibrium with O from several sources: ET from Fe^{2+} to Ru^{3+} ($k_{ET}[R]$), direct flash reduction of Ru^{3+} ($\Phi_{Ru}C$), and bimolecular reactions ($k_2[R][OO]$).

Error Analysis

The error (based on reproducibility) for k_{obs} was estimated to be ±10%. Since k_{ET} values were obtained from zero intercepts in k_{obs} vs. concentration plots, the estimated uncertainty in k_{ET}'s were calculated as follows: least-squares analysis was used to find the best line through the data. The ordinate value of this line (the ideal k_{obs}) at the lowest experimental concentration was defined as k_L, and that at the highest concentration, k_H (Figure 31). Two limiting lines (- - - -) were calculated using ±10% errors in k_L and k_H, and the difference in their intercepts from k_{ET} was taken to be the error.

For the temperature-dependence study, the errors in k_{ET} values were propagated by standard methods. The graphical approach using error bars was then used to approximate the range of slopes and intercepts possible in the Eyring plot.

Figure 31. A graphical approach to estimating uncertainty in slopes and intercepts. Refer to the text for an explanation of the method. The plot shown is of actual kinetics data for Ru(H26)WT-b_5 (see Results and Discussion Section).

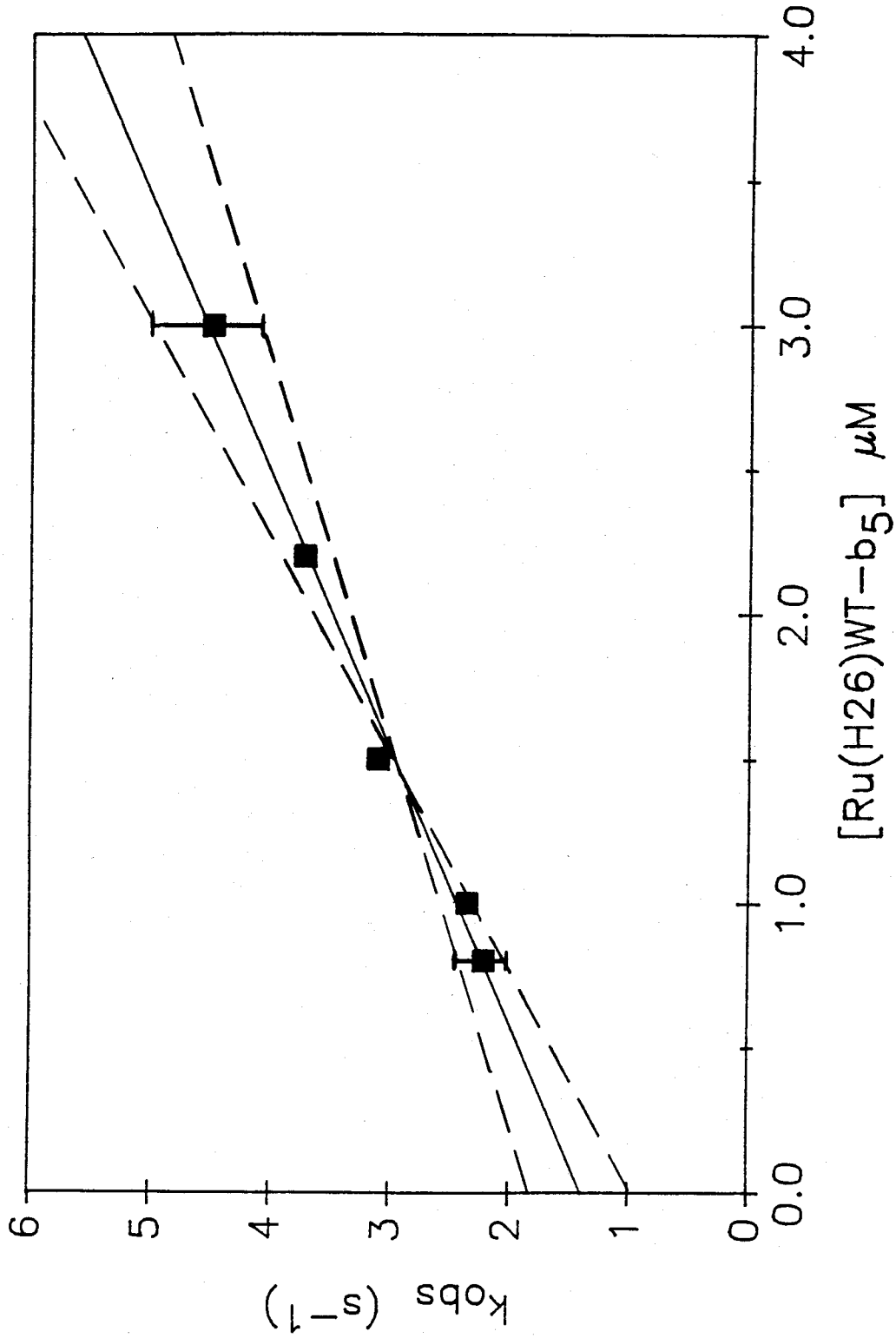
k_{obs} (s^{-1})
0
1
2
3
4
5
6
0.0
1.0
2.0
3.0
4.0
[Ru(H26)WT-b_5] μM

Stern-Volmer Quenching Experiment

In this experiment, the quenching of $[Ru(bpy)_3]^{2+*}$ phosphorescence by a varied concentration of cyt b_5 was studied. Detailed descriptions of the pulsed Nd:YAG laser system used can be found elsewhere.[1,13] Specifically, the frequency-doubled 532 nm line (8 ns pulse width) was used for $[Ru(bpy)_3]^{2+}$ excitation with a pulse frequency of 20 Hz. Light was collected perpendicular to the excitation beam and passed through 3-66 and 3-57 Corning filters. The $[Ru(bpy)_3]^{2+*}$ emission was monitored at 610 nm at a Biomation time base of 2 or 5 ns per point. A Digital PDP 11/03-L computer was used to initiate runs and to acquire and analyze data. Signal-to-noise ratios were improved by averaging data from 200 iterations for each run.

A teflon-stopcocked EPR tube was loaded in the glove box with previously degassed components. Samples consisted of 100 μL of 26.7 μM $[Ru(bpy)_3]Cl_2$ in μ = 100 mM or 500 mM NaPi, pH 7.0, plus successive aliquots (10 - 100 μL) of protein (stock solution 2 - 3 mM). Final protein concentrations ranged from 0 to 3 mM.

Molecular Modeling

All measurements of intramolecular distances were made using BIOGRAF, version 2.1 (written by S. L. Mayo, B. D. Olafson, and W. A. Goddard III). The coordinates for bovine cyt b_5 with the corrected major heme orientation [14] were kindly provided by F. S. Mathews (heme atom connectivities were added manually to the coordinate file). A model for DP-b_5 was made by deleting the 2- and 4-vinyl groups from the WT-b_5 structure. The crystal structure for a cyt b_5 triple mutant (Asn-57 to Asp, Gln-13 to Glu, Glu-11 to Gln)[15] was used for measurements pertaining to LM-b_5. The two additional mutations in LM-b_5 (His-15 to Asn and His-80 to Asn) are conservative surface substitutions and are thus expected to be nonperturbative.[16]

Pathway Calculations

The program "PATHWAY," [17-18] was used to search crystallographic coordinates (plus heteroatom hydrogens to allow estimation of hydrogen-bonding interactions) for ET pathways expected to provide the best electronic coupling between donor and acceptor. Although in a_5Ru-modified cyt b_5 the heme is the electron donor, to accommodate the program requirements, all searches were initiated at C_γ of the surface histidine of interest. The final atom was designated as Fe; then the pathway was truncated to the first atom conjugated to the heme.

Since in modified proteins the His side chain is expected to be pulled out into solvent, a manual rotation of this side chain (around the C_α-C_β and C_β-C_γ bonds) was performed (using BIOGRAF) in models of some proteins. This prevented pathways from starting by jumping from the side chain directly to a nearby surface residue; such pathways are likely peculiar to the native structure. Attempts to search for pathways using models of cyt b_5 constructed by substituting His with a_5Ru-His were unsuccessful; the PATHWAY program was incompatible with the resulting coordinate files. As a result, possible pathways involving jumps to surface residues from a_5Ru-His complexes were not considered.

RESULTS AND DISCUSSION

Optimizing Flash-Photolysis Conditions

At the beginning of this project, flash photolysis had been used by the Gray group to study ET in ruthenium-modified derivatives of cytochrome *c*,[1,2] myoglobin,[5] and *Pseudomonas aeruginosa* azurin.[19] Thus, the techniques and methods for this experiment had been developed using positively charged (or close to neutral) proteins with driving forces favoring ET from a surface a_5Ru^{2+} to the native metal center. The high negative charge, solvent-exposed heme, and low heme-reduction potential posed new technical challenges for making flash photolysis measurements. The methods detailed in the

Experimental Section and discussed below evolved during the investigation of several cyt b_5 derivatives (both native and ruthenium-modified), but primarily of WT-b_5 and LM-b_5.

Ni(MAC)/RBr Scavenging System

An assumption was made that like cytochrome *c* and myoglobin, the surface a_5Ru would be more reactive than the heme towards $[Ru(bpy)_3]^{2+*}$. Since $\Delta G°$ favors ET out from the heme to a surface ruthenium complex, the first attempt to induce intramolecular ET in ruthenium-modified WT-b_5 employed the Ni(MAC)/RBr oxidative scavenging system and doubly reduced protein (Scheme Ib).[3] After surmounting technical problems (i.e., keeping the protein reduced until flashed), no ET was evident; only a nativelike kinetics trace was observed (Figure 32). Since the EDTA reductive quenching system was found to be successful, the Ni(MAC)/RBr approach was abandoned. In retrospect, several advances in the technique developed later may have led to the ultimate success of the initially reduced method. However, starting with the oxidized protein allowed the same ET process (Fe^{2+} to Ru^{3+}) to be studied more easily and reliably.

EDTA Scavenging System

Still incorrectly assuming that the buried heme would be much less reactive than a surface a_5Ru^{3+} towards $[Ru(bpy)_3]^{2+*}$, it was hoped that enough a_5Ru^{2+} could be generated at the flash to allow observation of ET from Ru^{2+} to Fe^{3+} (Scheme Ia). In fact, a strong reductive spike in flash traces of unmodified WT-b_5 (Figure 33) indicated significant penetration of the heme area by $[Ru(bpy)_3]^{2+*}$ reducing equivalents.† With modified samples, a slow decay was observed (Figure 34) as the Fe^{2+} was oxidized by the remote a_5Ru^{3+}.

---

† Reduced cyt b_5 absorbs more strongly at 555 nm than does the oxidized protein (Figure 6). In the flash-photolysis traces, positive changes in voltage indicate iron reduction.

Figure 32. A flash-photolysis voltage/time trace for reduced WT-b_5 using the Ni(MAC)/RBr oxidative scavenging system. (1.2 μM WT-b_5 in μ = 100 mM NaPi, pH 7.0. Reaction followed at 555 nm; see Experimental Section for more details.)

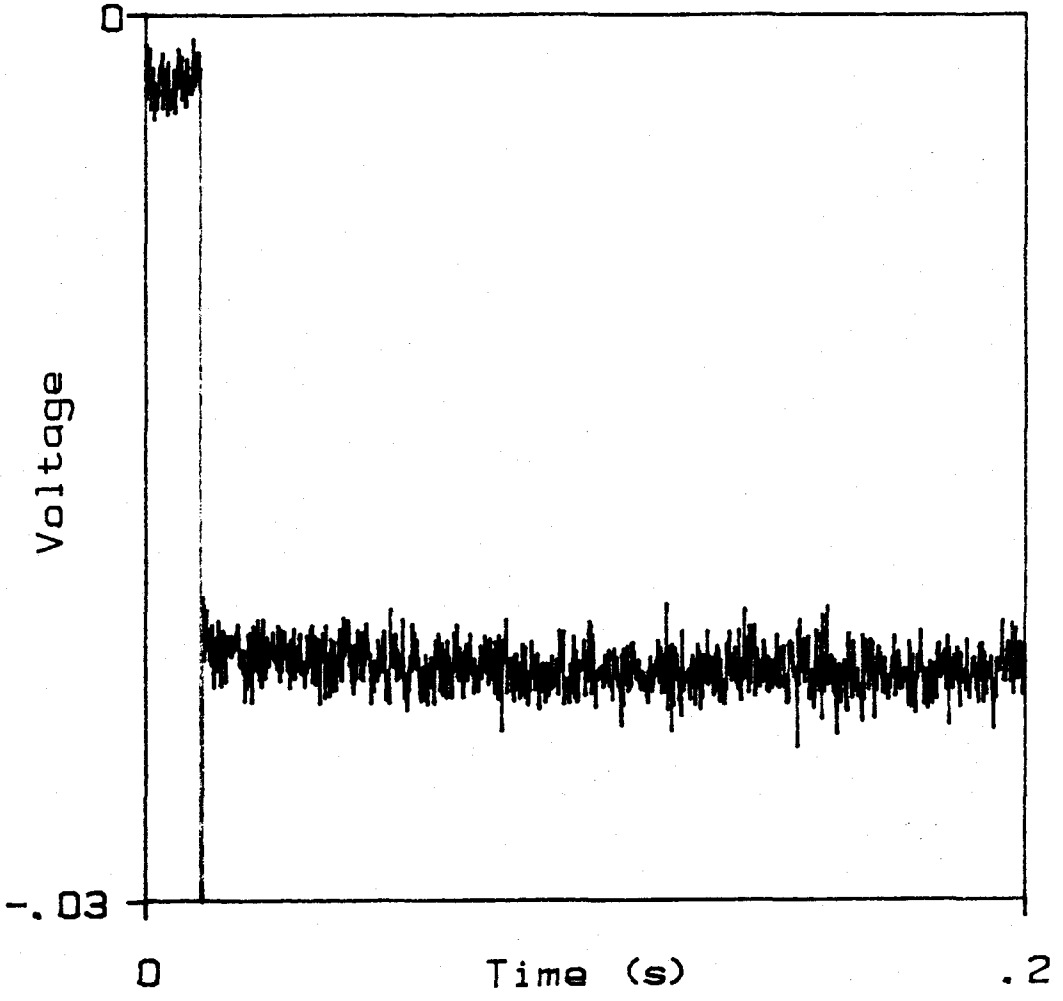
0
Voltage
-.03
0
Time (s)
.2

Figure 33. A flash-photolysis voltage/time trace for 1.0 μM of oxidized WT-b_5 using the EDTA reductive scavenging system (555 nm). Conditions for this and subsequent flash traces are provided in the Experimental Section .

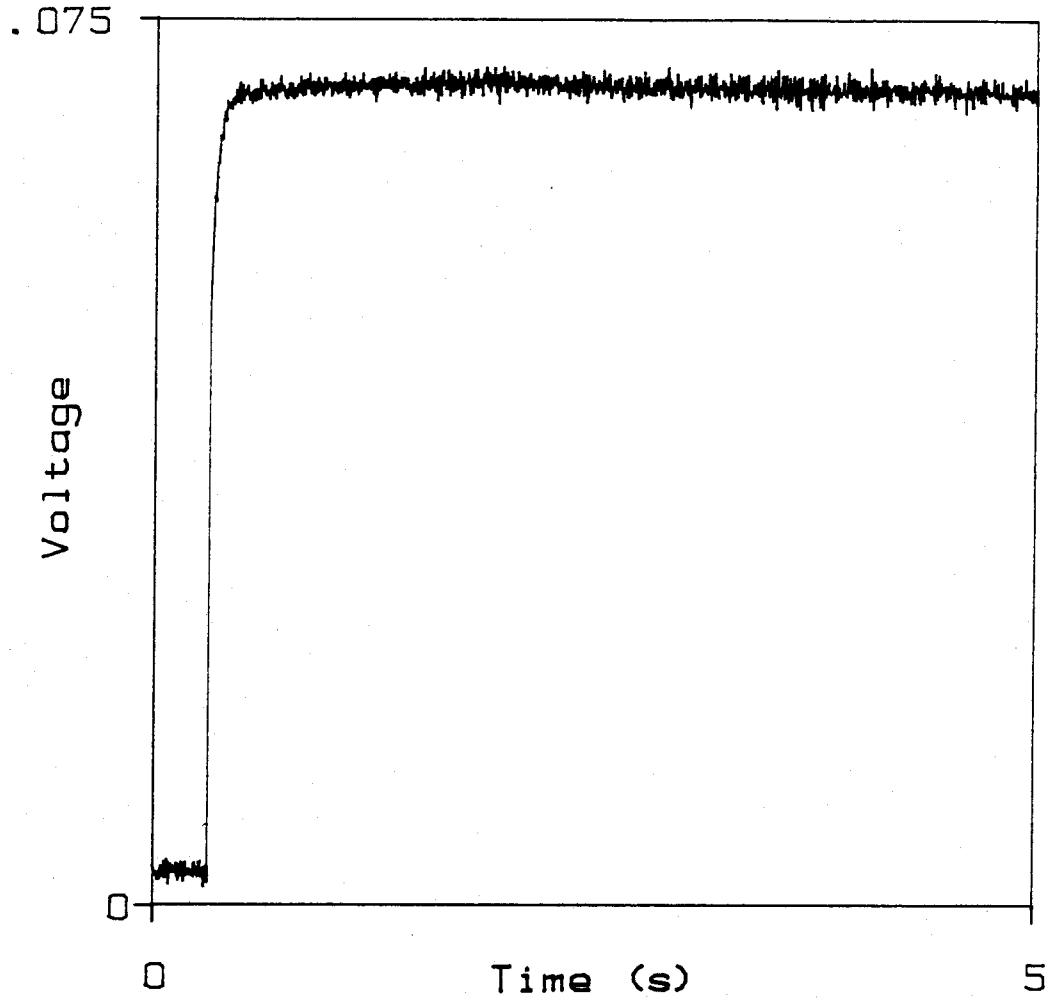
.075
Voltage
0
0
Time (s)
5

Figure 34. Flash-photolysis a) voltage/time and b) absorbance/time traces for 1 μM Ru(H26)WT-b_5 (555 nm). The data in trace a) were converted to those in trace b) by T2A.BAS. Analysis of points from t = 0.4 to 1.6 s using SI-FIT gave the fit shown (inset is a plot of residuals) and $k_{obs} = 2.2\ s^{-1}$.

a)

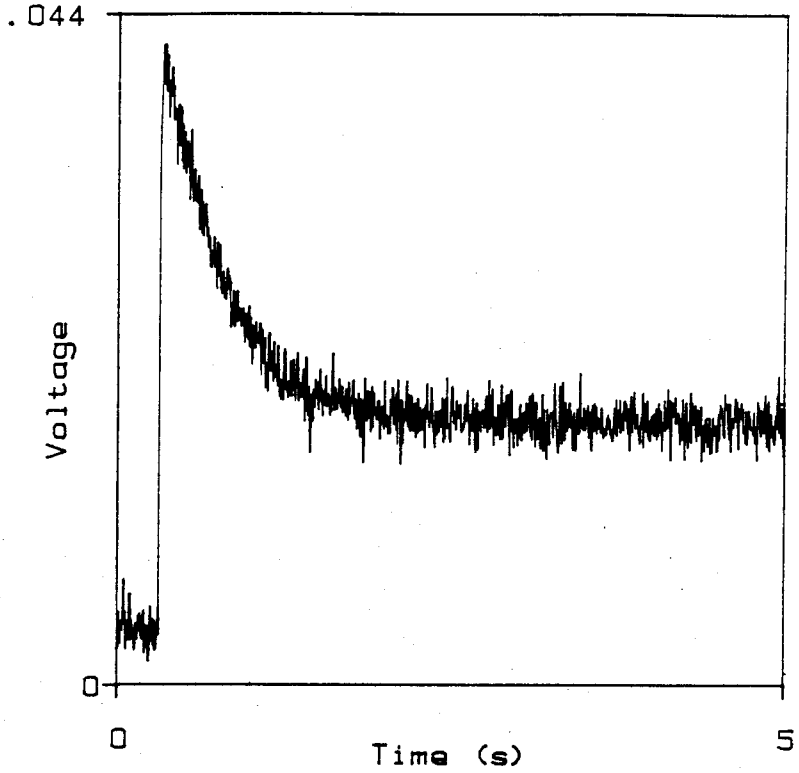
.044
Voltage
0
0
Time (s)
5

b)

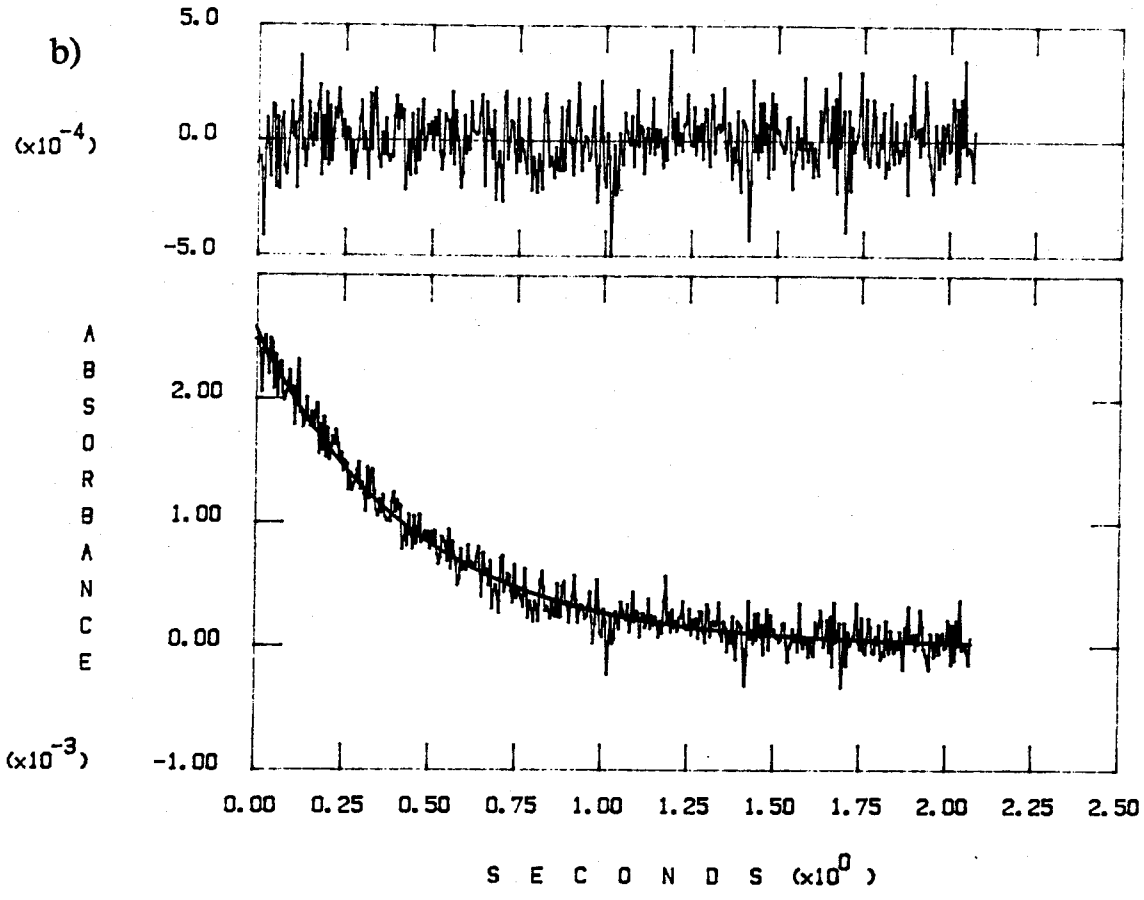
5.0
0.0
-5.0
(x10-4)
ABSORBANCE
2.00
1.00
0.00
-1.00
(x10-3)
0.00 0.25 0.50 0.75 1.00 1.25 1.50 1.75 2.00 2.25 2.50
SECONDS (x10^0)

At the flash, the reducing equivalents partition between Fe^{3+} and Ru^{3+}. Direct heme reduction is likely facilitated by the high solvent exposure of the heme edge (the heme fraction of the protein surface area is five times greater in cyt b_5 than in cyt *c*) [20] and by $[Ru(bpy)_3]^{2+*}$ binding in the negative heme area. Cyt b_5 is known to bind small, positively charged metal complexes with a 3-/4- binding site.[21] To determine whether $[Ru(bpy)_3]^{2+*}$ was binding, a Stern-Volmer experiment was performed.

Stern-Volmer Experiment

$[Ru(bpy)_3]^{2+*}$ phosphorescence at 610 nm was quenched by incremental concentrations of WT-b_5. For a simple bimolecular-quenching reaction, the observed emission-decay rate ($1/\tau$) is composed of the unimolecular decay rate ($1/\tau_0$) and a quenching rate constant (k_q),

$$1/\tau = k_qQ + 1/\tau_0, \qquad (7)$$

where Q is the quencher concentration. A plot of ($1/\tau - 1/\tau_0$) vs. Q for experimental data obtained at μ = 100 mM (Figure 35) shows that at high values of Q the linear dependence predicted by Equation 7 is not obeyed. The observed saturation behavior is consistent with a mechanism involving a preequilibrium-binding step,

$$Fe^{3+}b_5 + [Ru(bpy)_3]^{2+*} \overset{K}{\Leftrightarrow} (Fe^{3+}b_5,[Ru(bpy)_3]^{2+*}),$$

with a binding constant, K. The quenching (rate constant k_{qc}) occurs within the electrostatic complex in a second step,

$$(Fe^{3+}b_5,[Ru(bpy)_3]^{2+*}) \overset{k_{qc}}{\rightarrow} (Fe^{2+}b_5,[Ru(bpy)_3]^{3+}).$$

The kinetics of this preequilibrium-intracomplex mechanism can be described by

$$(1/\tau - 1/\tau_0) = k_{obs} = Kk_{qc}Q / (1 + KQ). \qquad (8)$$

At low concentrations (Q) Equation 8 reduces to Equation 7 with $k_q = Kk_{qc}$.

A nonlinear, least-squares fit of the data to Equation 8 gave K = 500 M^{-1} and k_{qc} = 1.2 x 10^7 s^{-1} for μ = 100 mM (Figure 35). The binding constant is similar to that

Figure 35. Stern-Volmer plot of $[Ru(bpy)_3]^{2+*}$ quenched by cyt b_5. The data collected at two ionic strengths (as shown) were fit by nonlinear and linear least-squares methods to Equation 8 (solid line, μ = 100 mM) and to Equation 7 (dotted line, μ = 100 mM, first eight points only; dashed line, μ = 500 mM).

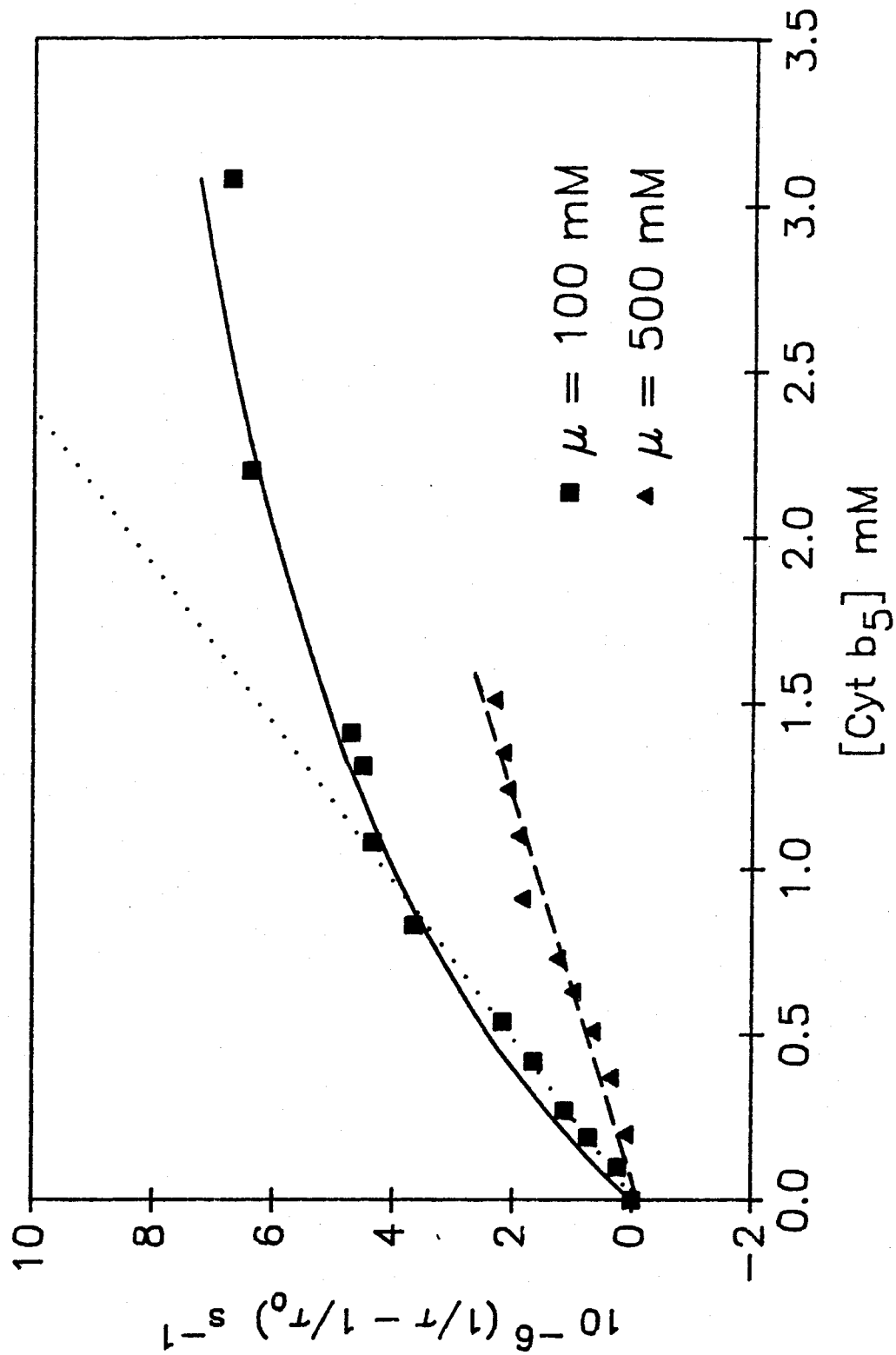
μ = 100 mM
μ = 500 mM
[Cyt b5] mM
10 −6 (1/τ − 1/τo) s−1
10
8
6
4
2
0
−2
0.0
0.5
1.0
1.5
2.0
2.5
3.0
3.5

found for the bimolecular oxidation of cyt b_5 with $[Co(NH_3)_6]^{3+}$ (K = 600 M^{-1}, pH 7.0, μ = 100 mM).[21] A linear regression used to fit Equation 7 to the first eight points (Q < 1.1 mM) yielded an approximation for $k_q = 4.2 \times 10^9$ M^{-1} s^{-1}, which agrees with Kk_{qc} above. Performing the quenching study at μ = 500 mM showed no indication of saturation below Q = 1.5 mM. A fit to Equation 7 gave $k_q = 1.7 \times 10^9$ M^{-1} s^{-1}. This result is consistent with a smaller K at high ionic strength.

The same factors leading to increased heme reduction probably contribute to bimolecular ET by attracting the positively charged a_5Ru^{3+} from another protein in a stacking arrangement. As a result, high ionic strengths were necessary to obtain reproducible intramolecular kinetics results as in the experiments described below.

Electron Transfer in a_5Ru(His-26) Derivatives of WT-*b*$_5$, LM-*b*$_5$, and DP-*b*$_5$

A parallel study of ET from Fe^{2+} to Ru^{3+} in Ru(H26)WT-b_5, Ru(H26)LM-b_5, and Ru(H26)DP-b_5 was investigated by flash photolysis. As discussed above, the proteins were initially oxidized (Fe^{3+}, Ru^{3+}), and the $[Ru(bpy)_3]^{2+}$/EDTA reductive scavenging system was employed. Figures 34,36, and 37 show representative voltage vs. time data, which were converted to absorbances for fitting. The traces were found to obey first-order decay kinetics for at least three half-lives. In order to identify any bimolecular (pseudo-first order) components contributing to the observed rate constants, a concentration dependence was carried out for each protein. A mild concentration dependence was indeed evident (Figure 38); thus values of k_{ET} were obtained by extrapolation to zero concentration (see the Experimental Section). For Ru(H26)WT-b_5, Ru(H26)LM-b_5, and Ru(H26)DP-b_5 , k_{ET} = 1.4(4), 6(1), and 0.2(1) s^{-1}. The magnitude of the differences in ET rates for the three samples is particularly evident in an overlay of kinetic traces for the modified proteins with that of native WT-b_5 (Figure 39). In view of their structural similarities, it is somewhat surprising that the ET rates in the

Figure 36. Flash-photolysis a) voltage/time and b) absorbance/time traces for 1 μM Ru(H26)LM-b_5 (555 nm). Analysis using SI-FIT gave the fit shown and $k_{obs} = 9.0\ s^{-1}$.

a)

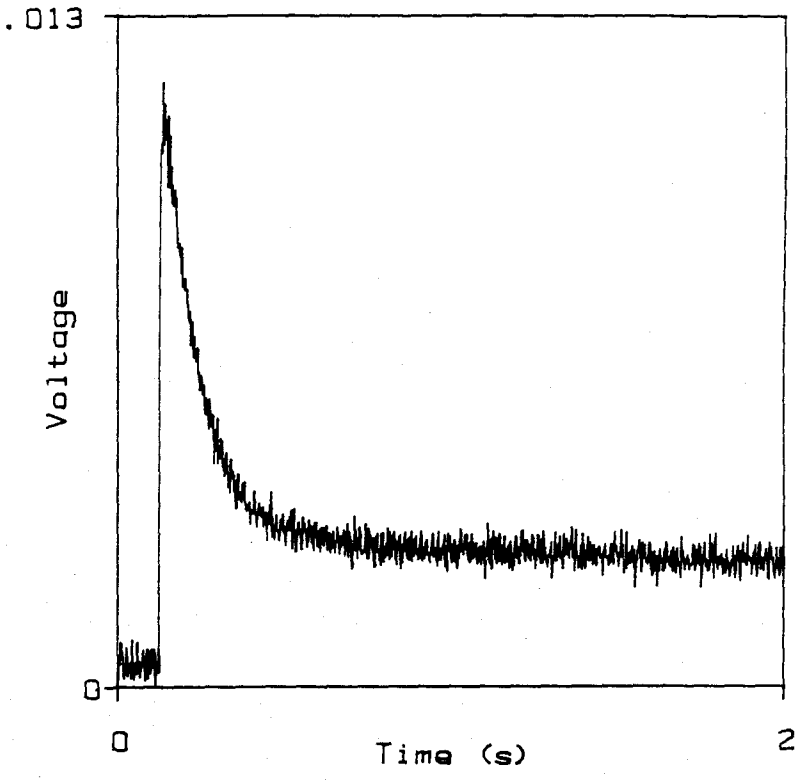
.013
Voltage
0
0
Time (s)
2

b)

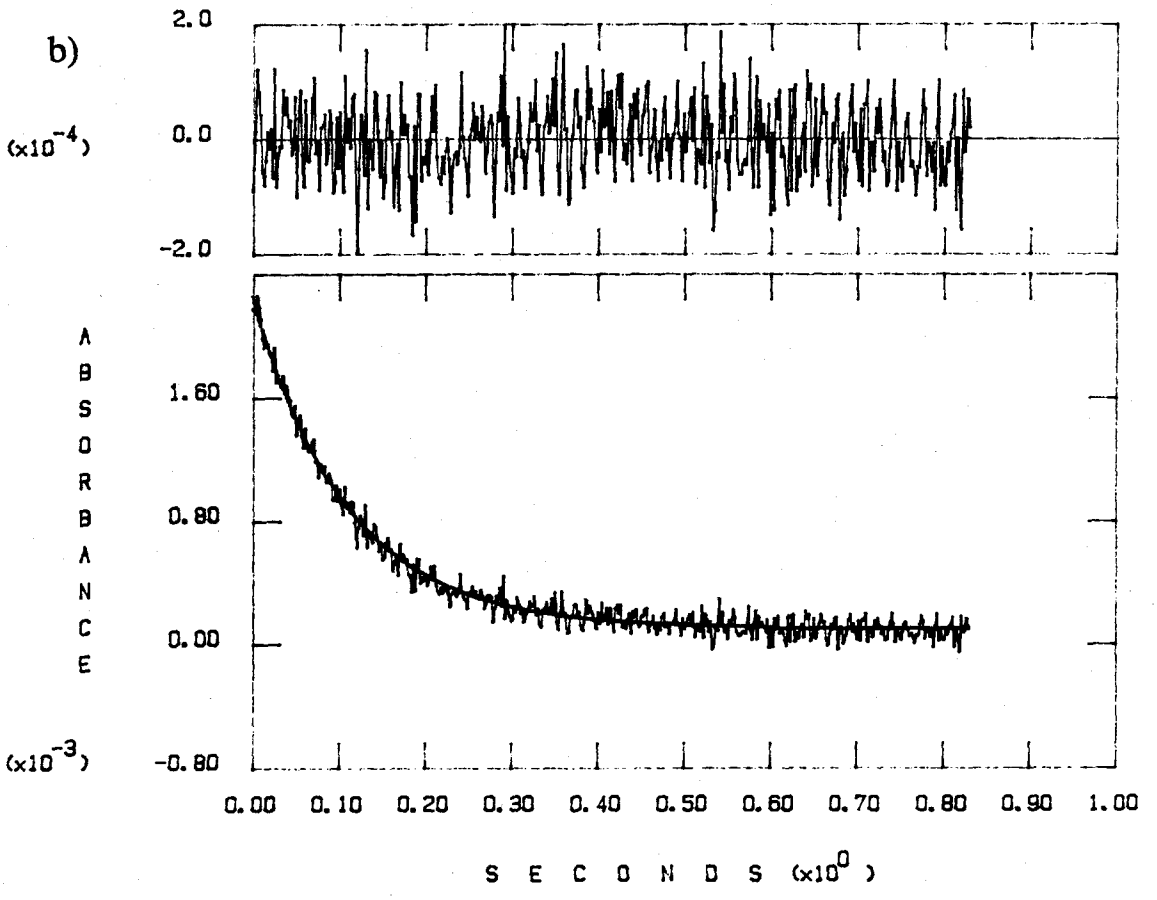
2.0
0.0
-2.0
(x10-4)
ABSORBANCE
1.60
0.80
0.00
-0.80
(x10-3)
0.00 0.10 0.20 0.30 0.40 0.50 0.60 0.70 0.80 0.90 1.00
SECONDS (x10^0)

Figure 37. Flash-photolysis a) voltage/time and b) absorbance/time traces for 1 μM Ru(H26)DP-b_5 (545 nm). Analysis using SI-FIT gave the fit shown and $k_{obs} = 0.3\ s^{-1}$.

a)

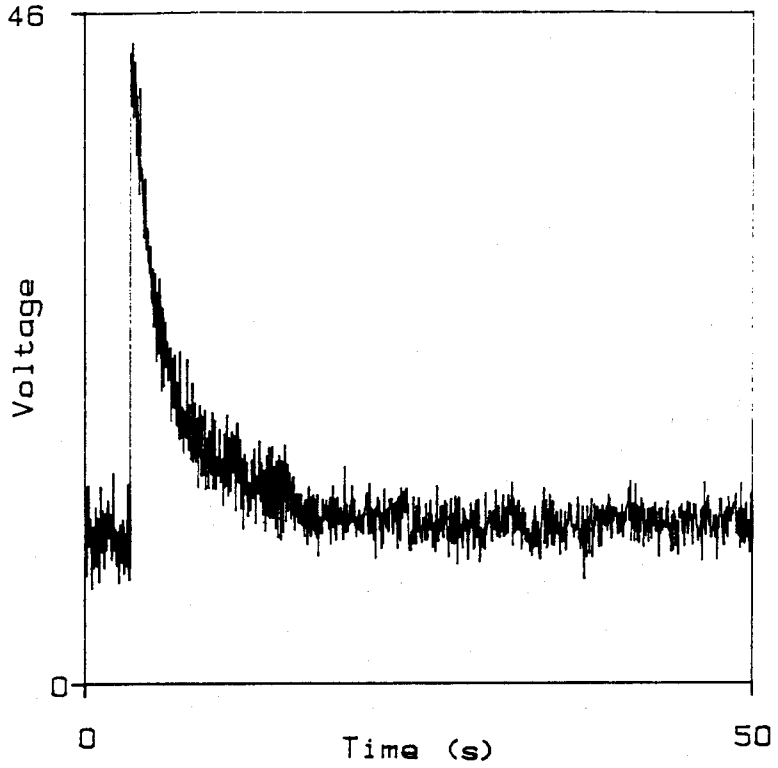
.0146
Voltage
0
0
Time (s)
50

b)

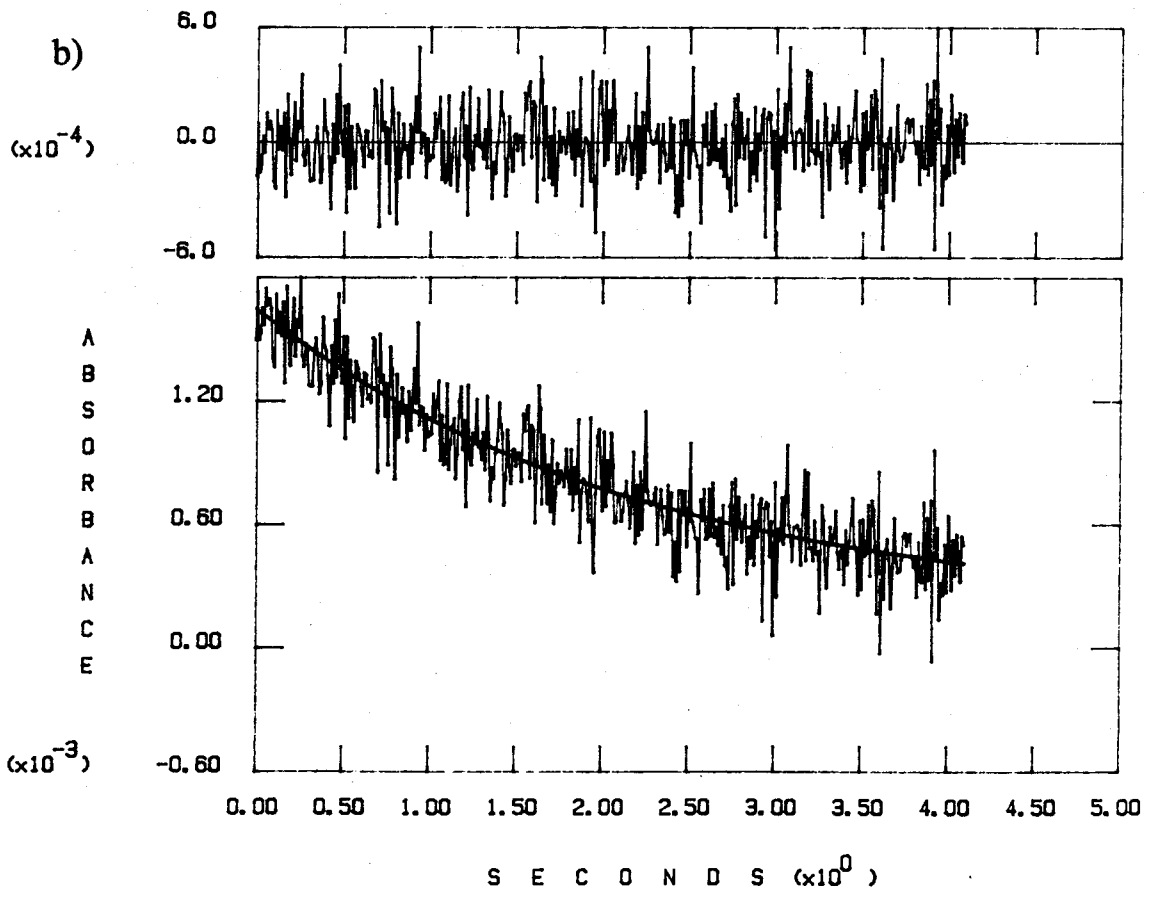
6.0
0.0
-6.0
(x10-4)
ABSORBANCE
1.20
0.60
0.00
-0.60
(x10-3)
0.00 0.50 1.00 1.50 2.00 2.50 3.00 3.50 4.00 4.50 5.00
SECONDS (x10^0)

Figure 38. A plot of the concentration dependence of k_{obs} for Ru(H26)LM-b_5, Ru(H26)WT-b_5, and Ru(H26)DP-b_5. The lines are least-squares fits to the data. Intramolecular rate constants for ET from Fe^{2+} to Ru^{3+} were obtained by extrapolation to zero concentration. For the three proteins, k_{ET} = 6(1), 1.4(4), and 0.2(1) s^{-1}.

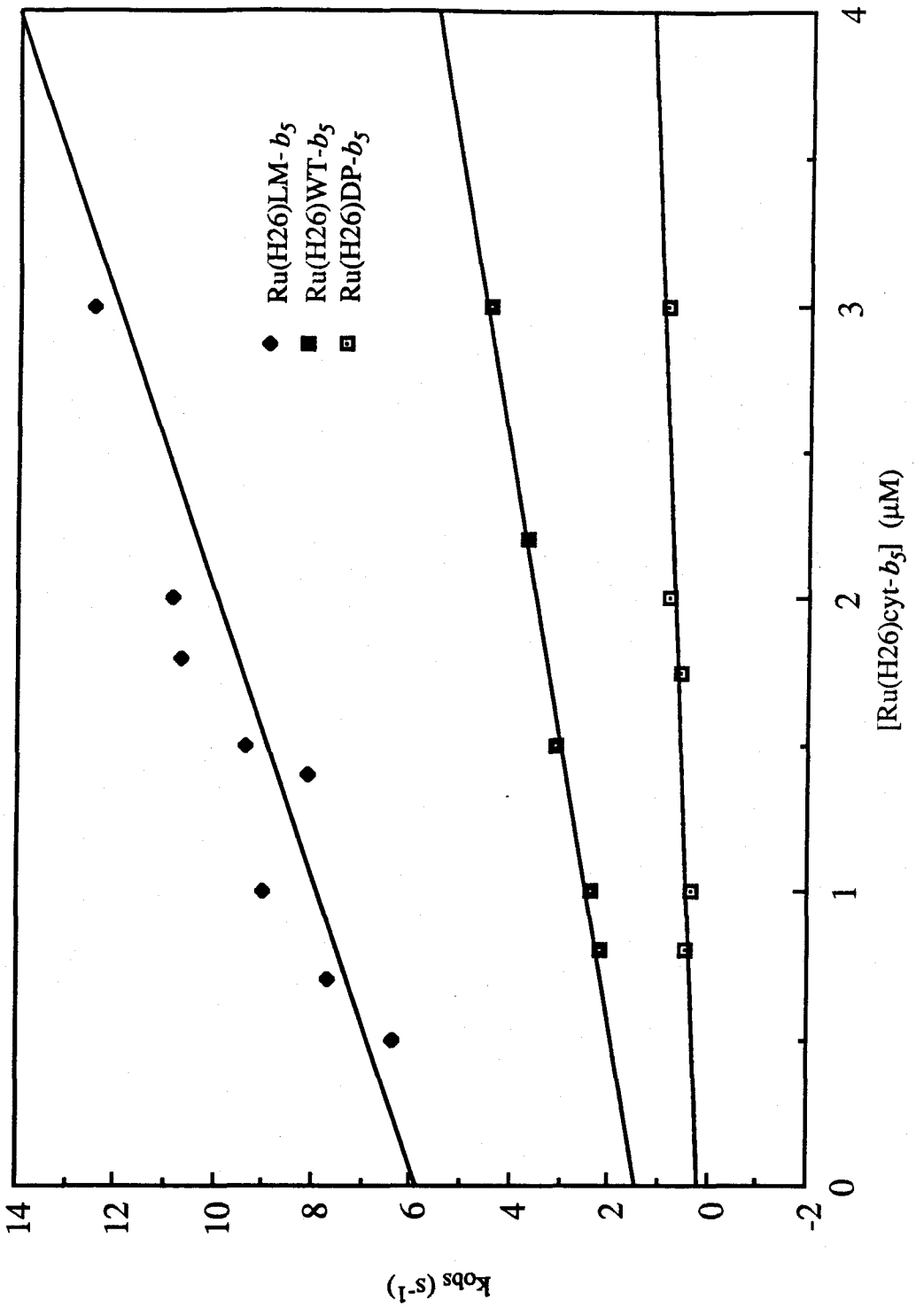
Ru(H26)LM-b_5
Ru(H26)WT-b_5
Ru(H26)DP-b_5
k_{obs} (s^{-1})
[Ru(H26)cyt-b_5] (μM)
14
12
10
8
6
4
2
0
-2
0
1
2
3
4

Figure 39. An overlay of flash-photolysis voltage traces for a) WT-b_5, b) Ru(H26)DP-b_5, c) Ru(H26)WT-b_5, and d) Ru(H26)LM-b_5. Since the data were collected at different time bases, the spikes were aligned by omitting points in the preflash baselines of traces a), b), and c).

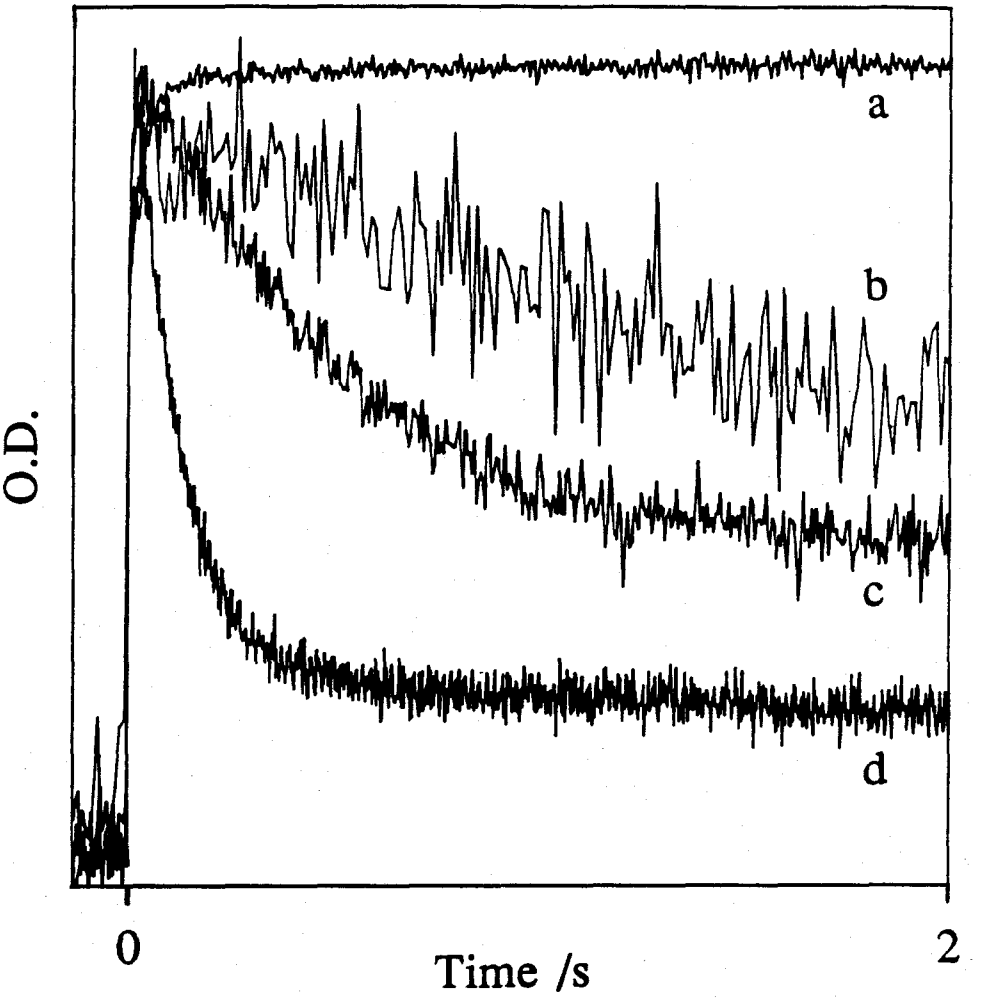
O.D.
a
b
c
d
0
2
Time /s

three a_5Ru(His-26)-modified proteins differ by over an order of magnitude. It is also striking that Ru(H26)DP-*b*$_5$, which has the largest driving force for Fe^{2+} to Ru^{3+} ET, exhibits by far the slowest rate. The implications of these results are discussed below.

Evaluating the ET Rates for Ru(H26)WT-*b*$_5$, Ru(H26)LM-*b*$_5$, and Ru(H26)DP-*b*$_5$ with Theoretical Models

The ET rate constant in the weak overlap (nonadiabatic) limit is given by the following expression:[22]

$$k_{ET} = (4\pi^2/h)\,(H_{AB})^2\,(FC). \qquad (9)$$

In Eq. 9, H_{AB} is the electronic coupling between the donor and acceptor, and the Franck-Condon term (FC) contains details of the nuclear motion coupled to the transfer. In the one-mode, high-temperature, harmonic limit,

$$FC = (4\pi k\lambda T)^{-1/2} \exp\{-(\lambda + \Delta G^\circ)^2 / 4\lambda kT\}. \qquad (10)$$

Thus, k_{ET} is expected to depend on the electronic coupling (H_{AB}), the driving force of the reaction ($-\Delta G^\circ$), and the reorganization energy (λ) of solvent dipoles and redox center ligands.

In the three systems studied, the trend in rates clearly does not follow ET driving forces since Ru(H26)DP-*b*$_5$ has the highest ΔG° but the lowest k_{ET}. Also, the iron porphyrin donors are very similar both structurally and electronically, and the acceptors are the same; hence, it is unlikely that the ET reorganization energies are very different in the three modified proteins.† Therefore, we believe that the ET rates reflect changes in the long-range donor-acceptor electronic coupling.

---

† This assertion may not be strictly true for RuDP-*b*$_5$. For example, the activation parameters for $Fe(EDTA)^{2-}$ reduction of WT-*b*$_5$ [$\Delta H^\ddagger$ = 5.4(2) kcal/mol, $\Delta S^\ddagger$ = -29.2(8) eu] [6] and of DP-*b*$_5$ [$\Delta H^\ddagger$ = 6.8(1) kcal/mol, $\Delta S^\ddagger$ = -26.5(4) eu][23] have been measured. The resulting $\Delta G^\ddagger$'s (298K) of 14.1(5) and 14.6(2) kcal/mol are the same within error. Since $\Delta G^\ddagger = (\lambda + \Delta G^\circ)^2/4\lambda$,[22] the difference in ΔG° between RuWT-*b*$_5$ and RuDP-*b*$_5$

It is commonly assumed that H_{AB} decays exponentially with the donor-acceptor separation (D):[1,22,24-26]

$$H_{AB} = H_{AB}^{\circ} H_{AB}'$$

$$H_{AB}' = \exp[-\beta(D-D_0)/2],$$

with values of β in the range 0.8 to 0.9 $Å^{-1}$. H_{AB}° is the matrix element at donor-acceptor contact ($D_0 \approx 3$ Å). Gingrich *et al.* compared ET from electronically excited ZnPP and ZnDP to $Fe^{3+}(H_2O)$PP (PP = protoporphyrin; DP = deuteroporphyrin) in hemoglobin hybrids and reported $k_{ET}(ZnPP)/k_{ET}(ZnDP) = 2.8$.[27] They credited a vinyl group in the ZnPP-substituted protein with extending the conjugation of the porphyrin, thus reducing D by 1 Å. Their ratio of k_{ET} values agrees with $\exp(-\beta\Delta D) \approx 2.5$ ($\beta = 0.9$ $Å^{-1}$). In the present work, comparing Ru(H26)WT-b_5 and Ru(H26)DP-b_5 also gives $\Delta D \approx 1$Å (Figure 40ab). However, in order to reproduce the observed ratio of ET rate constants with a simple exponential distance decay model, a value of $\beta = 1.9$ $Å^{-1}$ is required.

Onuchic and Beratan have developed a model of long-range interactions in proteins in which H_{AB}' is a function of the specific composition of the medium between the donor and the acceptor.[17] This electron-tunneling pathway model has been successful in predicting ET rate constants for several ruthenium-modified cytochrome *c* mutants.[28,29] In calculating ET pathways, the peptide network that bridges the electron donor and acceptor is partitioned into three types of interactions: covalent bonds (C), hydrogen bonds (H), and through-space jumps (S). The coupling is estimated to decay by a fixed amount over each covalent bond in the pathway; hydrogen bonds and through-space jumps are expected to result in more rapid decay. At this level of theory, no attempt has been made to qualify covalent bond types; thus pathways involving double bonds or

---

necessarily gives rise to a difference in λ (approximately 0.1 eV). However, because the $\Delta G^{\ddagger}$'s are the same, the FC's differ only by the prefactor $(4\pi k\lambda T)^{-1/2}$, which makes the difference in λ negligible with respect to k_{ET}.

Figure 40. ET distances in a_5Ru(His-26)-modified cyt b_5 derivatives. Edge-to-edge distances from the histidine C_γ to the nearest heme atom (- - -) for a) Ru(H26)DP-b_5 (12.9 Å), b) Ru(H26)WT-b_5 (11.9 Å), and c) Ru(H26)LM-b_5 (12 Å).

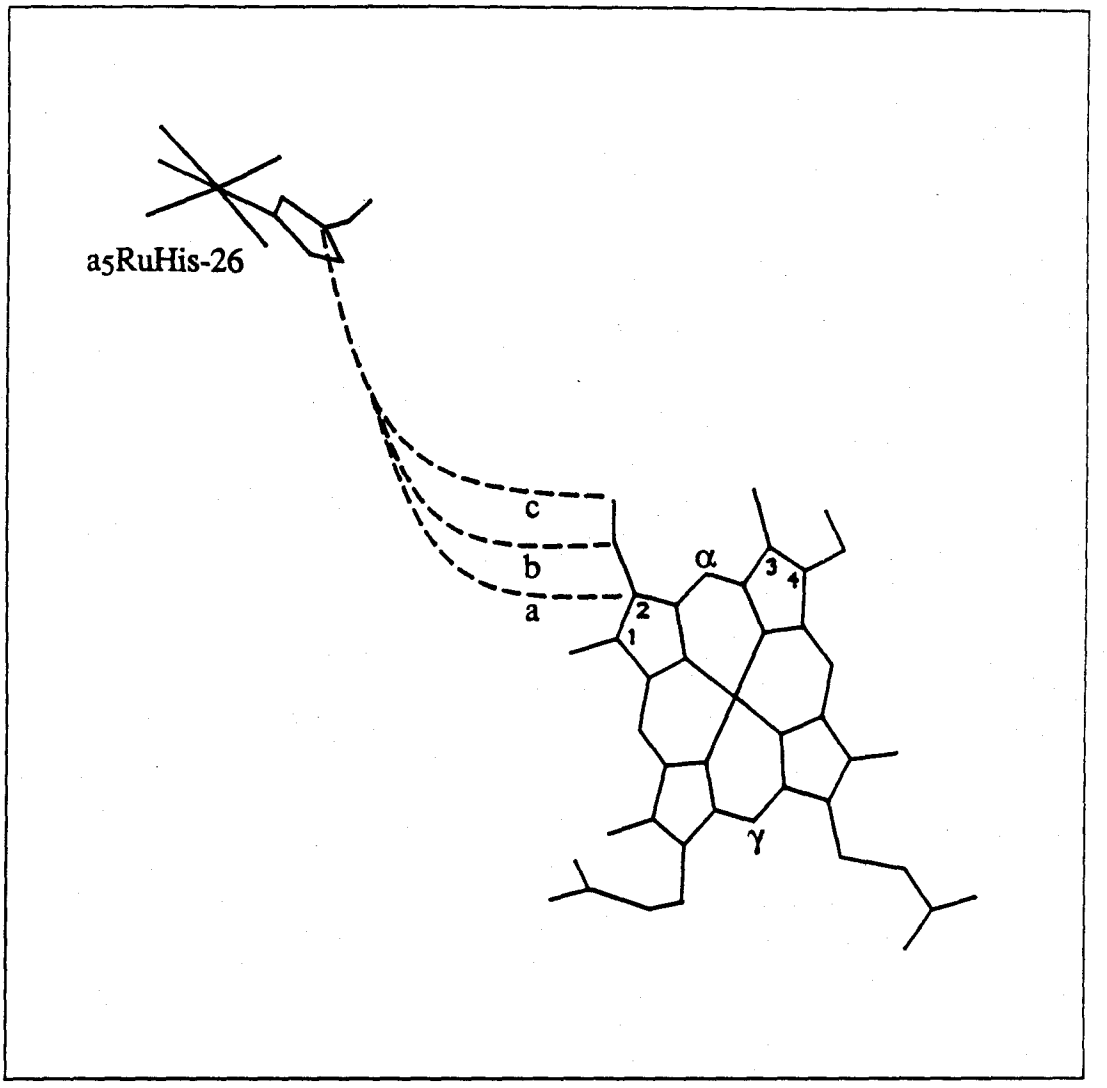
a5RuHis-26
c
b
a
α
γ
1
2
3
4

electron lone pairs are not exceptional. The electronic coupling matrix element H_{AB}' associated with each ET pathway is calculated as follows:

$$H_{AB}' = \prod_{i=1}^{N_C} \varepsilon_C(i) \prod_{j=1}^{N_B} \varepsilon_H(j) \prod_{k=1}^{N_S} \varepsilon_S(k)$$

$\varepsilon_C = 0.6$

$\varepsilon_H = 0.36 \exp [-1.7 (R - R_0)]$; $R_0 = 2.9$ Å

$\varepsilon_S = 0.6 \exp [-1.7 (R - R_0)]$; $R_0 = 1.4$ Å.

A computer program has been written employing this formalism to search crystallographic coordinates for the optimum ET pathways through proteins.[18]

Pathways for Ru(H26)WT-b5

A search of the medium between His-26 and Fe in WT-*b5* revealed that the pathway with the largest H_{AB}' consists of eight covalent bonds from C_γ of His-26 to the end ($C_{\delta 1}$) of the Leu-25 side chain; the pathway is completed by a 3.8 Å through-space jump to the closest heme atom, C_α of the 2-vinyl (Figure 41). Because the vinyl group is conjugated with the porphyrin π-system, the bond counting considers it to be part of the delocalized iron center. The $(H_{AB}')^2$ for this pathway is given in Table 2.

Most of the other pathways found in the search were minor (longer) variations of the best path, e.g., eight covalent bonds to Leu-25 ($C_{\delta 2}$) and a longer (4.49 Å) jump to the heme 3-methyl. One interesting alternative pathway shown in Figure 41 continues from the Leu-25 backbone to the Ile-24 carbonyl oxygen. From there it takes advantage of a hydrogen bond (2.94 Å) to Ala-54, but there remains a 3.8 Å space jump to the heme, making the overall $(H_{AB}')^2$ over 10^4 smaller than for the best pathway. Since the porphyrin ring lacks bonds to the protein, the only possible routes from His-26 to Fe that avoid the large space jump to the heme must follow a longer, more circuitous path through the axial ligand, His-63 (see Ru(H26)DP-*b5* in the section below).

Figure 41. Possible ET pathways for His-26 to heme in WT-b_5. Protein bonds are shown in green, and heme bonds are black. Pathways are drawn in red or blue with covalent links (—), H-bonds (– – –), and space jumps (- - -) as indicated. See the text for a thorough discussion. CAB = 2-vinyl C_α, CBB = 2-vinyl C_β, and CMC = 3-methyl.

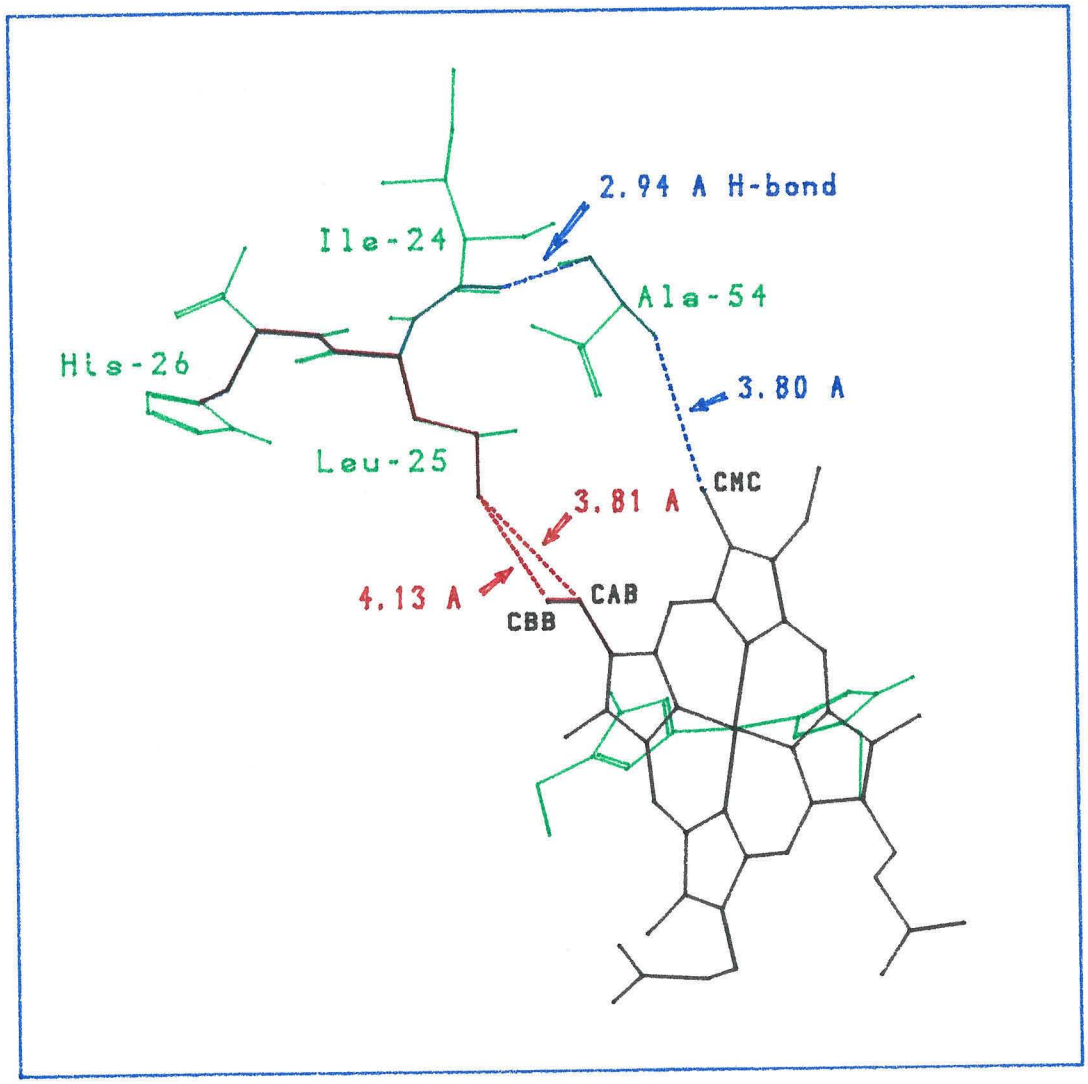
2.94 A H-bond
Ile-24
Ala-54
His-26
3.80 A
Leu-25
CMC
3.81 A
4.13 A
CAB
CBB

Table 2. Rate Constants for Fe(II) to Ru(III) ET in Ru(H26)cyt b_5 Derivatives.

					k_{calc} (s^{-1})		
Sample	$\Delta G°$ (eV)[a]	k_{ET} (s^{-1})	Pathway	$(H_{AB}')^2$	λ_{b5} = 1.2 eV[b]	λ_{b5} = 1.4 eV[b]	Ru(H26)WT-b_5
Ru(H26)WT-b_5	-0.08	1.4(4)	8C, 1S (3.8 Å)	2.8×10^{-8}	1.9 [4.5]	0.27 [0.65]	--
Ru(H26)LM-b_5	-0.10	6(1)	8C, 1S (3.7 Å)	4.7×10^{-8}	4.4 [5.7]	0.66 [0.85]	3.3 [1.8]
Ru(H26)DP-b_5	-0.13	0.2(1)	9C, 1S (4.5 Å)	9.9×10^{-10}	0.16 [4.4]	0.02 [0.63]	0.12 [1.4]

[a] $E°(Fe^{3+/2+})$ = 5.1 mV, WT-$b5$;[7] -14 mV, LM-$b5$;[15] -44 mV, DP-$b5$ [23] (vs. NHE, 25 °C, μ=0.1 M(NaPi)). $E°$ $(Ru^{3+/2+})$ = 80 mV.[1,24]

[b] Referenced to Ru(H33)cyt *c*: $k_{ET} = 30\ s^{-1}$, $(H_{AB}')^2 = 8.0 \times 10^{-8}$. Rates in brackets were calculated using an exponential decay expression, $k_{calc} = (k_{ref}) \exp[-\beta (D - D_{ref})] (FC/FC_{ref})$, ($\beta = 0.9$ Å^{-1}).

There is some uncertainty in the vinyl orientations in WT-*b*5 that should be considered when evaluating the ET pathways. The dominant heme orientation in lipase-solubilized wild-type cyt *b*5, as determined by NMR [30] and by x-ray diffraction,[14] has the 2-vinyl in proximity to Leu-25. A minor form, with the heme rotated 180° about the α,γ meso axis (see Figure 7), is in slow equilibrium with the major form (major:minor = 90:10).[31] In WT-*b*5, the best pathway for the minor heme orientation would be insignificantly different: the space jump from Leu-25 $C_{\delta 1}$ would be of the same approximate distance to the 3-methyl as to C_α of the 2-vinyl in the major orientation. An extra covalent bond would be counted (a factor of 0.36 in $(H_{AB}')^2$) since the methyl is not conjugated with the porphyrin ring.

Pathways for Ru(H26)LM-b5

For LM-*b*5, the predicted ET pathways are analogous to those for WT-*b*5, but small changes in its relative structure make some of the important distances different. For instance, in LM-*b*5 the Leu-25-to-heme jump is only 3.7 Å to C_β of the 2-vinyl (Figure 42), because in this mutant the vinyl has pivoted relative to the WT-*b*5 structure. This shorter space jump leads to a calculated 1.7-fold increase in $(H_{AB}')^2$ compared to WT-*b*5 (Table 2). This prediction is encouraging, since k_{ET} for Ru(H26)LM-*b*5 was greater than that for Ru(H26)WT-*b*5. For a discussion of calculated rate constants, see below.

The other, less important, pathway through Ile-24 and Ala-54 is interesting because it highlights how a small overall perturbation in protein structure (Chapter II) can result in significant changes with respect to ET pathways. Comparing this path in LM-*b*5 (Figure 42) with the analog in WT-*b*5 (Figure 41) reveals that in the former the H-bond is 0.2 Å shorter, but the space jump is 0.6 Å greater. In a primary pathway such changes would have a considerable effect on the predicted coupling.

As with WT-*b*5, there is some uncertainty in the vinyl orientations in LM-*b*5.[15] The parent protein for LM-*b*5 (LTM-*b*5; see Experimental Section) has the same major

Figure 42. Possible ET pathways for His-26 to heme in LM-b_5 (LTM-b_5 structure). Note the changes in H-bond and space-jump distances from WT-b_5, Figure 41.

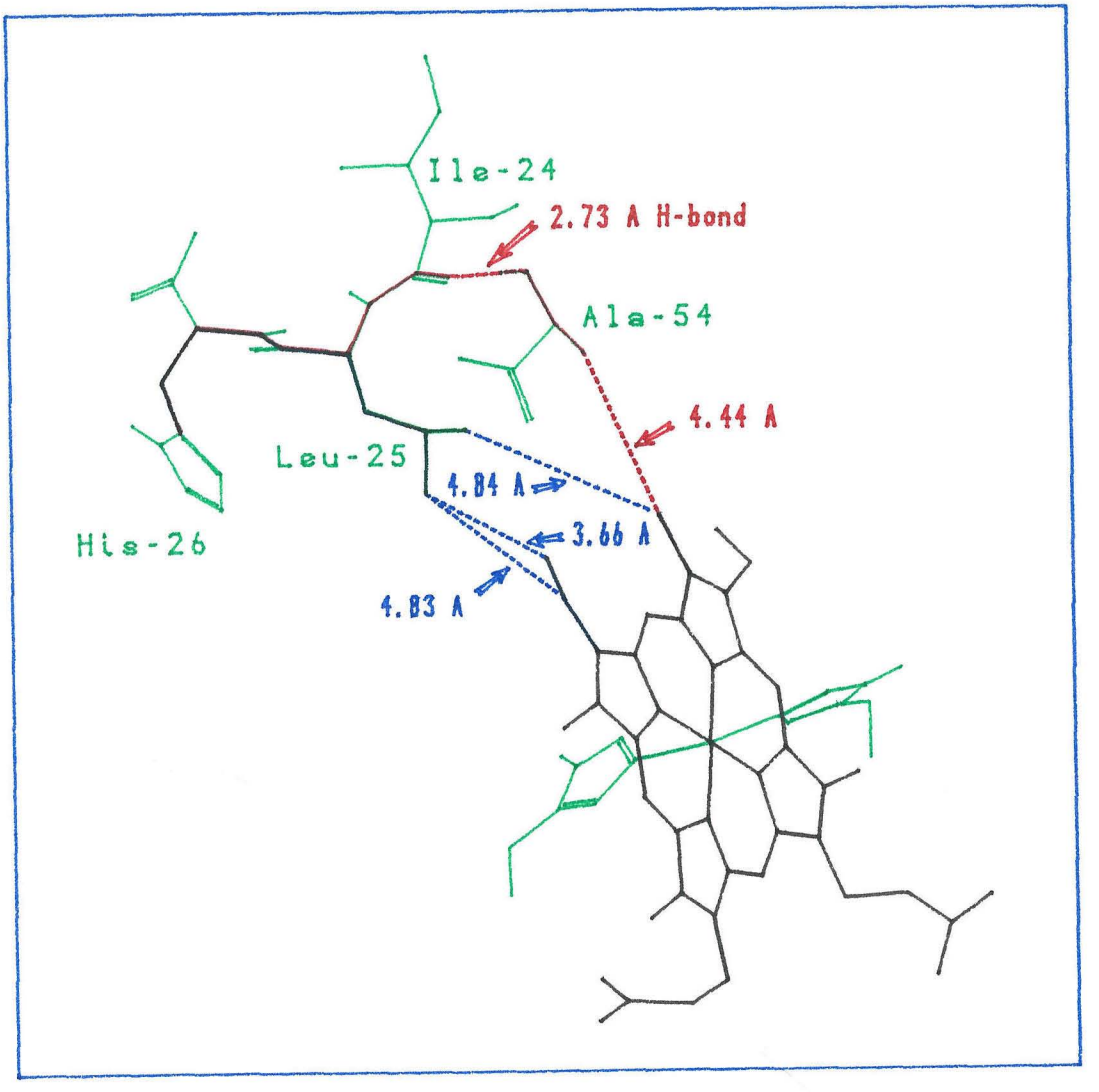
Ile-24
2.73 A H-bond
Ala-54
4.44 A
Leu-25
4.84 A
3.66 A
His-26
4.83 A

heme orientation but with an estimated 60:40 relative abundance. Consequently, there is some ambiguity in the exact positions of the 2- and 4-vinyl groups in the crystal structure.[15] Unlike the case of WT-*b*$_5$, the best pathway for LM-*b*$_5$ involves the C_β of the 2-vinyl. The jump from the Leu-25 $C_{\delta 1}$ to the 2-vinyl C_α is much longer (4.8 Å); thus this pathway (3-methyl replacing C_α) is likely to have poor coupling for LM-*b*$_5$ with the minor heme orientation. If the pathway analysis is correct, with both components in solution during a flash-photolysis experiment, their rates would differ by more than a factor of ten. However, no slow component in k_{obs} was observed in ET kinetics traces for Ru(H26)LM-*b*$_5$.

Pathways for Ru(H26)DP-b$_5$

The native protoporphyrin was substituted with deuteroporphyrin (Figure 7) to test the pathway predictions directly. Since H_{AB}' decays rapidly with distance in through-space jumps, replacing the 2-vinyl group with a proton effectively shuts down the shortest pathway found for WT-*b*$_5$ and LM-*b*$_5$. In DP-*b*$_5$ the jump from Leu-25 ($C_{\delta 1}$) to the heme is 5 Å (Figure 43), cutting $(H_{AB}')^2$ for this pathway to 5×10^{-10}. As a result, less favored paths in the other proteins are more competitive in DP-*b*$_5$.

The best pathway in DP-*b*$_5$ involves nine covalent bonds and a 4.5 Å jump from Leu-25 to the heme 3-methyl (Figure 43; an extra covalent bond is counted since the methyl is not conjugated with the porphyrin ring). Consequently, the value of $(H_{AB}')^2$ in Ru(H26)DP-*b*$_5$ is predicted to be over an order of magnitude lower than the others (Table 2). From the microscopic perspective of the pathway model, a 0.7 Å difference in R has a dramatic effect on the ET rate. Once again, the predicted change in coupling parallels the observed k_{ET}.

Looking at an alternate pathway through the His-63 Fe ligand provides insight into the cyt *b*$_5$ system. Although this pathway (Figure 43) avoids the 3 - 4 Å jumps from Leu-25 or Ala-54 to the heme, it still involves a 3.7 Å jump to Phe-58 plus a 2.7 Å H-

Figure 43. Possible ET pathways for His-26 to heme in DP-b_5. With the 2-vinyl missing, pathways for this derivative must include longer space jumps or less direct routes to the heme.

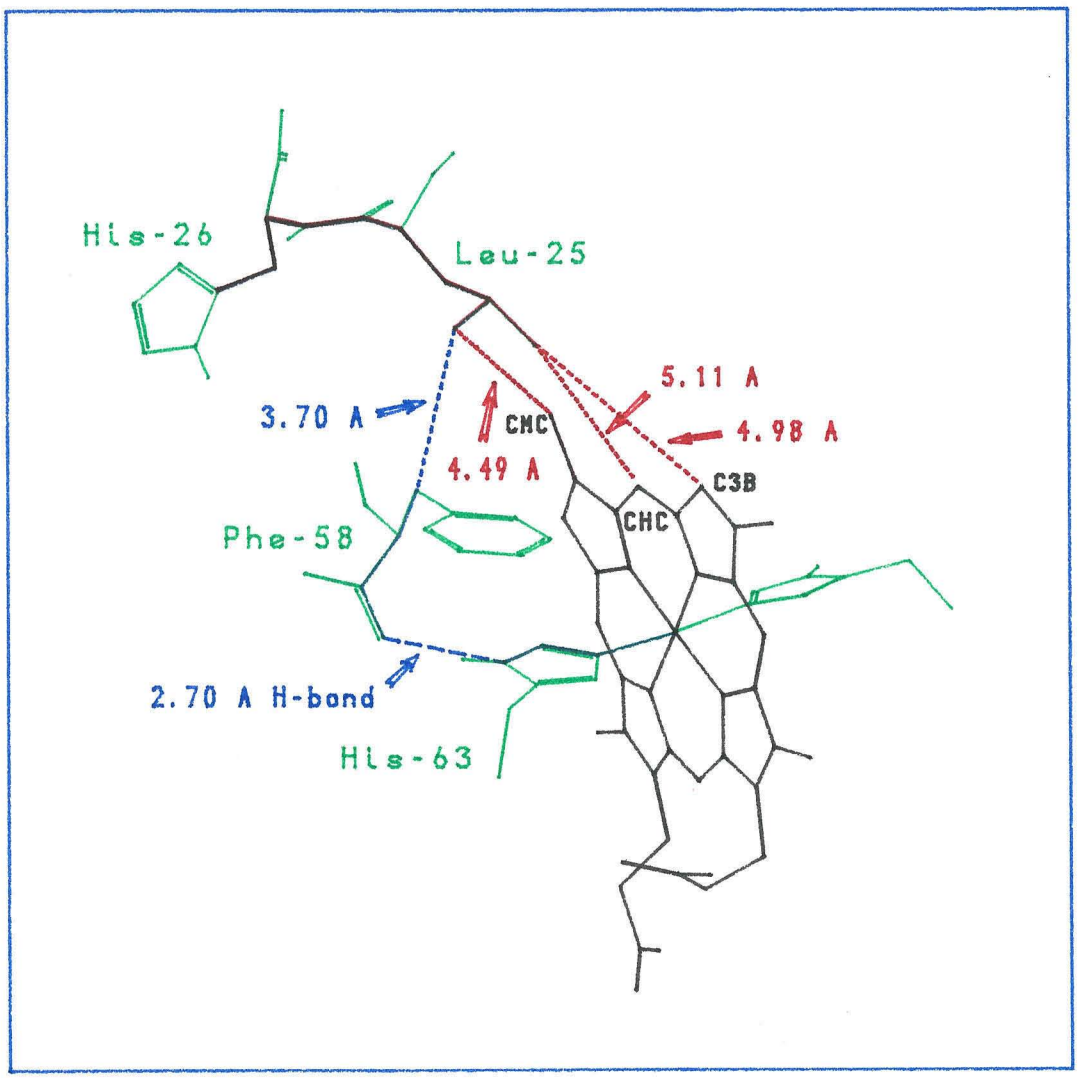
His-26
Leu-25
3.70 A
CMC
4.49 A
5.11 A
4.98 A
C3B
CHC
Phe-58
2.70 A H-bond
His-63

bond to His-63. The resulting $(H_{AB}')^2$ of 2.3 x 10^{-11} is on a par with values for other secondary ET pathways; all are 2 to 3 orders of magnitude lower that $(H_{AB}')^2$ for the pathway through the Leu-25 side chain. This observation is important because it means that in calculating k_{ET}, one can reasonably consider just $(H_{AB}')^2$ for this best pathway. In other words, according to the pathway model, k_{ET}'s for all three proteins studied should be reflected in the differences in the length of the Leu-25 ($C_{\delta 1}$)-to-heme through-space jump.

Calculating k_{ET} for Ru(H26)WT-b_5, Ru(H26)LM-b_5, and Ru(H26)DP-b_5

In order to calculate ET rate constants from H_{AB}' values (Eqs. 9,10), an estimate of the reorganization energy accompanying ET in ruthenium-modified cyt b_5 (λ_{b5}) is required. A reasonable approximation of λ_{b5} is 1.2 eV, which was obtained from an analysis of ET rates in Ru(H33)Cyt *c*.[32] Because some studies suggest that cyt b_5 may have a heme reorganization energy greater than that of cyt *c*, calculations using λ_{b5} = 1.4 eV were done for comparison.†

One more approximation was made in calculating ET rate constants. Since $H_{AB}°$ is not known, H_{AB}' was scaled to a reference value, H_{ABref}', and a corresponding experimental rate constant, k_{ref}, to give k_{calc}:

$$k_{calc} = k_{ref} [(H_{AB}')^2 / (H_{ABref}')^2] (FC/FC_{ref}).$$

The rate constants calculated using this approach, referenced both to the well-studied His-33 cyt *c* system [32] and to Ru(H26)WT-b_5 itself, are given in Table 2. The ratio of Franck-Condon factors corrects for differences in $\Delta G°$ and/or λ. Rate constants

---

† Calculations based on self-exchange reactions for cyt b_5 and cyt *c* give values of λ_{heme} = 0.6 and 0.35 eV (per heme).[20] Subtracting the λ_{heme} for cyt *c* from λ_{total} = 1.2 eV obtained for ruthenium-modified cyt *c* [32] provides an estimate of $\lambda_{Ru,solvent}$ = 0.85 eV. For modified cyt b5, then, $\lambda_{heme} + \lambda_{Ru,solvent} \approx \lambda_{total}$ = 1.45 eV.

calculated in the same way but with an exponential decay model for H_{AB}' ($\beta = 0.9$ Å^{-1}) are included for comparison.

It is clear from the calculated and observed ET rates in Table 2 that the pathway model is superior to an exponential distance decay relationship in predicting both the trends in rates and their orders of magnitude. The good fit for predictions referenced to Ru(H33)Cyt *c* ($\lambda_{b5} = 1.2$ eV) and the internally consistent values referenced to Ru(H26)WT-b_5 suggest that similar ET mechanisms operate in the two modified proteins. This observation also tends to discount an aromatic effect that is due to Phe-58. Of particular note is the relatively poor electronic coupling in Ru(H26)DP-b_5, which strongly indicates that through-space interactions can play a key role in controlling long-range ET rates in proteins.

Temperature Dependence of ET in Ru(H26)WT-b_5

In order to determine the activation parameters for the intramolecular ET reaction in cyt b_5, a temperature-dependence study was performed over the range 2 to 38 °C. The dependence of the ET rate on concentration for each temperature is shown in Figure 44. Unfortunately, the need for extrapolation to determine k_{ET}'s resulted in an Eyring plot (Figure 45) with experimental uncertainties too large for useful conclusions to be drawn ($\Delta H^{\ddagger} = 6(4)$ kcal/mol).

ET in Ru(H80)TR26-b_5

Ru(H80)TR26-b_5 was flashed under the same conditions used for the His-26 derivatives. At 0.8 to 2.5 mM protein concentrations, a first-order decay was observed (Figure 46), but the extrapolated k_{ET} was within experimental error of zero (Figure 47). Higher driving forces must be accessed before the intramolecular rate for this isomer can be distinguished from the bimolecular ET evident in the other modified samples.

Figure 44. A plot of the concentration dependence of k_{obs} for ET in Ru(H26)WT-b_5 at varied temperature. Lines are least-squares fits to the data. The extrapolated values of k_{ET} at the different temperatures are tabulated below.

Temperature (°C)	k_{ET} (s^{-1})
38.0	2.6 ± 1.0
30.0	1.4 ± 0.7
25.0	1.4 ± 0.4
20.0	1.2 ± 0.5
10.0	0.6 ± 0.3
2.0	0.9 ± 0.3

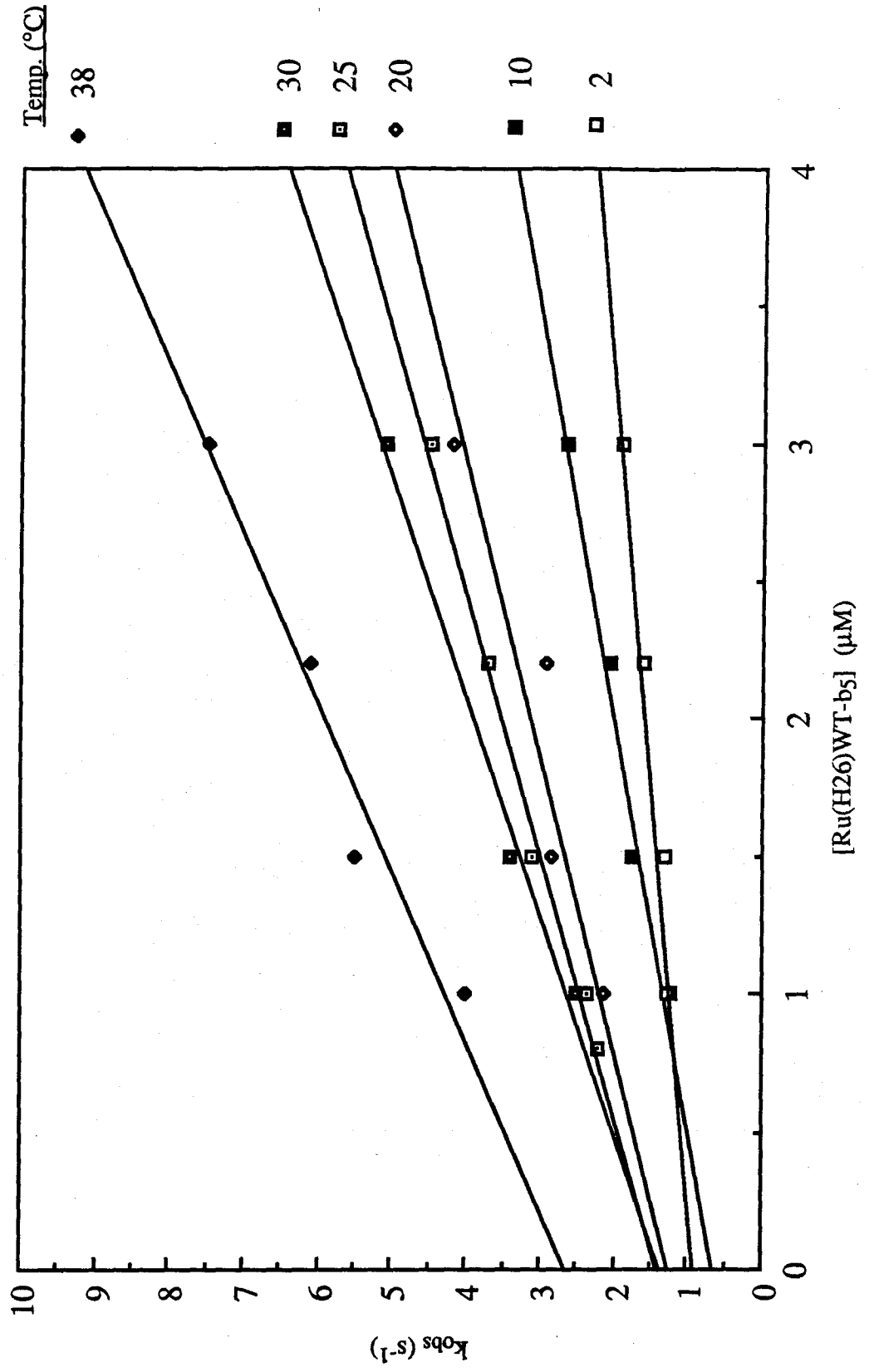
Temp. (°C)
38
30
25
20
10
2
k_{obs} (s^{-1})
0
1
2
3
4
5
6
7
8
9
10
[Ru(H26)WT-b5] (μM)

Figure 45. An Eyring plot for Ru(H26)WT-b_5 variable-temperature ET kinetics results. For a discussion of the error bars, refer to the Experimental Section.

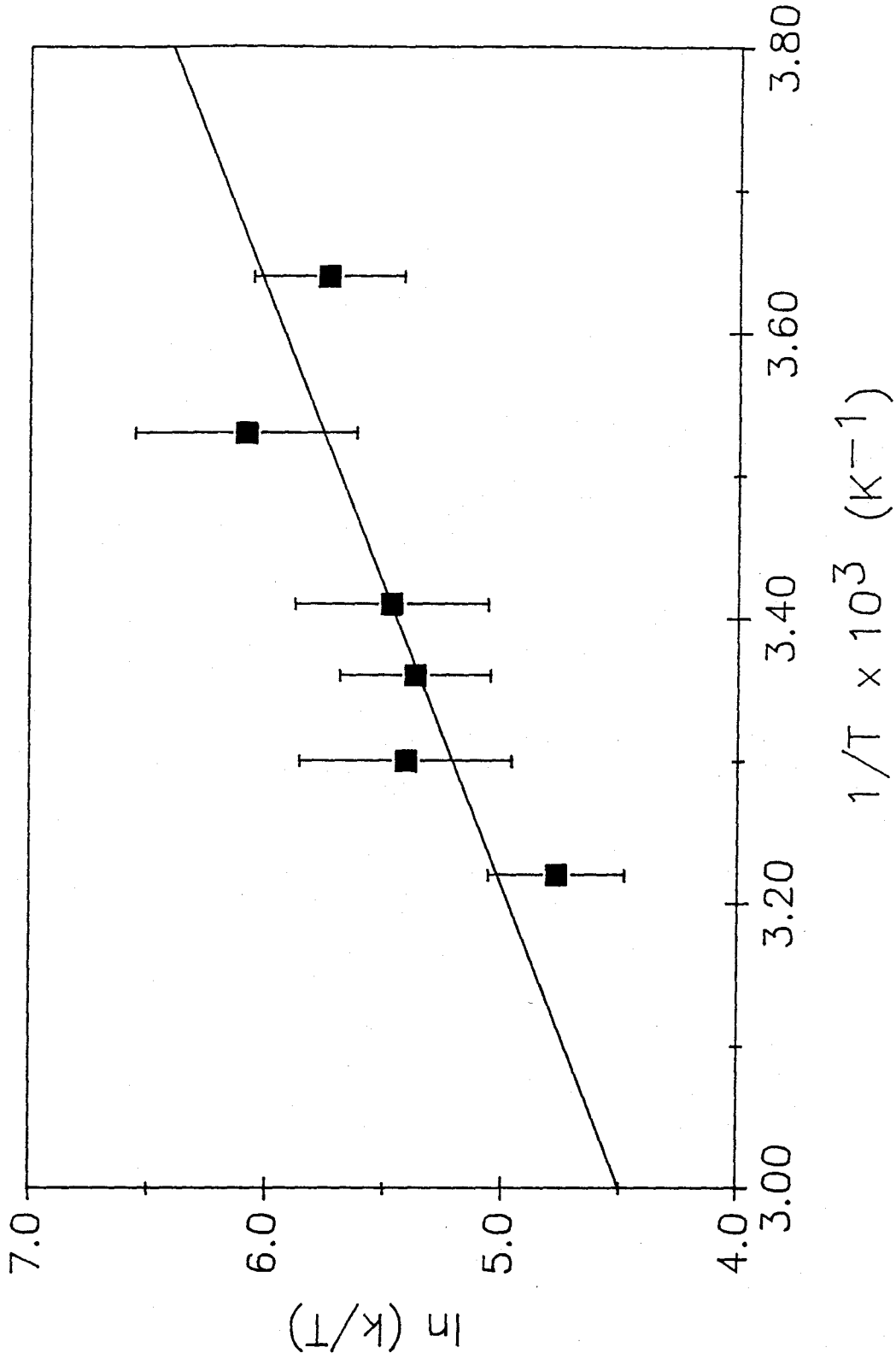
7.0
6.0
5.0
4.0
ln (k/T)
3.00
3.20
3.40
3.60
3.80
1/T x 10^3 (K^-1)

Figure 46. Flash-photolysis a) voltage/time and b) absorbance/time traces for 1 μM Ru(H80)TR26-b_5 (555 nm). Analysis using SI-FIT gave the fit shown and k_{obs} = 0.9 s^{-1}.

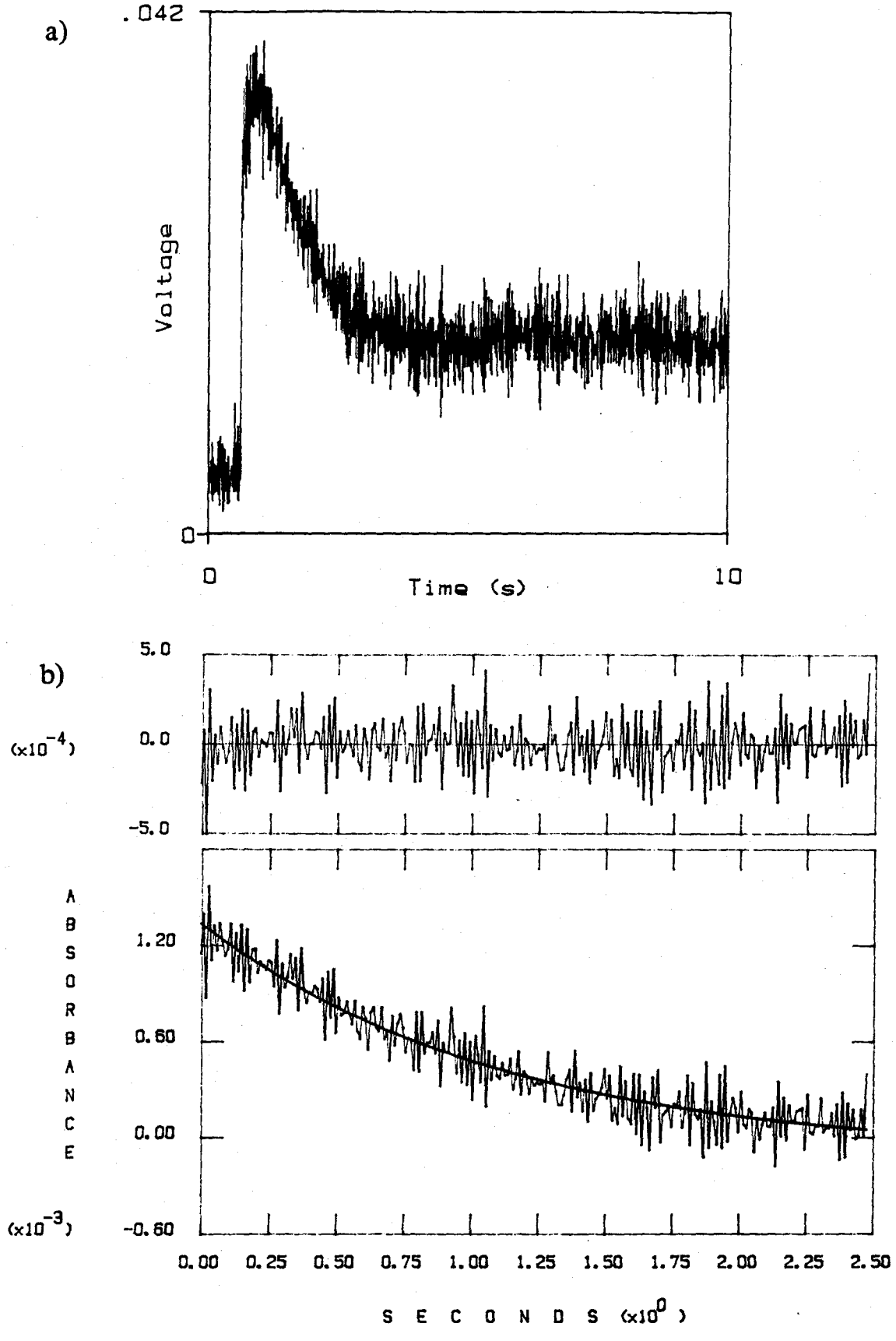
a)
.042
Voltage
0
0
Time (s)
10
b)
5.0
0.0
-5.0
(x10^{-4})
ABSORBANCE
1.20
0.60
0.00
-0.60
(x10^{-3})
0.00 0.25 0.50 0.75 1.00 1.25 1.50 1.75 2.00 2.25 2.50
SECONDS (x10^{0})

Figure 47. Plot of the k_{obs} concentration dependence for the ET reaction of Ru(H80)TR26-b_5. The intercept is within experimental error of 0 s^{-1}.

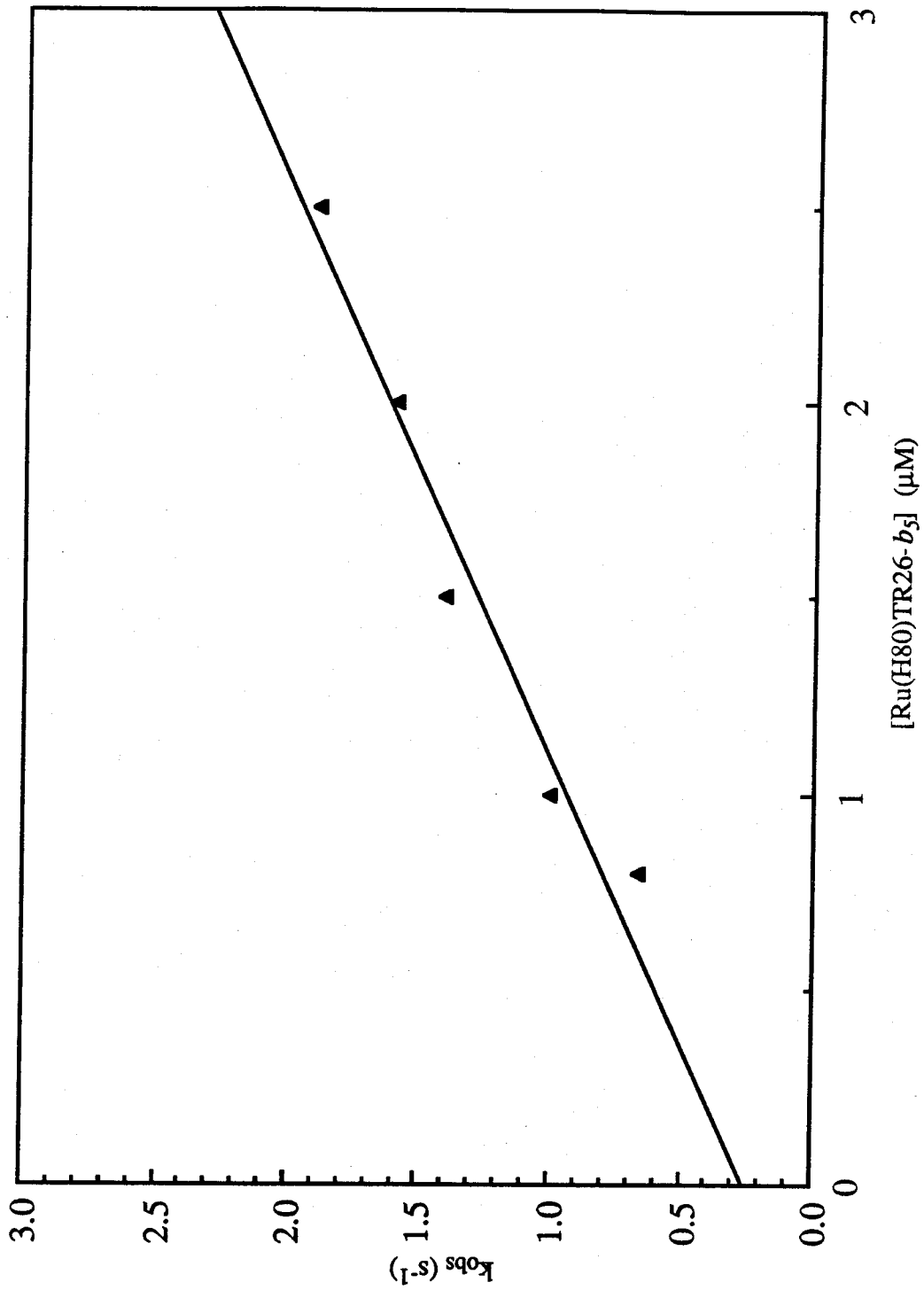
3.0
2.5
2.0
1.5
1.0
0.5
0.0
k_{obs} (s^{-1})
0
1
2
3
[Ru(H80)TR26-b_{51}] (μM)

Since His-80 is approximately 21 Å from the heme and the driving force is low (ΔG° = -0.08 eV; the same as in Ru(H26)WT-b_5), the rate of intramolecular ET for Ru(H80)TR26-b_5 is expected to be too low for observation by flash photolysis; k_{calc} = 1 x 10^{-3} s^{-1} by the exponential decay model. A search for ET pathways revealed that in addition to being much longer than those for His-26, the best His-80 pathways still encounter the long space jumps from Leu-25 to the heme (Figure 48). The shortest path consists of 12 covalent bonds, 2 H-bonds (2.87, 2.84 Å), and 2 space jumps (2.27, 3.81 Å), giving $(H_{AB}')^2$ = 5.5 x 10^{-13} and k_{calc} = 4 x 10^{-5} s^{-1}.

Of note is that the shortest pathway includes the carbonyl oxygen of Tyr-27, with the aromatic ring in close proximity (Figure 48). The present version of the pathway program does not account for any possible effects aromatic residues may have on the coupling, but perhaps future versions will. In any case, measuring the rate for a derivative with a higher driving force would be interesting because the rates predicted by the two models differ by more than an order of magnitude.

His-15 Pathways

Although no rates for His-15 derivatives were measured, the pathway analysis for this site was performed for completeness. Being on the other side of the protein from the the other two histidines, His-15 is expected to access different pathways. In fact, the shortest pathways are distinct from those described above, passing through either Leu-32 or Leu-23 (Figure 49). However, the jumps to the heme from these leucines are no shorter than from Leu-25 (3.8 to 4.6 Å), and $(H_{AB}')^2$ = 4 x 10^{-11}, giving k_{calc} = 3 x 10^{-3} s^{-1}. The exponential decay model predicts a faster rate for this 15 Å separation: k_{calc} = 0.3 s^{-1}.

Figure 48. Possible ET pathways from His-80 to the heme in WT-b_5. The long through-space jumps found in the His-26 pathways are evident here as well.

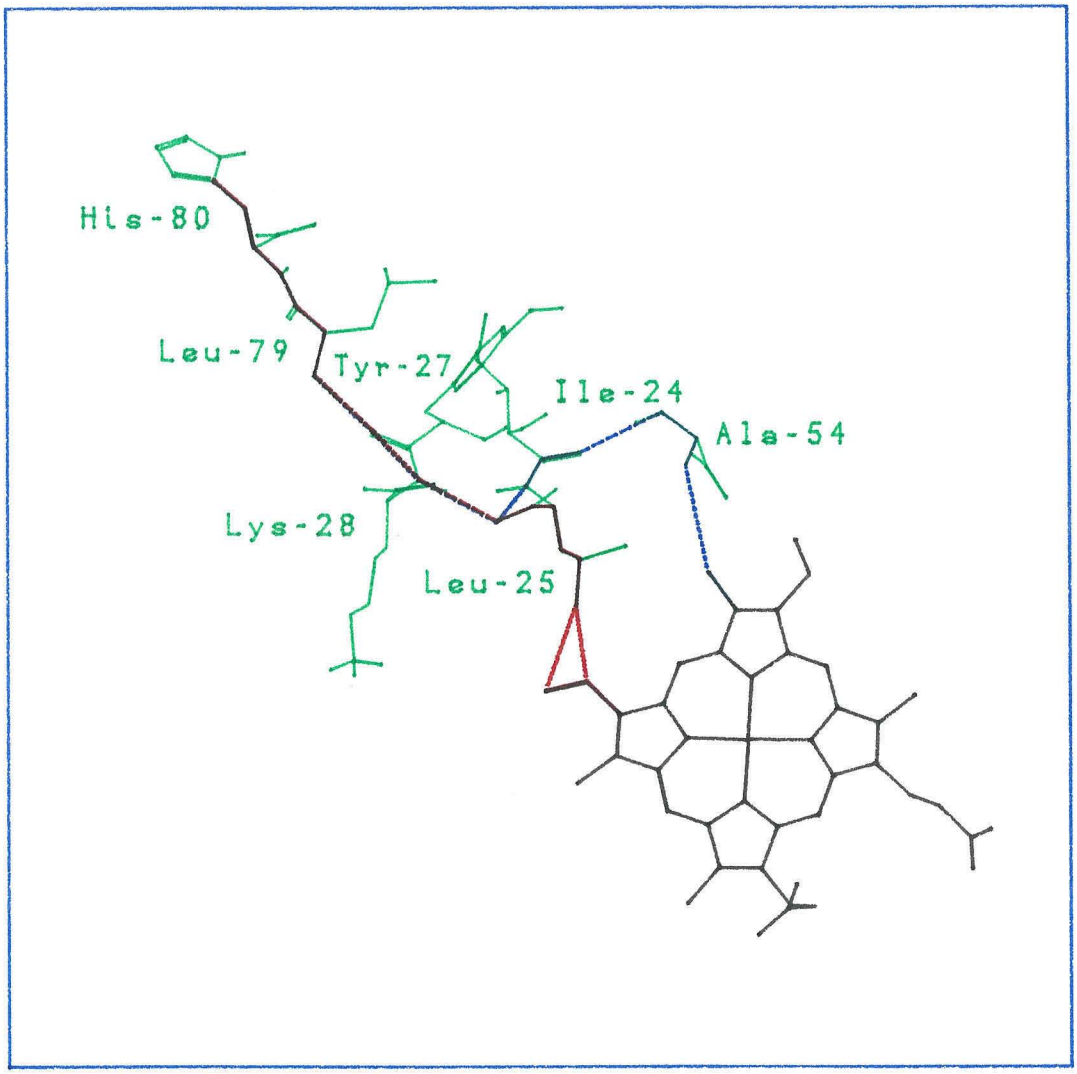
His-80
Leu-79
Tyr-27
Ile-24
Ala-54
Lys-28
Leu-25

Figure 49. Possible ET pathways from His-15 to the heme in WT-b_5. Although the pathways from this residue are distinct from those of His-26 and His-80, long space jumps are still required.

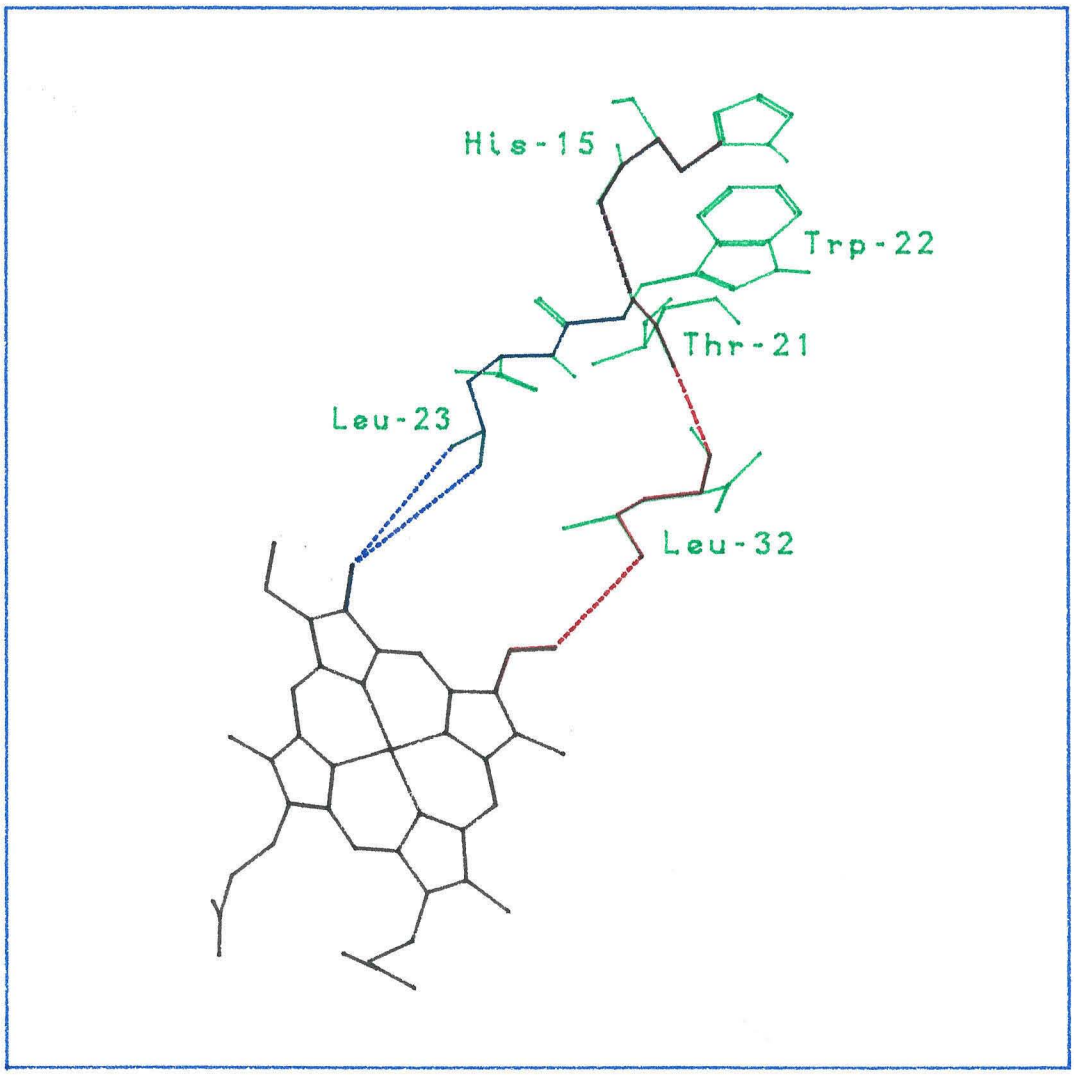
His-15
Trp-22
Thr-21
Leu-23
Leu-32

Summary

Flash photolysis conditions for studying intramolecular ET from Fe^{2+} to Ru^{3+} in ruthenated cyt b_5 were developed. The best method employed a $[Ru(bpy)_3]^{2+*}$ initiator quenched reductively by EDTA, and initially oxidized protein in a high ionic-strength buffer. The observed rate constants for a_5Ru(His-26) derivatives of WT-b_5, LM-b_5, and DP-b_5 displayed a mild concentration dependence; the k_{ET}'s determined by extrapolation to zero concentration were 1.4(4), 6(1), and 0.2(1) s^{-1}. The differences in these rates did not correlate with donor-acceptor separation, driving force, or reorganization energy.

A search of the protein structures for possible ET pathways indicated that the dominant pathway from His-26 to the heme involves a through-space jump from Leu-25 to the closest heme atom, a distance that differs for the three proteins. Since alternate pathways were found to have significantly lower predicted electronic coupling, according to the pathway model, the variation in the Leu-25-to-heme space jump should be reflected in the observed ET rates. In fact, rate constants calculated using the best pathway $(H_{AB}')^2$ values (referenced to Ru(H33)Cyt *c* and to Ru(H26)WT-b_5) successfully reproduced the experimental ET rates for the three proteins. This correlation suggests that a similar ET mechanism is operative in cytochromes b_5 and *c*, and also that through-space jumps in ET pathways can control ET rates.

Flash photolysis of a His-80-modified cyt b_5 derivative (Ru(H80)TR26-b_5) was also studied. As expected from the long edge-to-edge distance and poor electronic coupling predicted by pathway analysis, k_{ET} was within experimental error of 0 s^{-1}. Higher driving forces must be employed to study intramolecular ET in this isomer.

REFERENCES

(1) Nocera, D. G.; Winkler, J. R.; Yocom, K. M.; Bordignon, E.; Gray, H. B. *J. Am. Chem. Soc.* **1984**, *106*, 5145-5150.

(2) Winkler, J. R.; Nocera, D. G.; Yocom, K.M.; Bordignon, E.; Gray, H. B. *J. Am. Chem. Soc.* **1982**, *104*, 5798-5800.

(3) Lieber, C. M.; Karas, J. L.; Gray, H. B. *J. Am. Chem. Soc.* **1987**, *109*, 3778-3779.

(4) Mayo, S. L.; Ellis, W. R., Jr.; Crutchley, R. J.; Gray, H. B. *Science* **1986**, *233*, 948-952.

(5) Crutchley, R. J.; Ellis, W. R.,Jr.; Gray, H. B. *J. Am. Chem. Soc.* **1985**, *107*, 5002-5004.

(6) Reid, L. S.; Mauk, A. G. *J. Am. Chem. Soc.* **1982**, *104*, 841-845.

(7) Reid, L. S.; Taniguchi, V. T.; Gray, H. B.; Mauk, A. G. *J. Am. Chem. Soc.* **1982**, *104*, 7516-7519.

(8) Rillema, D. P.; Endicott, J. F.; Papaconstantinou, E. *Inorg. Chem.* **1971**, *10*, 1739.

(9) Milder, S. J.; Goldbeck, R. A.; Kliger, D. S.; Gray, H. B. *J. Am. Chem. Soc.* **1980**, *102*, 6761-6764.

(10) Guggenheim, E. A. *Philos. Mag.* **1926**, *2*, 538-543.

(11) Albin, M.; Gray, H. B. *Computers and Chemistry* **1989**, *13*, 173-177.

(12) Osvath, P.; Salmon, G. A.; Sykes, A. G. *J. Am. Chem. Soc.* **1988**, *110*, 7114-7118.

(13) Karas, J. L. Ph.D. Thesis, California Institute of Technology, 1989.

(14) Mathews, F. S. *Biochim. Biophys. Acta* **1980**, *622*, 375-379.

(15) Funk, W. D.; Lo, T. P.; Mauk, M. R.; Brayer, G. D.; MacGillivray, R. T. A.; Mauk, A. G., *Biochemistry* **1990**, *29*, 5500-5508.

(16) a) Go, M.; Miyazawa, S. *Int. J. Pept. Protein Res.* **1980**, *15*, 211-224. b) Alber, T.; Dao-pin, S.; Nye, J. A.; Muchmore, D. C.; Matthews, B. W. *Biochemistry* **1987**, *26*, 3754-3758. c) Baldwin, R. L.; Eisenberg, D. In *Protein Engineering*; Oxender, D. L. and Fox, C. F., Eds.; Alan R. Liss: New York, 1987, pp. 127-148.

(17) a) Beratan, D. N.; Onuchic, J. N. *Photosynthesis Research* **1989**, *22*, 173-186. b) Beratan, D. N.; Onuchic, J. N.; Hopfield, J. J. *J. Phys. Chem.* **1987**, *86*, 4488-4498.

(18) Beratan, D. N.; Onuchic, J. N.; Betts, J. N.; Bowler, B. E.; Gray, H. B. *J. Am. Chem. Soc.*, in press.

(19) Kostic, N. M.; Margalit, R.; Che, C. -M.; Gray, H. B. *J. Am. Chem. Soc.* **1983**, *105*, 7765-7767.

(20) Dixon, D. W.; Hong, X.; Woehler, S. E.; Mauk, A. G.; Shishta, B. P. *J. Am. Chem. Soc.* **1990**, *112*, 1082-1088.

(21) Chapman, S. K.; Davies, D. M.; Vuik, C. P. J.; Sykes, A. G. *J. Am. Chem. Soc.* **1984**, *106*, 2692-2696.

(22) Marcus, R. A.; Sutin, N. *Biochim. Biophys. Acta* **1985**, *811*, 265-322.

(23) Reid, L. S.; Lim, A. R.; Mauk, A. G. *J. Am. Chem. Soc.* **1986**, *108*, 8197-8201.

(24) Axup, A. W.; Albin, M.; Mayo, S. L.; Crutchley, R. J.; Gray, H. B. *J. Am. Chem. Soc.* **1988**, *110*, 435-439.

(25) a) Elias, H.; Chou, M. H.; Winkler, J. R. *J. Am. Chem. Soc.* **1988**, *110*, 429-434. b) Durham, B.; Pan, L. P.; Long, J. P.; Millett, F. *Biochemistry* **1989**, *28*, 8659-8665.

(26) Peterson-Kennedy, S. E.; McGourty, J. L.; Kalweit, J. A.; Hoffman, B. M. *J. Am. Chem. Soc.* **1986**, *108*, 1739-1746.

(27) Gingrich, D. J.; Nocek, J. M.; Natan, M. J.; Hoffman, B. M. *J. Am. Chem. Soc.* **1987**, *109*, 7533-7534.

(28) a) Therien, M. J.; Chang, J.; Raphael, A. R.; Bowler, B. E.; Gray, H. B. *Stucture and Bonding*; Palmer, G., Ed.; in press. b) Therien, M. J.; Bowler, B. E.; Selman, M. A.; Gray, H. B.; Chang, I. -J.; Winkler, J. R. *ACS Symposium Series*, in press.

(29) Bowler, B. E.; Meade, T. J.; Mayo, S. L.; Richards, J. H.; Gray, H. B. *J. Am. Chem. Soc.* **1989**, *111*, 8757-8759.

(30) Keller, R. M.; Wuthrich, K. *Biochim. Biophys. Acta* **1980**, *621*, 204-217.

(31) a)La Mar, G. N.; Burns, P. D.; Jackson, J. T.; Smith, K. M.; Langry, K. C.; Strittmatter, P. *J. Biol. Chem.* **1981**,*256*, 6075. b) Walker, F. A.; Emrick, D. Rivera, J. E.; Hanquet, B. J.; Buttlaire, D. H. *J. Am. Chem. Soc.* **1988**, *110*, 6234-6240. c) McLachlan, S. J.; La Mar, G. N.; Burns, P. D.; Smith, K. M; Langry, K. C. *Biochim. Biophys. Acta* **1986**, *874*, 274-284.

(32) Meade, T. J.; Gray, H. B.; Winkler, J. R. *J. Am. Chem. Soc.* **1989**, *111*, 4353-4356.

CHAPTER IV

ELECTRON TRANSFER IN *ALCALIGENES DENITRIFICANS* AZURIN

INTRODUCTION

Azurin is a small (14 kdal) bacterial cupredoxin containing one type I (blue) copper per molecule. Its physiological role has not yet been clearly defined, but it may serve to transfer electrons from cytochrome c_{551} to cytochrome oxidase.[1] The azurins from two species of bacteria have been crystallographically characterized: *Pseudomonas aeruginosa* (*P. a.*) to 2.7 Å,[2] and *Alcaligenes denitrificans* (*A. d.*) to 1.8 Å.[3,4] They share a common general structure that has been described as a β-barrel; eight β-strands surround a central core, with the copper bound in a hydrophobic pocket near one end (Figure 50).

One feature of azurin that attracted early attention was its deep-blue color, later determined to arise from charge transfer from cysteine sulfur to Cu(II).[5] The intense visible absorption (~ 620 nm), a low hyperfine coupling constant in the EPR spectrum, and a high reduction potential (245 - 308 mV vs. NHE)[6] are the result of the unusual arrangement of ligands around the copper imparted by the protein. Figure 51 shows the copper site of *A. d.* azurin. The coordination sphere includes a sulfur from Cys-112 and nitrogens from two histidines (His-46 and His-117) in an approximate trigonal planar geometry. Axially, a methionine sulfur (Met-121) and possibly the carbonyl oxygen from Gly-45 form long, weak bonds to the copper.[4] This ligand geometry is peculiar to protein complexes of copper and is thought to have evolved to minimize structural reorganization on reduction or oxidation.[7]

Azurin is interesting for intramolecular ET investigations because unlike the cytochromes and myoglobin, the redox prosthetic group is a copper rather than an iron heme. Also, the secondary structure of azurin is almost entirely β-sheet, while the heme proteins are largely α-helical. In order to determine how azurin's distinctive properties affect ET, His-83 on the surface of *P. a.* azurin (11.7 Å from the copper) was modified with ruthenium, and the intramolecular ET rate was measured.[8] Although the donor-

Figure 50. The crystal structure of *Alcaligenes denitrificans* azurin.[3,4] The peptide backbone is shown in green, the copper site in blue, and the surface histidines in red. The azurin structure consists of eight β–strands forming a "β–barrel" with a hydrophobic interior. The one α-helical flap can be seen on the left.

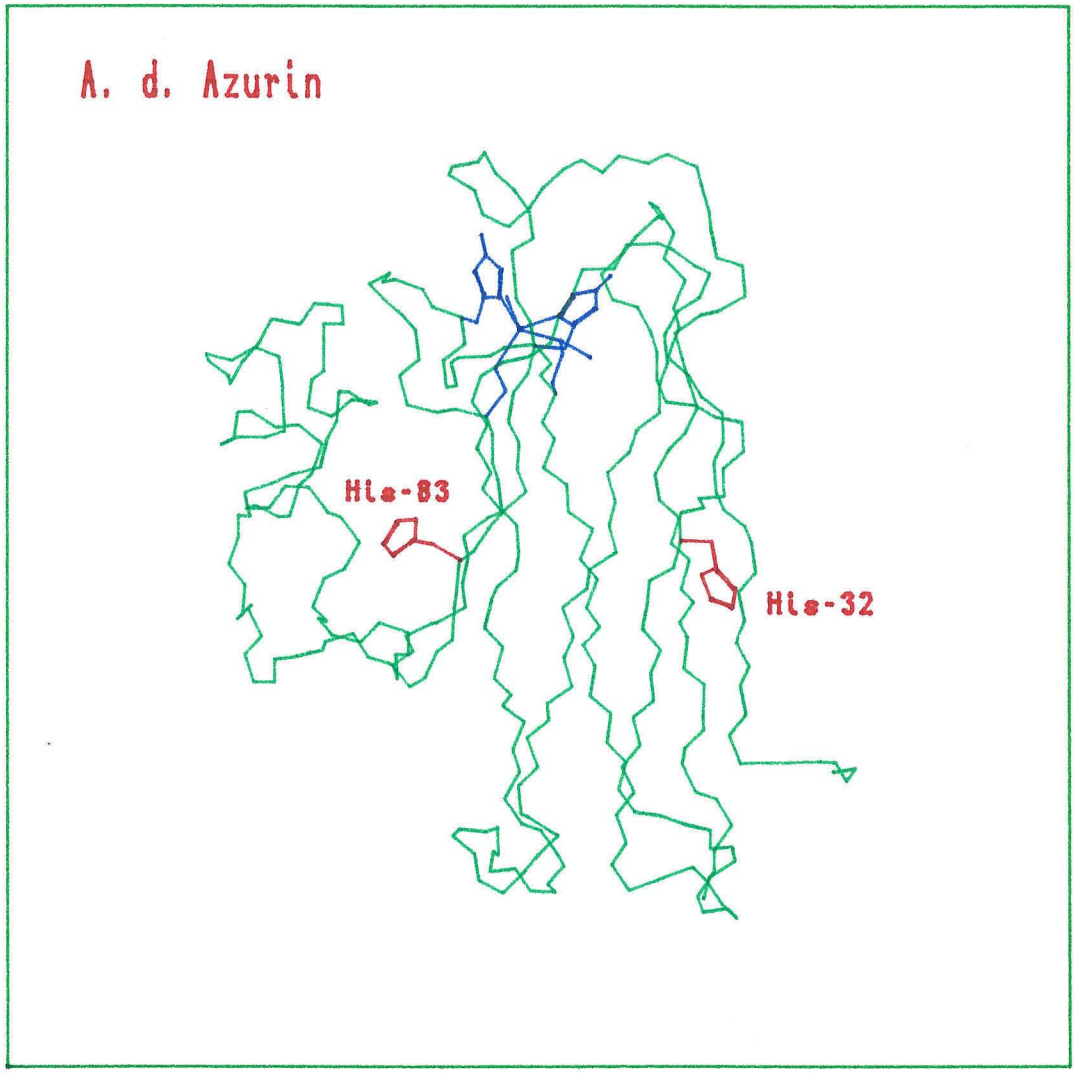
A. d. Azurin
His-83
His-32

Figure 51. The copper site of *A. d.* azurin.[4] The bond lengths (Å) between copper and the ligands are as follows: Cys-112 (S), 2.13; His-46 (N), 2.06; His-117 (N), 1.96; Met-121 (S), 3.13; Gly-45 (O), 3.11.

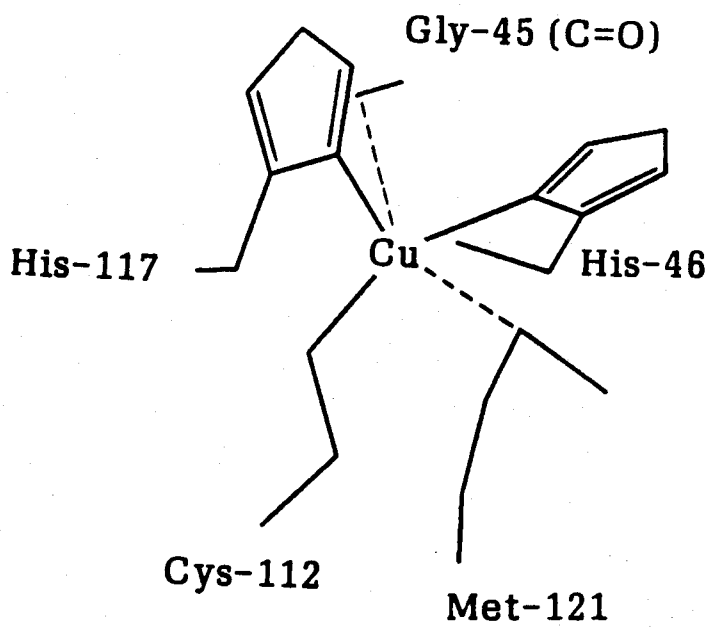
Gly-45 (C=O)
His-117
Cu
His-46
Cys-112
Met-121

acceptor separation and ET driving force are comparable to those in modified cytochrome *c*, ET in ruthenated *P. a.* azurin was an order of magnitude slower. From a variable temperature study of the ET rate, the authors were able to calculate an upper limit of 7.1 kcal/mol for the blue-copper site reorganizational enthalpy.[9]

Since a high reorganization energy in azurin is unlikely, the reason for the slow rate in azurin may be that there is poor electronic coupling between ruthenium and copper. Of interest for ET studies, then, is how the rate of ET in azurin depends on the separation of the two redox sites. Does a simple exponential decay with distance explain the rate behavior (perhaps with a different value of β than with the cytochromes), or do the pathways permitted by the β-barrel structure limit the rate, and if so, how? Also, is the distance dependence isotropic, or does the ET rate vary with the orientation of the ruthenium tag relative to the copper center?

Some of these questions can be addressed by studying *A. d.* azurin, which is 64% homologous in amino-acid sequence to *P. a.* azurin. This protein shares His-83 as a surface residue and has another histidine (His-32) at a slightly longer distance from the copper (12.7 Å). Computer modeling indicates that His-83 and His-32 have the same solvent-accessible surface area (46 $Å^2$); thus they are expected to be equally reactive towards ruthenium modification.[6] ET from the His-32 site would help to elucidate the effect of relative donor-acceptor orientation and would also provide an indication of the distance dependence of ET in azurin. Studying ET in *A. d.* azurin modified at His-83 is also attractive because small differences in the structure from that of *P. a.* azurin might alter the electronic coupling enough to change k_{ET}, and thus allow a probe of medium effects.

With these goals in mind, Cindy St. Clair performed preliminary ruthenium-modification and characterization studies of *A. d.* azurin.[6] In the present work, the modification conditions were re-examined, the characterization was completed, and ET rates were measured.

EXPERIMENTAL

Unless noted otherwise, the materials and methods used in the study of azurin were the same as those detailed in Chapters II and III.

Preparation of Ruthenium-Modified *A. d.* Azurin

There is a lack of agreement in the literature over the absorbance extinction coefficient for *A. d.* azurin. Groeneveld and Canters used $\varepsilon_{625} = 4800\ M^{-1}\ cm^{-1}$,[10] C. St. Clair chose the *P. a.* value ($5700\ M^{-1}\ cm^{-1}$),[6] and Ainscough *et al.* reported $\varepsilon_{619} = 5100\ M^{-1}\ cm^{-1}$.[11] For determining concentration of protein in this work, a compromise value of $\varepsilon_{620} = 5000\ M^{-1}\ cm^{-1}$ was used.

The procedure for modifying azurin was similar to that employed for cyt b_5 (Chapter II). (C. St. Clair prepared some of the modified protein used in this project by a slightly different, but equivalent method.)[6] A concentrated solution of about 30 mg (MW 14,000) *A. d.* azurin in 325 mM HEPES, pH 7.5, and extra HEPES in a separate flask were degassed by the Ar-purge method. A 10-fold molar excess of $[a_5Ru(OH_2)](PF_6)_2$ was taken into the glove box as a solid, dissolved in the extra HEPES, and filtered (Millipore 0.2 μm) into the protein solution (5 mg/mL final protein concentration). The resulting pale yellow, reduced protein solution was stirred briefly, then allowed to react at room temperature for 30 min. The reaction was quenched by addition of an excess of Na[Co(EDTA)], and the protein was allowed to oxidize overnight at 4 °C before removal of small molecules by gel filtration. The product mixture was washed with several Centricon ultrafiltration cycles into $\mu = 50$ mM $NH_4(CH_3CO_2)$, pH 5.2, in preparation for FPLC chromatography. More Na[Co(EDTA)] was often added at this stage to maintain the cupric oxidation state.

Solutions of ruthenium-modified azurin were separated using a Pharmacia FPLC chromatography system with a Mono S (HR 5/5 or 10/10) cation-exchange column eluted

with a gradual salt gradient at room temperature (according to the gradient programs in Figure 52). Buffer A was μ = 50 mM $NH_4(CH_3CO_2)$, pH 5.2, and buffer B was A + 1 M NaCl. The eluate was monitored at 280 nm, and fractions were collected at regular volume intervals (1 - 4 mL).

NMR Spectra

Spectra were recorded on a Bruker AM500 spectrometer at 309 K, and referenced to DSS. Samples were prepared by washing the fully oxidized protein into D_2O ($\geq$ 4 times) and then into μ = 20 mM NaPi in $D_2O \geq 4$ times by Centricon ultrafiltration. Resonance from residual water was not suppressed. The sharp histidine C_2H resonances were enhanced by Gaussian multiplication, and their assignments [12] were verified by pH titration with DCl and NaOD.

Differential Pulse Voltammetry

The methods and conditions used for this experiment were identical to those outlined in Chapter II.

Flash Photolysis

Flash photolysis was carried out using a 15-cm pathlength, water-jacketed (25 °C) cell containing approximately 11 mL of the following solution: 7.25 mM Na_2EDTA, 65 μM $[Ru(bpy)_3]Cl_2$ (bpy = 2,2'-bipyridine),[13] and 1.2 to 4 μM oxidized protein, in μ = 500 mM NaPi, pH 7.0. (The protein was maintained in the cupric state by storing it with an excess of Na[Co(EDTA)], then removing the oxidant by gel filtration on the day of use.) The component solutions were degassed separately and mixed in a glove box. To prevent premature $[Ru(bpy)_3]^{2+}$ excitation, the loaded cell was kept dark prior to flashing, and the probe light was filtered (cutoff < 602 nm). Electron-transfer reactions

Figure 52. FPLC gradient programs for the separation of ruthenium-modification product mixtures for *A. d.* azurin. The program for the Mono S 10/10 column was patterned after that for the Mono S 5/5 column (4-fold increase in volumes) to facilitate direct scale-up of separations and to allow easy comparison of chromatograms from each. Buffer A: 50 mM $NH_4(CH_3CO_2)$, pH 5.2. Buffer B: A + 1 M NaCl. In each program, the numbers in the left-hand column are in mL eluate.

Mono S 5/5

0.0	CONC %B	0.0
0.0	ML/MIN	0.20
0.0	CM/ML	0.20
1.0	VALVE.POS	1.2
1.0	PORT.SET	6.1
2.0	VALVE.POS	1.1
2.0	ML/MIN	1.00
2.0	CONC %B	0.0
58.0	CONC %B	14.0
69.0	CONC %B	25.0
79.0	CONC %B	100
79.0	PORT.SET	6.0
79.0	ML/MIN	2.00
84.0	CONC %B	100
89.0	CONC %B	0.0
99.0	CONC %B	0.0

Mono S 10/10

0.0	CONC %B	0.0
0.0	ML/MIN	2.00
0.0	CM/ML	0.07
1.0	VALVE.POS	1.2
1.0	PORT.SET	6.1
4.0	VALVE.POS	1.1
4.0	CONC %B	0.0
4.0	ML/MIN	4.00
240.0	CONC %B	14.0
265.0	CONC %B	100
265.0	PORT.SET	6.0
265.0	ML/MIN	6.00
270.0	CONC %B	100
270.0	CONC %B	0.0
280.0	CONC %B	0.0

were followed by monitoring the protein oxidation state by visible absorption at 620 nm, and only data from the first flash were used.

Instrumentation and methods of data treatment were unchanged from the cyt b_5 work (Chapter III).

RESULTS AND DISCUSSION

Modification and Characterization

A. d. azurin has two surface histidines (His-83 and His-32) potentially accessible to ruthenium modification. By introducing a second metal center into the protein at either of these residues, a two-site, donor-acceptor system can be produced for intramolecular ET investigations; ideally, two singly modified isomers would be prepared and isolated. Preliminary studies indicated that *A. d.* azurin could be effectively modified with a 10-fold molar excess of $[a_5Ru(OH_2)]^{2+}$ in Tris HCl, pH 7.2, for 45 minutes.[6] FPLC separated one major and two later-eluting, minor modified bands from the native azurin, which eluted with the void volume (a similar trace is shown in Figure 53, from the present work).

Since the two histidines were expected to modify equally well,[6] several changes in the procedure were made in an effort to effect modification of the other residue. As described in the experimental section, a higher pH and a different modification buffer were tried, and the $[a_5Ru(OH_2)]^{2+}$ was isolated as the PF_6 salt before use. In addition, the reaction was quenched after different times using the Bio-Gel centrifugation method (Chapter II) both before and after oxidation with Na[Co(EDTA)]. Longer reaction times slightly increased the yields (and number) of late eluting bands, but otherwise the variations tried were inconsequential. The 30 min reaction time was chosen to maximize peak 2 (Figure 53).

By using the absorbances at 620 and 304 nm in the UV-vis spectrum of FPLC peak 2, a Ru/Fe ratio of 1/1 was determined.[6] The site of modification for this singly

Figure 53. Elution profile by FPLC (Mono S 10/10; see conditions and the gradient program in Figure 52) of the reaction mixture from a_5Ru-modification of *A. d.* azurin quenched after 30 min. Native azurin and Co(EDTA)$^-$ oxidant co-elute at the void volume. Peak 2 is singly modified Ru(H83)Az. Peak 3 is singly modified (probably at His-32), and peak 4 is a multiply modified product.[5]

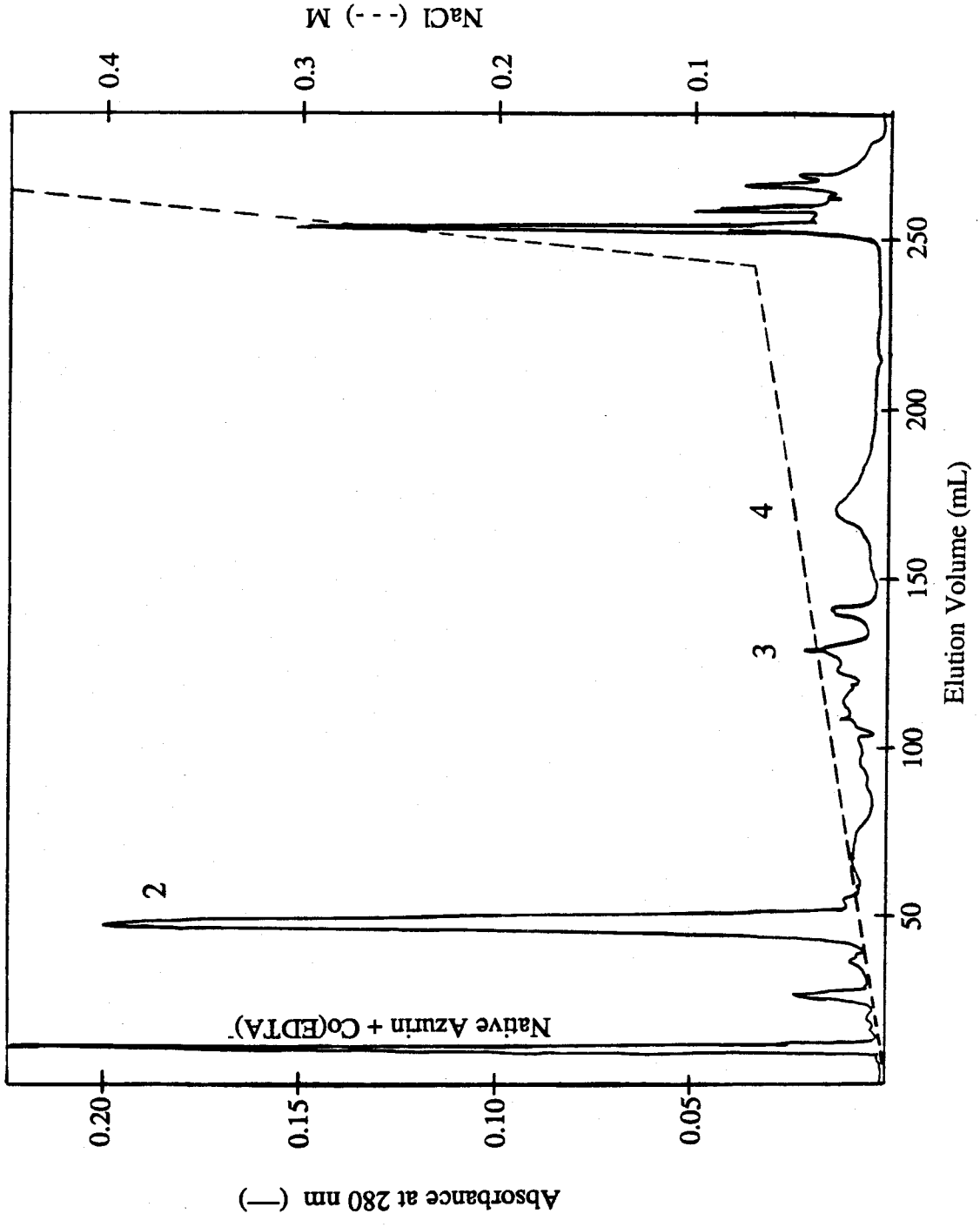
Absorbance at 280 nm (—)
0.20
0.15
0.10
0.05
Native Azurin + Co(EDTA)
2
3
4
50
100
150
200
250
Elution Volume (mL)
NaCl (- - -) M
0.4
0.3
0.2
0.1

ruthenated derivative was identified by proton NMR. Figure 54 shows the aromatic regions of ^{1}H NMR spectra for native azurin and for FPLC peak 2. The two sharp, histidine imidazole C_2H resonances are easily identified in the spectrum of the native protein (8.23 and 7.65 ppm; pH 6.8, 36 °C) and correlate well with literature assignments for surface histidines 83 and 32.[12] The His-32 C_4H is also evident at 6.54 ppm. In the spectrum of peak 2 the His-83 resonance is absent, indicating modification at that site: Ru(H83)Az.

As with cyt b_5, differential pulse voltammetry was employed to verify the reduction potentials of the two metal centers in modified azurin. Unlike the heme protein, however, reduction waves from both sites were resolved, giving values of $E°(Cu^{2+/+})$ = 278(5) mV and $E°(Ru^{3+/2+})$ = 118(5) mV vs. NHE in μ = 100 mM NaPi, pH 7.0 with 10 mM 4,4'-bipyridine added to enhance heterogeneous electron transfer (Figure 55). The former potential is the same as that already reported,[14] while the latter is 40 mV higher that expected.[15-16] (Sykes has found similar potentials for $[a_5Ru\text{-}His]^{3+/2+}$ in other modified blue-copper proteins.)[17] As a result, the net driving force favors ET from Ru^{2+} to Cu^{2+}, $\Delta G°$ = -0.16 eV.

Electron Transfer in *A. d.* Azurin

ET was studied by flash photolysis, using the initially oxidized protein and the $[Ru(bpy)_3]^{2+}$/EDTA system. Since Cu^+ does not absorb at 620 nm, the flash-photolysis voltage trace of native azurin (Figure 56) shows a sharp bleach caused by direct reduction of Cu^{2+} by $[Ru(bpy)_3]^{2+*}$. In the modified sample, continued reduction by the remote Ru^{2+} site results in an additional, slower bleaching (Figure 57). This slow component was found to decay according to first-order kinetics for over >3 half-lives. The value of k_{obs} displayed a mild concentration dependence (1.2 to 4 μM), extrapolating to k_{ET} = 1.0(3) s^{-1} (Figure 58). This rate constant is comparable to that obtained for His-83-modified *P. a.* azurin (1.9(4) s^{-1}); the implications are discussed below.

Figure 54. The aromatic region of the ^1H NMR spectra (Bruker AM500, 20 mM D_2O NaPi, pH 6.8) of a) FPLC peak 2 (Figure 53), assigned as Ru(H83)Az and b) unmodified *A. d.* azurin. The His-83 C_2H resonance is absent (*) in the modified sample.

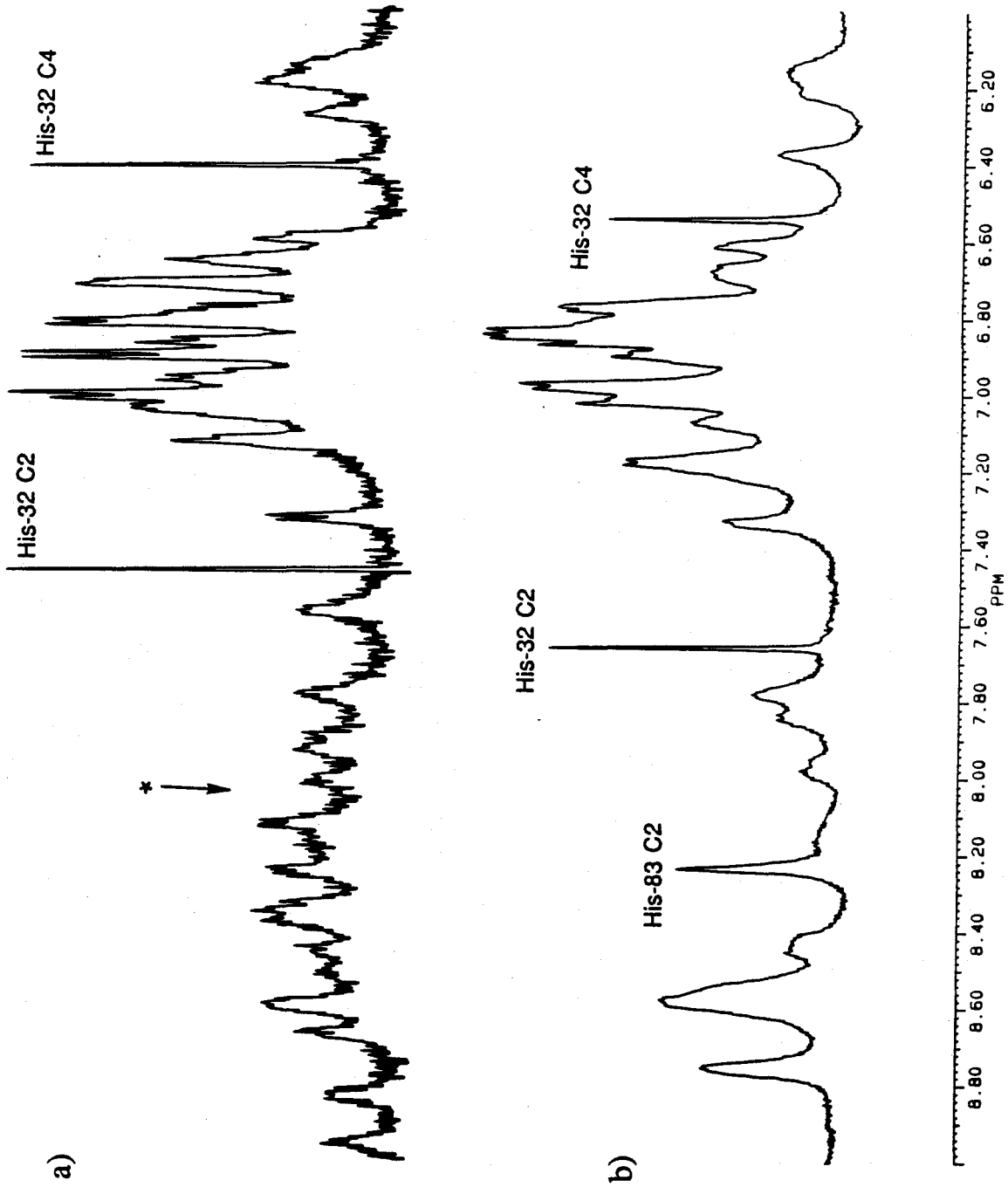
a)
His-32 C2
His-32 C4
*
b)
His-83 C2
His-32 C2
His-32 C4
8.80
8.60
8.40
8.20
8.00
7.80
7.60
7.40
PPM
7.20
7.00
6.80
6.60
6.40
6.20

Figure 55. Differential pulse voltammogram of Ru(H83)Az in μ = 100 mM NaPi, pH 7.0, plus 10 mM 4,4'-bipyridine (25 °C). Reduction waves for both metal centers were resolved: $E°(Cu^{2+/+})$ = 278(5) mV, and $E°(Ru^{3+/2+})$ = 118(5) mV vs. NHE. Refer to the Experimental Section for more details.

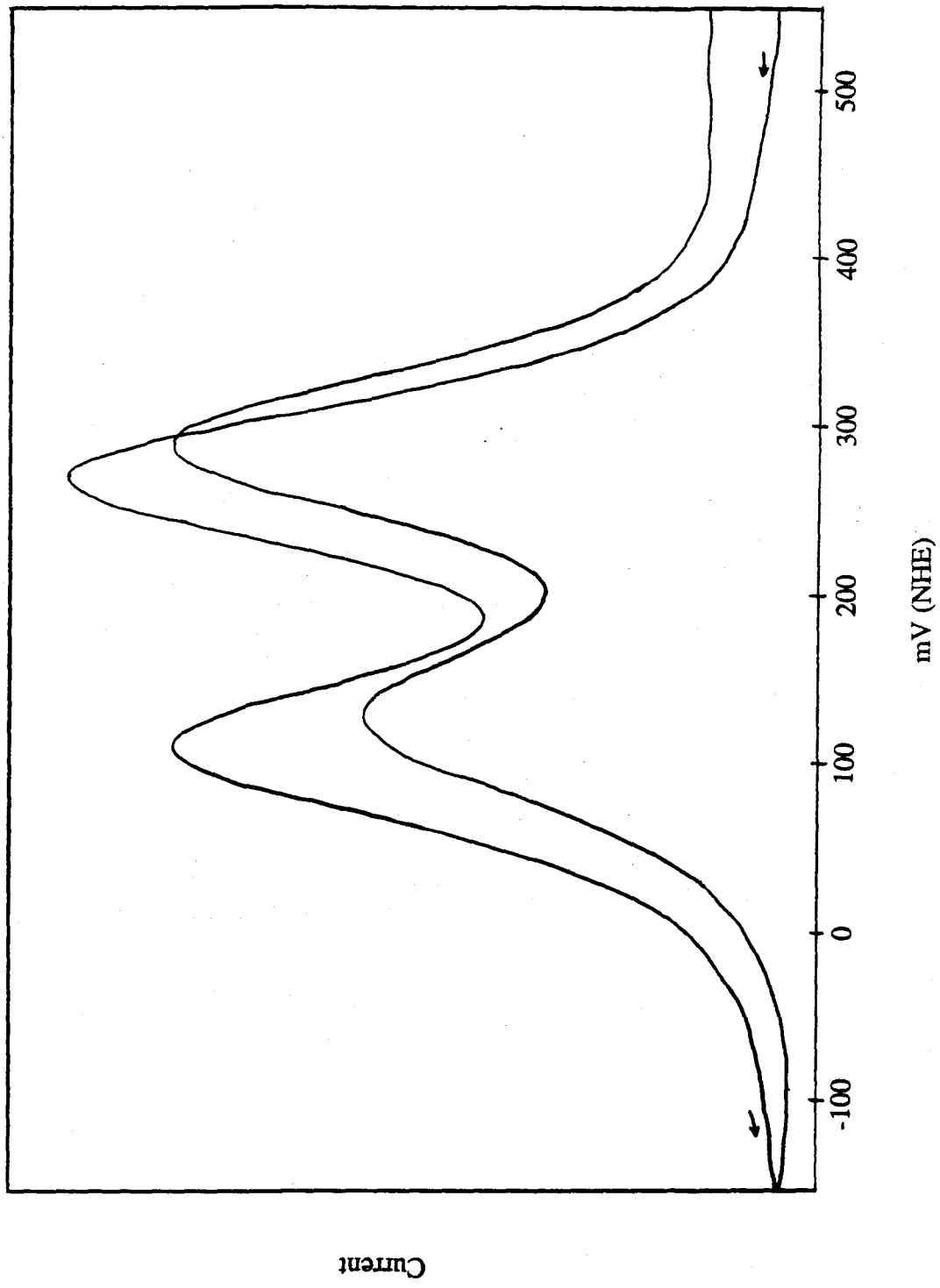
Current
-100
0
100
200
300
400
500
mV (NHE)

Figure 56. A flash-photolysis voltage/time trace for 1.5 μM of oxidized *A. d.* azurin using the EDTA reductive scavenging system (620 nm). Conditions are provided in the Experimental Section .

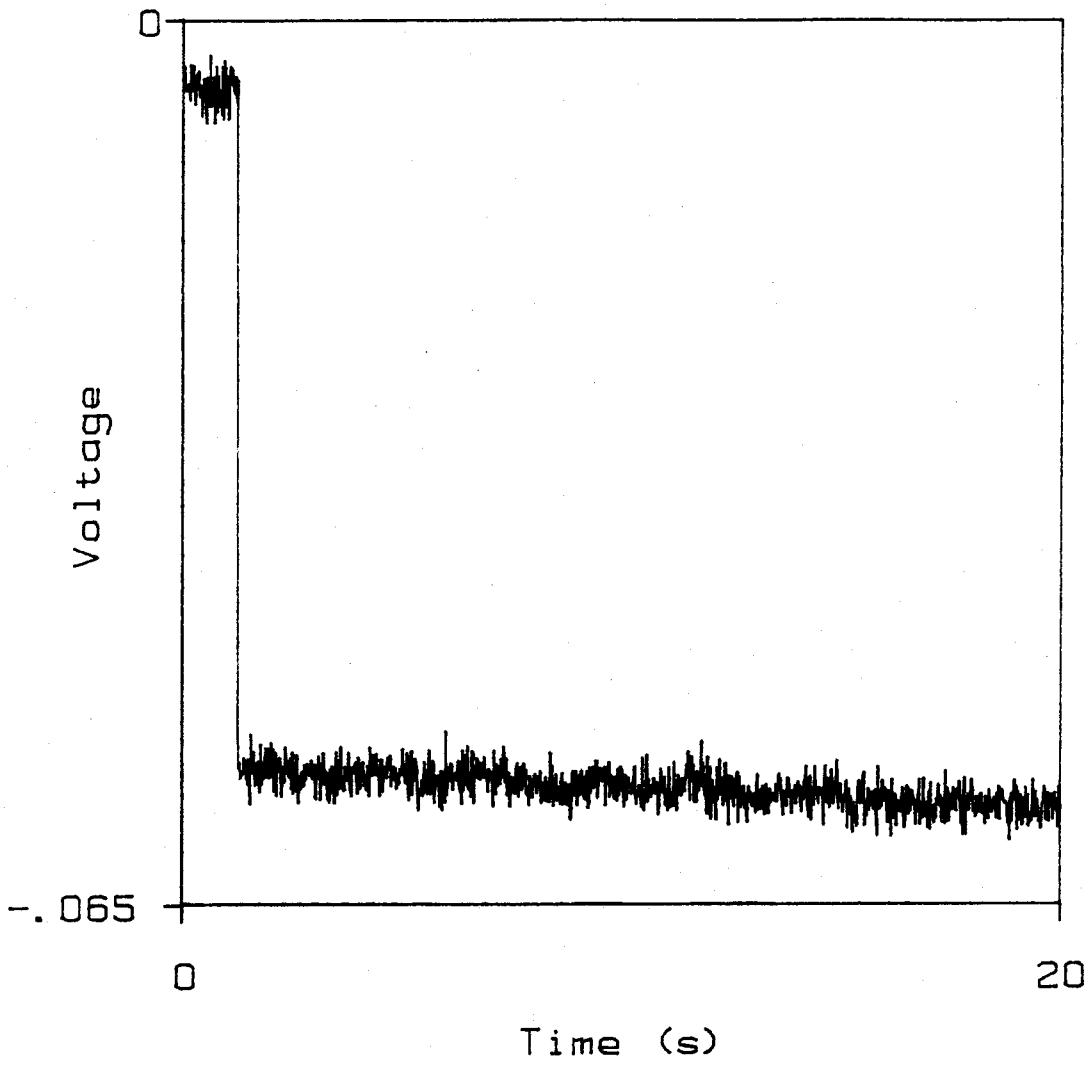
0
Voltage
-.065
0
20
Time (s)

Figure 57. Flash-photolysis a) voltage/time and b) absorbance/time traces for 1.5 μM Ru(H83)Az (620 nm). The data in trace a) were converted to those in trace b) by T2A.BAS. Analysis of points using SI-FIT gave the fit shown (inset is a plot of residuals) and $k_{obs} = 1.6\ s^{-1}$.

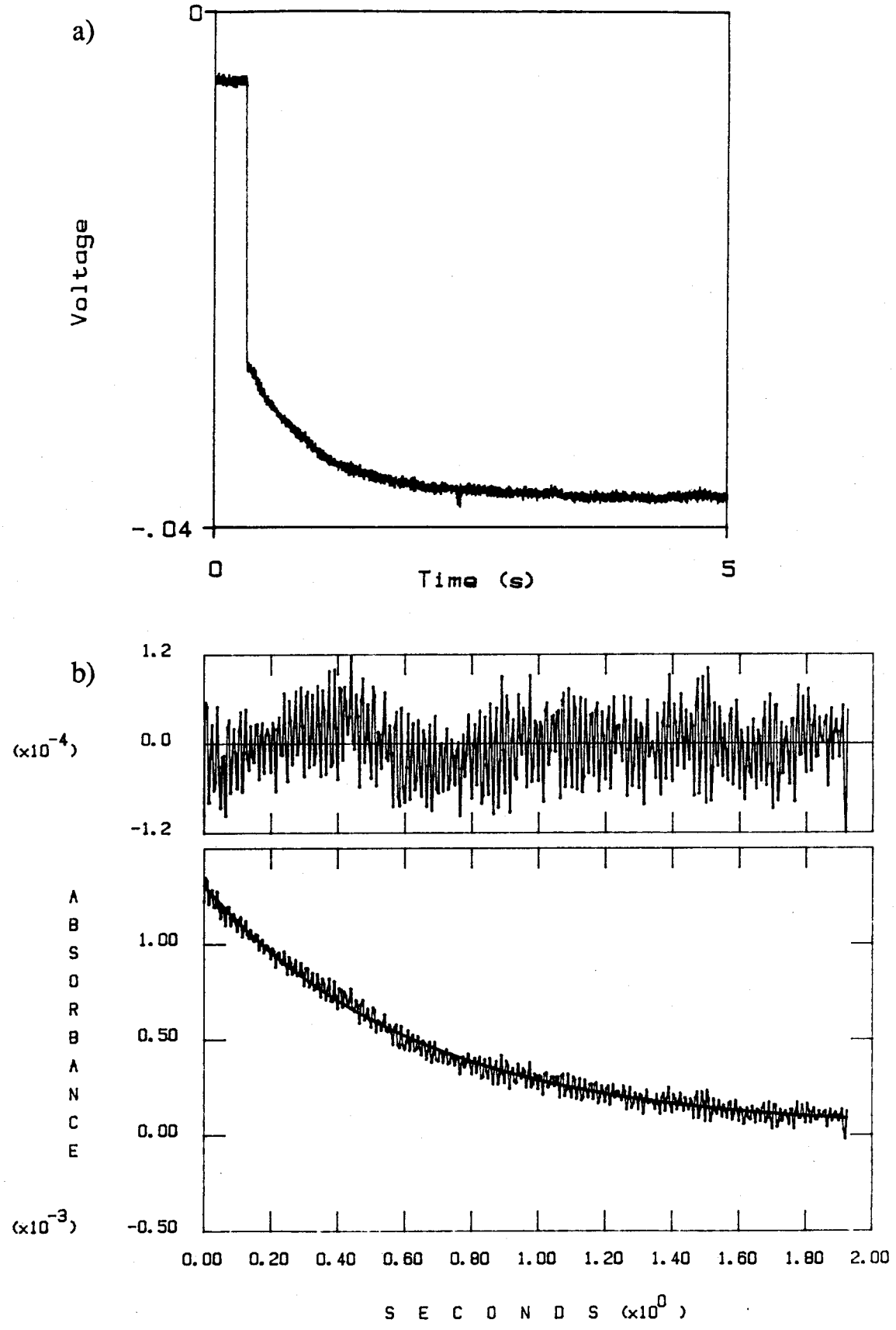
a)
0
Voltage
-.04
0
Time (s)
5
b)
1.2
0.0
-1.2
(x10^-4)
ABSORBANCE
1.00
0.50
0.00
-0.50
(x10^-3)
0.00
0.20
0.40
0.60
0.80
1.00
1.20
1.40
1.60
1.80
2.00
SECONDS (x10^0)

Figure 58. A plot of the concentration dependence of k_{obs} for Ru(H83)Az. The line is a least-squares fit to the data. The intramolecular rate constant for ET from Ru^{2+} to Cu^{2+} was obtained by extrapolation to zero concentration: $k_{ET} = 1.0(3)\ s^{-1}$.

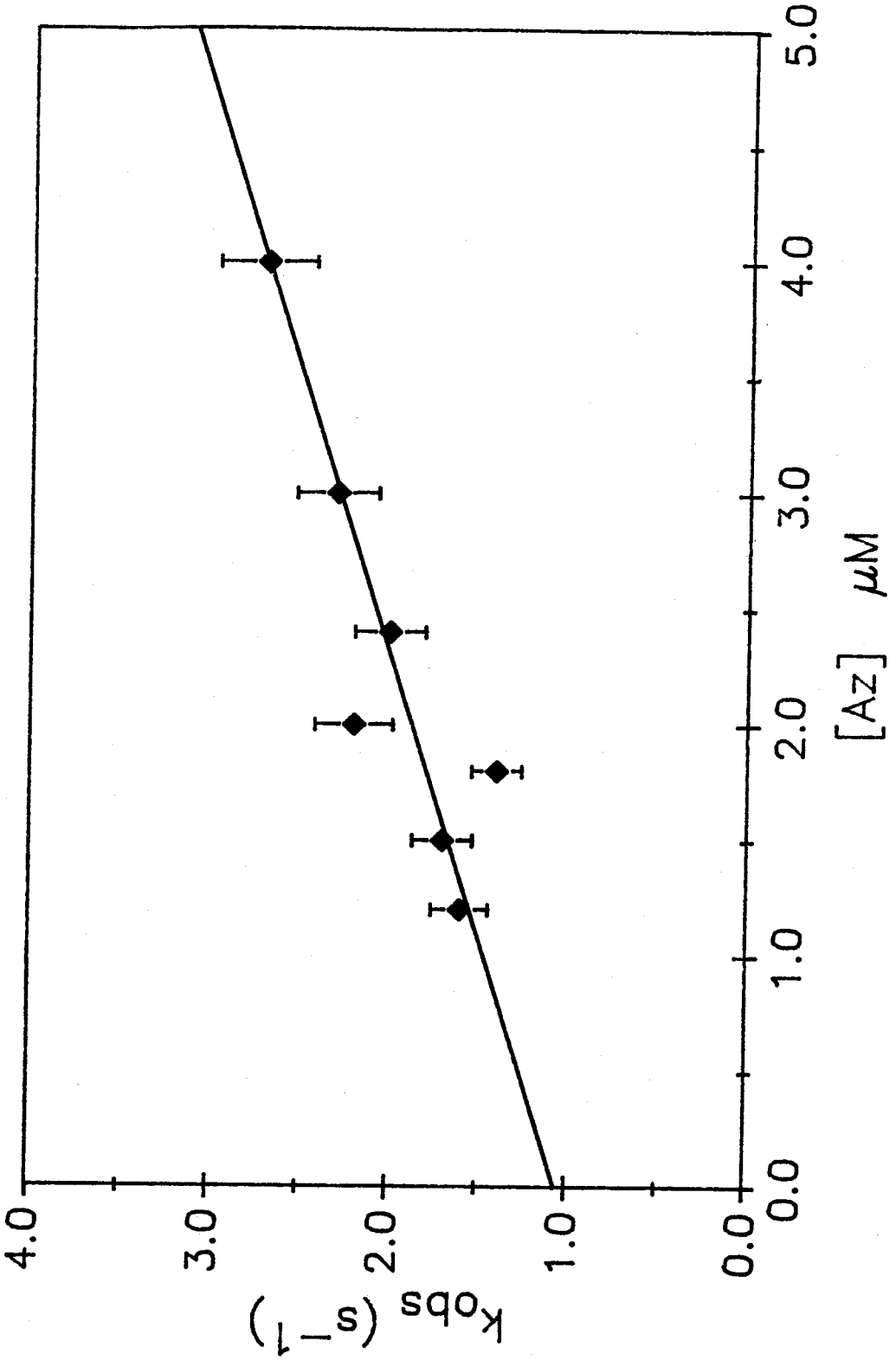
4.0
3.0
2.0
1.0
0.0
k_{obs} (s^{-1})
0.0
1.0
2.0
3.0
4.0
5.0
[Az] μM

Evaluating the ET Rate for Ru(H83)Az With Theoretical Models

For Ru(H83)Az the edge-to-edge, donor-acceptor separation (D = 11.3 Å) is similar to that for Ru(H26)WT-b_5, and the ET driving force ($\Delta G°$ = -0.16 eV) is twice as great. If, as in Chapter III, the rate constant is calculated from D and $\Delta G°$ (scaled to Ru(H33)Cyt *c*; λ = 1.2 eV), the exponential decay model [18] predicts $k_{calc} = 30\ s^{-1}$. (In fact, D and $\Delta G°$ for Ru(H83)Az are nearly identical to D = 11.7 Å and $\Delta G°$ = -0.18 eV for Ru(H33)Cyt *c*; $k_{ET} = 30\ s^{-1}$.) Why the actual rate ($k_{ET} = 1.0(3)\ s^{-1}$) is low in the copper protein is curious. As discussed above, the reorganization enthalpy for Cu^{2+} reduction in azurin is small ($\Delta H^{\ddagger}$ = -7.1 kcal/mole);[9] thus the observed rate is expected to be due to poor electronic coupling rather than to a high value of λ.

One explanation for the lower electronic coupling in azurin could be that the β-sheet secondary structure permits few good ET pathways. To address this hypothesis, a search of the possible ET pathways from His-83 to Cu was performed (see Chapter III).[19] The best pathway (Figure 59) consists of eleven covalent bonds and two hydrogen bonds (3.01, 2.97 Å) from His-83 (C_γ) to Cys-112 (S_γ), giving $(H_{AB}')^2 = 1.2 \times 10^{-7}$ (calculated rate constants can be found in Table 3). This value of $(H_{AB}')^2$ is greater than that calculated for Ru(H26)WT-b_5. Therefore, according to the pathway analysis, the β-sheet secondary structure in Ru(H83)Az imposes no unusual barriers to ET.

Another difference azurin has from the cytochromes is the redox prosthetic group. The copper center in azurin is smaller and is expected to be less delocalized than an iron heme; thus electronic coupling to copper may be inherently lower than to an iron heme. If so, including a simple prefactor (< 1) might satisfactorily adjust rates predicted for azurin from a heme protein reference. On the other hand, orientational effects may play a significant role in ET to copper. The sulfur of Cys-112 is implicated in a ligand-to-metal, charge-transfer transition (giving azurin its blue color);[5] thus Cys-112 may be a special ligand through which there is enhanced electronic coupling. If this is true, then ET

Figure 59. The shortest ET pathway found from His-83 to copper in *A. d.* azurin. Protein bonds are shown in green, and the copper site is blue. Pathways are drawn in red with covalent links (—), and H-bonds (– – –) as indicated. See the text for a thorough discussion.

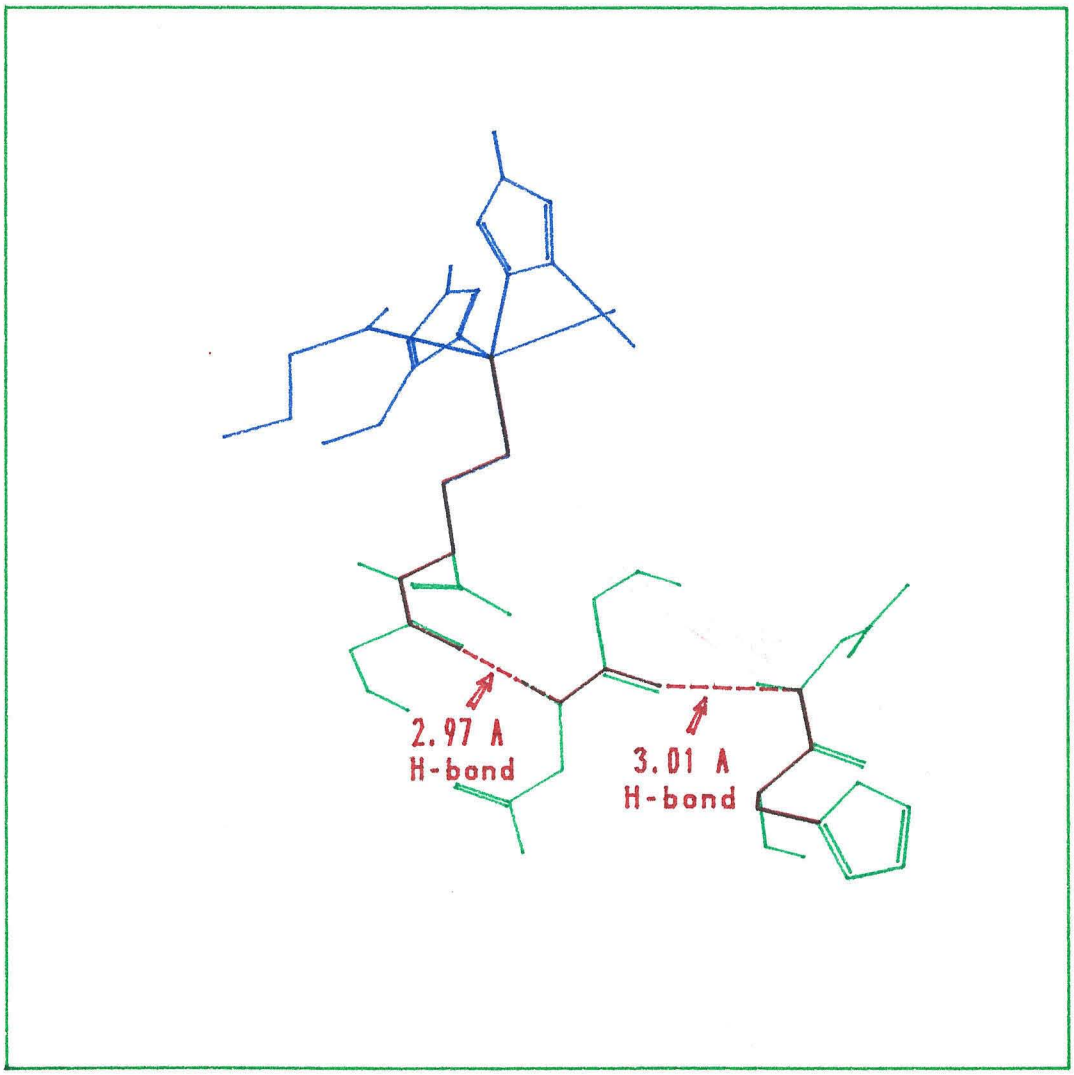
2.97 A
H-bond
3.01 A
H-bond

Table 3. Rate Constants for Ru(II) to Cu(II) ET in a_5Ru-Azurin Derivatives.

Sample	$\Delta G°$ (eV)[a]	k_{ET} (s^{-1})	Pathway	$(H_{AB}')^2$	k_{calc} (s^{-1}) Path[b]	k_{calc} (s^{-1}) Exp. Decay[c]
A. d.-Ru(H83)Az	-0.16	1.0(3)	11C, 2H (3.01, 2.97 Å)	1.2×10^{-7}	30	30
P. a.-Ru(H83)Az	-0.23	1.9(4)	13C, 2H (2.69, 2.66 Å)	1.3×10^{-7}	130	70
A. d.-Ru(H32)Az	-0.16	---	11C, 1H (2.86 Å), 1S (3.81 Å)	2.0×10^{-10}	0.05	10

[a] $E°(Cu^{2+/+}) = 276$ mV, *A.d.* azurin;[14] 308 mV, *P. a.* azurin;[6] $E°(Ru^{3+/2+}) = 80$ mV.[15,16] (vs. NHE, 25 °C).

[b] $k_{calc} = (k_{ref}) \{(H_{AB}')^2 / (H_{ABref}')^2\}(FC / FC_{ref})$.[d]

[c] $k_{calc} = (k_{ref}) \exp[-\beta (D - D_{ref})] (FC/FC_{ref})$, ($\beta = 0.9$ Å^{-1}).[d]

[d] Referenced to Ru(H33)Cyt *c*: $k_{ref} = 30$ s^{-1}, $(H_{ABref}')^2 = 8.0 \times 10^{-8}$, $D_{ref} = 11.7$ Å, $\lambda = 1.2$ eV.

involving Cys-112 (either as the end of a pathway or as the nearest Cu ligand) could be faster than ET from other donor-acceptor orientations. By this argument, electronic coupling through the long Met-121(S) to Cu bond (3.13 Å)[4] would be weaker than through the cysteine or histidine ligands, and coupling through the Gly-45 (carbonyl O) to Cu bond (3.11 Å)[4] would be particularly small.

Two alternate pathways from His-83 to Cu were found that pass through His-46 and the Gly-45 carbonyl (Figure 60). With no weighting of orientational effects, each of these pathways has $(H_{AB}')^2 = 3.5 \times 10^{-8}$, a value on par with $(H_{AB}')^2$ for Ru(H26)WT-b_5. Since the $(H_{AB}')^2$ for the Cys-112 pathway is ten times greater, however, any contribution by these paths is likely to be negligible. More experiments with primary pathways through ligands other than Cys-112 are necessary to elucidate the effect of orientation on ET in azurin.

Comparison to P. a. Azurin

One reason for studying *A. d.* azurin was to allow a comparison of ET rates from the same modification site in proteins from different species of bacteria. A pathway search from His-83 to Cu using the crystallographic coordinates for *P. a.* azurin [2] revealed that the structures were different enough to change the preferred pathway. Figure 61 depicts some of the pathways found. The pathway in *P. a.* azurin with the largest coupling includes two more covalent bonds (13) than that for *A. d.* azurin, but because its two hydrogen bonds (2.69, 2.66 Å) are shorter, the net coupling is coincidentally equivalent: $(H_{AB}')^2 = 1.3 \times 10^{-7}$. Likewise, the edge-to-edge distances for *P. a.* and *A. d.* azurins are similar (11.7, 11.3 Å), making the coupling values calculated by exponential decay approach the same for the two proteins.

However, the higher reduction potential of *P. a.* azurin ($E°(Cu^{2+/+}) = 308$ mV vs. NHE) results in a larger ET driving force ($\Delta G° = -0.23$ eV, using $E°(Ru^{3+/2+}) = 80$ mV vs. NHE);[15-16] thus k_{calc}(*P. a.*) is significantly higher than k_{calc}(*A. d.*) according to both

Figure 60. Alternate ET pathways from His-83 to copper in *A. d.* azurin. The possible pathways passing through copper ligands His-46 and Gly-45 are shown compared to the Cys-112 pathway (Figure 59).

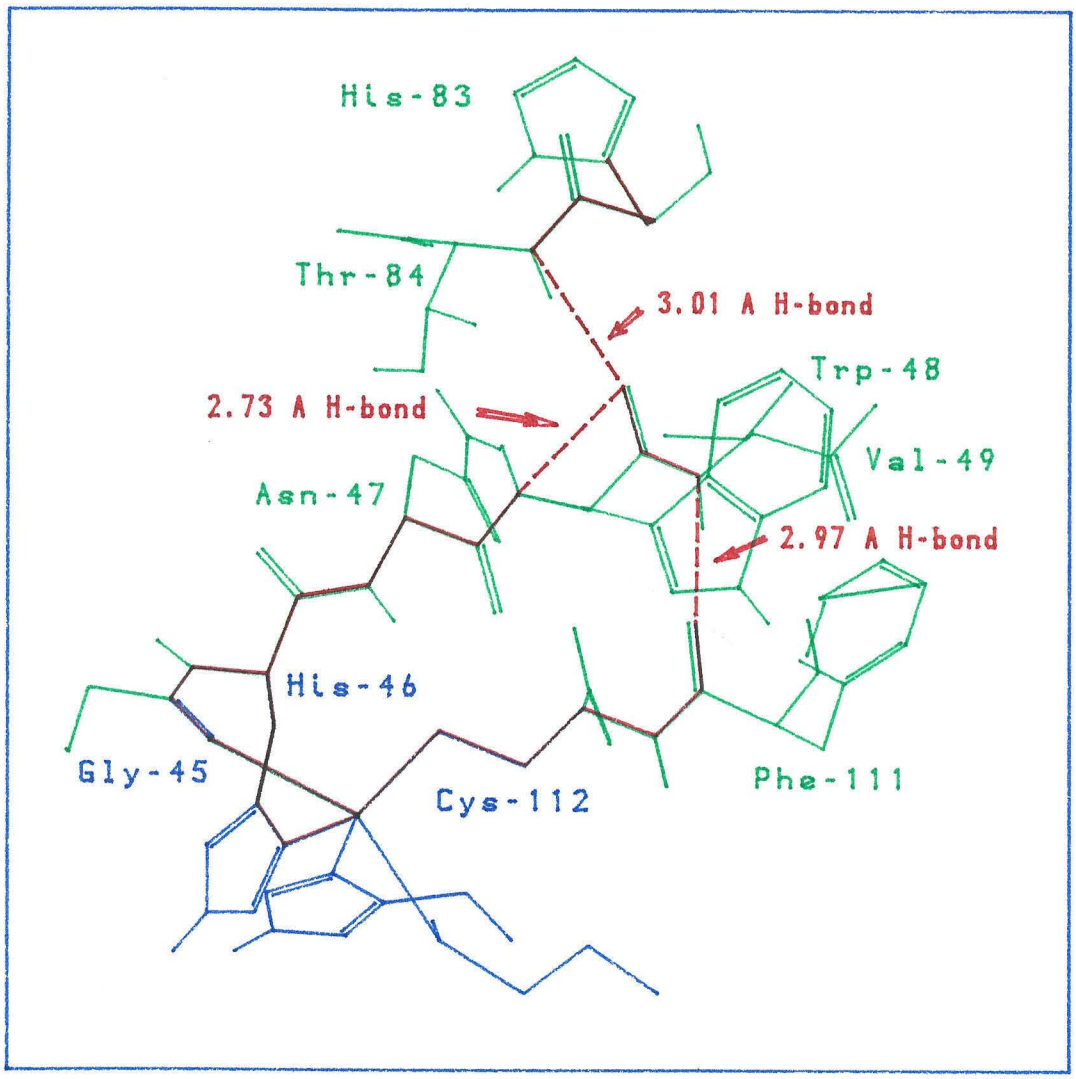
His-83
Thr-84
3.01 A H-bond
Trp-48
2.73 A H-bond
Val-49
Asn-47
2.97 A H-bond
His-46
Gly-45
Cys-112
Phe-111

Figure 61. Possible ET pathways for His-83 to copper in *P. a.* azurin. Pathways are drawn in red with covalent links (—), H-bonds (– – –), and space jumps (- - -) as indicated. As with *A. d.* azurin, the best pathway passes through Cys-112 after negotiating two H-bonds (2.69, and 2.66 Å; pathway to far right). The central pathway includes a 3.61 Å space jump from His-83 (C_α) to Trp-48 (O), and the leftmost pathway crosses three successive H-bonds (2.54, 2.90, and 3.22 Å).

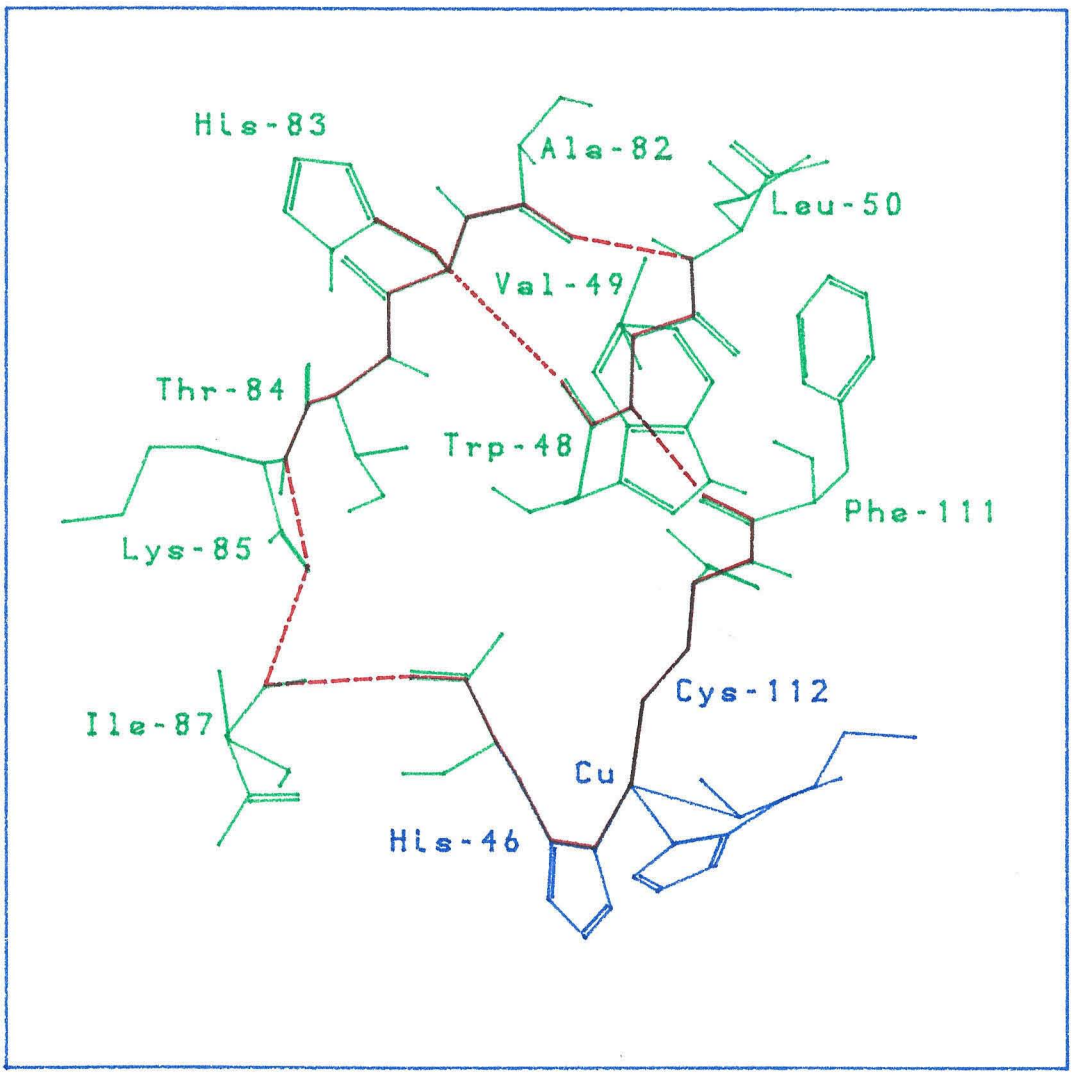
His-83
Ala-82
Leu-50
Val-49
Thr-84
Trp-48
Phe-111
Lys-85
Cys-112
Ile-87
Cu
His-46

the exponential decay and the pathway models (Table 3). Since the differences in predicted rates arise from the driving forces in the two modified proteins, possible errors in their estimation should be considered. The $E°(Ru^{3+/2+})$ measured in the modified *P. a.* azurin was 50 mV vs. NHE,[9] but the preferred value used later was 80 mV.[20] In the present work, $E°(Ru^{3+/2+})$ as measured by DPV was 120 mV, a high value that was accepted since the $Cu^{2+/+}$ reduction potential determined in the same voltammogram (Figure 55) was identical to the value measured by spectroelectrochemical methods.[14] Using a more typical value of $E°(Ru^{3+/2+})$ = 80 mV for the *A. d.* azurin system increases $\Delta G°$ to 0.2 eV, resulting in $k_{calc}(path) = 60\ s^{-1}$ and $k_{calc}(exp.\ decay) = 60\ s^{-1}$. The ratio of these values to those calculated for *P. a.* azurin are quite close to the ratio of k_{ET}'s for the two proteins. One should avoid adjusting experimental results to accommodate theory, but this example serves to illustrate how the predicted and observed rates can be reconciled with allowance for experimental error.

His-32 Modified A. d. Azurin

The low reactivity of His-32 towards a_5Ru was unexpected. According to computer-graphics modeling, His-83 and His-32 have identical solvent accessibilities,[6] and neither residue is involved in hydrogen bonding. Inspection of the crystal structure reveals that the imidazole ring of His-83 points out into solvent, thus exposing the ε-nitrogen (which is reactive towards ruthenation). One explanation of the relative inertness of His-32 is that although the side chain has good solvent accessibility it lies flat on the protein surface.

The low reactivity of His-32 is unfortunate because ET from this site would be interesting and informative. An exponential decay calculation using the 12.7 Å separation between His-32 and Cu gives $k_{calc} = 10\ s^{-1}$. On the other hand, the pathway model predicts a much smaller value (Table 3) because of the reduced coupling across an

Figure 62. Possible ET pathways for His-32 to copper in *A. d.* azurin. Pathways are drawn in red with covalent links (—), H-bonds (– – –), and space jumps (- - -) as indicated. Unlike searches initiated from His-83, Cys-112 is not involved in pathways from His-32. In addition, even the best pathway includes a 3.81 Å space jump, making the predicted electronic coupling low from this site.

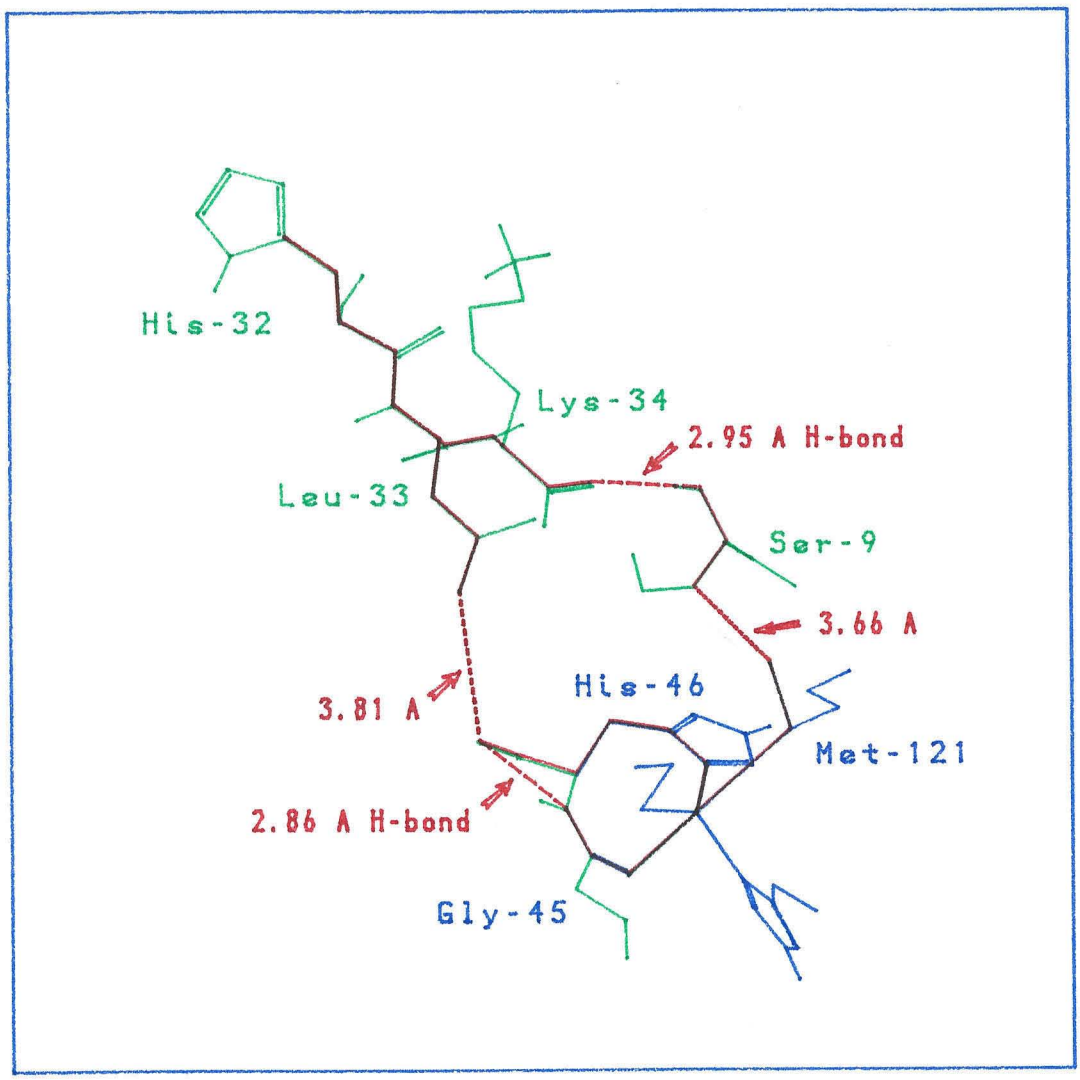
His-32
Lys-34
2.95 A H-bond
Leu-33
Ser-9
3.66 A
3.81 A
His-46
Met-121
2.86 A H-bond
Gly-45

obligatory 3.81 Å space jump (Figure 62). In fact, the best pathway passes through the Gly-45 carbonyl to the copper; hence, measuring the rate in this derivative (particularly at a higher driving force with a different modification reagent) would test the importance of the copper ligand in the ET pathway. Alternate pathways from this site pass through His-46 or Met-121, but not Cys-112. Now that *P. a.* azurin has been expressed in *E. coli*,[21] mutants in neighboring (but perhaps more solvent-exposed) positions would allow some interesting ET experiments.

Summary

A. d. azurin was singly modified at His-83 with a_5Ru^{3+} and was characterized by UV-vis, DPV, and ^1H NMR. The other surface histidine, His-32, was not successfully modified, contrary to expectations. The intramolecular k_{ET} for Ru(H83)Az was measured (1.0(3) s^{-1}) and was found to be comparable to that reported for the analogous ruthenium-modified *P. a.* azurin. These rates are slower than would be expected for a similar distance in cytochrome *c*. Pathway and exponential decay theoretical models were applied to both the *P. a.* and *A. d.* azurin systems. No evidence was found by the pathway model that the β-sheet secondary structure of azurin precludes effective electronic coupling. In fact, when referenced to Ru(H33)Cyt *c*, both models overestimate the ET rate constant by an order of magnitude. This suggests that weak electronic coupling to the copper site itself is responsible for the low k_{ET}'s in azurin. More experiments are necessary to identify any relationships between the nonisotropic electronic properties of the blue-copper center and orientation effects for electron transfer.

REFERENCES

(1) Farver, O.; Pecht, I. In *Copper Proteins and Copper Enzymes*; Lontie, R., Ed.; CRC Press, Inc.: Boca Raton, Florida, 1984; Vol. I., Chapter 7.

(2) a) Adman, E. T.; Stenkamp, R. E.; Sieker, L. C.; Jensen, L. H. *J. Mol. Biol.* **1978**, *123*, 35. b) Adman, E. T.; Jensen, L. H. *Isr. J. Chem.* **1981**, *21*, 8.

(3) Norris, G. F.; Anderson, B. F.; Baker, E. N. *J. Mol. Biol.* **1983**, *165*, 501-521.

(4) Norris, G. F.; Anderson, B. F.; Baker, E. N. *J. Am. Chem. Soc.* **1986**, *108*, 2784-2785.

(5) a) Solomon, E. I.; Hare, J. W.; Dooley, D. M.; Dawson, J. H.; Stephens, P. J.; Gray, H. B. *J. Am. Chem. Soc.* **1980**, *102*, 168. b) Gray, H. B.; Solomon, E. I. In *Copper Proteins*; Spiro, T., Ed.; Wiley-Interscience: New York, 1981; pp. 1-40.

(6) St. Clair, C. S. Ph. D. Thesis, California Institute of Technology, 1989.

(7) Gray, H. B.; Malmstrom, B. G. *Comments Inorg. Chem.* **1983**, *2*, 203-209.

(8) Kostic, N. M.; Margalit, R.; Che, C. -M.; Gray, H. B. *J. Am. Chem. Soc.* **1983**, *105*, 7765-7767.

(9) Margalit, R.; Kostic, N. M.; Che, C. -M.; Blair, D. F.; Chiang, H. -J.; Pecht, I.; Shelton, J. B.; Shelton, J. R.; Shroeder, W. A.; Gray, H. B. *Proc. Nat. Acad. Sci. USA* **1984**, *81*, 6554-6558.

(10) Groeneveld, C. M.; Canters, G. W. *Eur. J. Biochem.* **1985**, *153*, 555-564.

(11) Ainscough, E. W.; Bingham, A. G.; Brodie, A. M.; Ellis, W. R., Jr.; Gray, H. B.; Loehr, T. M.; Plowman, J. E.; Norris, G. E.; Baker, E. N. *Biochemistry*, **1987**, *26*, 71-82.

(12) Groeneveld, C. M.; Ouwerling, M. C.; Erkelens, C.; Canters, G. W. *J. Mol. Biol.* **1988**, *200*, 198-199.

(13) Winkler, J. R.; Nocera, D. G.; Yocom, K.M.; Bordignon, E.; Gray, H. B. *J. Am. Chem. Soc.* **1982**, *104*, 5798-5800.

(14) Ellis, W. R., Jr. Ph. D. Thesis, California Institute of Technology, 1986.

(15) Axup, A. W.; Albin, M.; Mayo, S. L.; Crutchley, R. J.; Gray, H. B. *J. Am. Chem. Soc.* **1988**, *110*, 435-439.

(16) Nocera, D. G.; Winkler, J. R.; Yocom, K. M.; Bordignon, E.; Gray, H. B. *J. Am. Chem. Soc.* **1984**, *106*, 5145-5150.

(17) Sykes, A. G., personal communication.

(18) Marcus, R. A.; Sutin, N. S. *Biochim. Biophys. Acta* **1985**, *811*, 265-322.

(19) a) Beratan, D. N.; Onuchic, J. N. *Photosynthesis Research* **1989**, *22*, 173-186. b) Beratan, D. N.; Onuchic, J. N.; Hopfield, J. J. *J. Phys. Chem.* **1987**, *86*, 4488-4498. c) Beratan, D. N.; Onuchic, J. N.; Betts, J. N.; Bowler, B. E.; Gray, H. B. *J. Am. Chem. Soc.*, in press.

(20) Gray, H. B. *Chem. Soc. Rev.* **1986**, *15*, 17-30.

(21) a) Chang, T., unpublished work. b) Pascher, T.; Bergstrom, J.; Malmstrom, B. G.; Vanngard, T.; Lundberg, L. G. *FEBS Lett.* **1989**, *108*, 2784.